SOME TECHNIQUES RELEVANT TO THE DEVELOPMENT OF A LONG BASELINE GRAVITATIONAL WAVE DETECTOR USING LASER INTERFEROMETRY

By

John B. Mangan

Presented as a thesis for the degree of Ph.D. in the University of Glasgow

September 1987

ProQuest LLC.
789 East Eisenhower Parkway
P.O. Box 1346
Ann Arbor, MI 48106 – 1346

Contents

Acknowledgments

Firstly I would like to thank my supervisor, Jim Hough, whose guidance and advice (and patience) have been invaluable. I would like to thank Prof. R. W. P. Drever, Prof. E. Laing and Prof. I. Hughes for their interest and support during the period of this work. I am particularly grateful to Jim Hough and to Norna Robertson for many helpful discussions and suggestions which they provided during the writing of this thesis. I am would like to express my gratitude to Gavin Newton and Brian Meers, for many helpful discussions on optical fibres, and Norman Mackenzie without whom this thesis would have taken very much longer to print. I would also like to thank all the other members of the gravitational wave group at Glasgow - Harry Ward, Stuart Hoggan, Graham Kerr and David Robertson - for their help and support during my work. Excellent technical assistance was provided by Angus Mckellar, Jim Pittillo, Allan Latta, John Jarvis and the staff of the departmental mechanical workshop.

In conclusion I would like to thank my family and friends for all their support which has always been very much appreciated.

I would like to thank the SERC and the University of Glasgow for financial support during the course of this work.

Preface

In 1978 construction began on a 10 metre baseline prototype gravitational radiation detector at Glasgow. This followed on from previous work with both split bar and separated mass detectors. Since this time work has continued towards the development of the techniques necessary to construct and operate a long baseline gravitational wave antenna employing optical interferometry. This thesis describes work done between October 1983 and September 1987 with the aim of furthering this development.

Chapter 1 introduces the concept of gravitational radiation and gives a broad overview of the expected properties. The chapter continues with a survey of some of the best understood sources and indicates the likely amplitudes which a terrestrial detector could expect to observe. There are many different types of possible detector systems and a summary of the most promising is included.

Chapter 2 provides a broad overview of the Glasgow prototype detector, which uses laser interferometry to monitor the positions of essentially free test masses, and the major sources of noise which must be overcome if detectors of sufficient sensitivity are to be operated. The work in these two chapters is gathered from several sources including theses and publications from the group at Glasgow. The provision of laser light that is stable in frequency, intensity and geometry is an important requirement in this work.

Chapter 3 covers work done in collaboration with Dr. N. A. Robertson and Mr. S. Hoggan on the investigation of the factors limiting the observed performance of a laser intensity stabilisation servosystem employing an electrooptic modulator as the control element.

Chapter 4 outlines the development of two feedback circuits -

one for the intensity stabilisation and the other for the fast frequency stabilisation of an Argon Ion laser - designed by Prof. J. Hough and constructed by the author. This required writing a computer program to calculate values of the circuit frequency response. This information was used to improve the circuit parameters prior to, and during, operation. The program is included in Appendix B with a brief explanation of the method employed.

In Chapter 5 the possibility of using optical fibres to reduce geometry fluctuations in the laser light illuminating the interferometer is investigated. Following on from these results the efficiency of transmission of a fundamental Gaussian mode which could be achieved with an ideal stepped-index, mono-mode optical fibre is calculated. This latter work was carried out at the suggestion of Dr. G. Newton.

The design and development of a data collection system is described in Chapter 6. The design parameters were outlined by Prof. J. Hough and this chapter explains some of the problems which had to be overcome in the realisation of the system. The computer program which was devised to overcome these problems is included in Appendix B.

The thesis concludes in Chapter 7 with a brief look at the prospects for experimental gravitational wave work in the near future and at the state of development in the community at large.

Summary

SOME TECHNIQUES RELEVANT TO THE DEVELOPMENT OF A LONG BASELINE GRAVITATIONAL WAVE DETECTOR USING LASER INTERFEROMETRY

Gravitational radiation is a travelling distortion in four-dimensional space-time which is predicted by most relativistic theories. This distortion may be detected by monitoring the changes in the separation of test masses. Since the gravitational interaction is so weak appreciable levels of gravitational radiation are only produced by violent astrophysical phenomena in which large masses are accelerated coherently to velocities approaching the speed of light. However, due to the conservation of momentum the lowest order of gravitational radiation is quadrupole and so the source must contain some asymmetry in its dynamics.

Chapter 1 is intended to introduce the reader to the concept of gravitational radiation by outlining its properties, describing some of the possible sources and indicating the levels which might be observed by a terrestrial detector. Chapter 1 also includes a brief overview of the main detection schemes currently being pursued.

Chapter 2 includes a brief overview of the current status of the prototype detector at Glasgow, which uses laser interferometry to monitor the relative lengths of two orthogonal optical cavities, before describing, briefly, the sources of noise which are most likely to limit the sensitivity of this type of system and the levels at which they become important. Theoretical work suggests that to see several gravitational wave events per year a sensitivity to strain, h $\sim 10^{-22}$ is required and so the levels have been scaled to the proposed 1km long observatory which should have this potential.

The following chapters are concerned with experiments related to reducing the effects of some of these possibly limiting sources of noise, in particular fluctuations in the quality of the laser light used to illuminate the optical cavities of the detector. Chapter 3 is concerned with the development of a laser intensity stabilisation system and investigations into limits to its observed performance which included geometry and frequency fluctuations in the laser light.

Chapter 4 covers the development of the feedback circuit for the intensity stabilisation system in more depth and describes another circuit designed for the fast frequency stabilisation of an Argon Ion laser.

The possible use of optical fibres to reduce the effects of geometry fluctuations in laser light is investigated in Chapter 5. This chapter describes the investigation of the suppression available from a sample fibre and calculates the efficiency with which a fundamental Gaussian beam may be transmitted through a mono-mode fibre.

Chapter 6 describes the construction of a data collection system designed to capture pulses in the output of an interferometric gravitational wave detector. Although the prototype detector is probably not sufficiently sensitive to detect likely levels of gravitational radiation the system was tested by sampling data from the prototype system. These data were then used to study the noise statistics of the detector to search for any non-random effects.

Chapter 7 briefly describes the state of the gravitational radiation detection effort world-wide and the prospects for future development.

'There is a pleasure sure
In being mad which none but madmen know'

John Dryden (The Spanish Friar, 1681)

'Contrariwise,' continued Tweedledee, 'if it was so, it might be; and if it were so, it would be; but as it isn't, it ain't. That's logic.'

Lewis Carroll (Alice's Adventures in Wonderland, 1865)

CHAPTER 1

GRAVITATIONAL RADIATION - SOURCES AND DETECTORS

1:1 INTRODUCTION

This chapter is intended to orient the reader by presenting an elementary description of gravitational radiation, its predicted properties, some likely astrophysical sources and their amplitudes and finally some of the techniques developed to detect them.

Gravitational radiation was first predicted in 1916 by Albert Einstein[1,2] as weak field wave solutions to the equations of his General Theory of Relativity. Gravitational waves are predicted by all currently viable relativity theories[3] though the expected amplitudes and properties vary slightly. In this thesis General Relativity will be assumed to be correct. The following summary of gravitational wave properties has been collated from review articles and other sources[3-6].

The acceleration of matter produces gravitational waves, which propagate at the speed of light, in a manner analogous to Maxwell's electromagnetic waves. However, due to the single sign of mass, conservation of momentum prevents the production of dipole radiation. Therefore the production of gravitational waves requires a time-varying quadrupole moment. The inefficiency of quadrupole wave generation means that large masses moving relativistically are required to produce appreciable levels of gravitational radiation.

The extreme weakness of the gravitational interaction means that gravitational radiation propagates virtually unimpeded through matter. In principal there are other reactions, such as dispersion

and backscatter for example, but in practice the effect of these is negligible. This property allows gravitational radiation to carry information on the bulk motions of matter in the cores of collapsing stars and other astrophysical phenomena that is unobtainable in any other way.

Gravitational radiation may be described in a straightforward way in terms of an extension of Newtonian gravity. In the neighbourhood of some fiducial point the gravitational potential, $\emptyset(\underset{\sim}{x})$, may be written:

$$\emptyset(\underset{\sim}{x}) = \emptyset_o - \sum_j g_j x_j + \sum_{j,k} \frac{1}{2} R_{joko}\, x_j x_k + \ldots \qquad (1.1)$$

Where x_j is the component of the vector $\underset{\sim}{x}$ from the fiducial point to the measuring point and g_j is the component of local g. R_{joko} measures the inhomogeneity of the gravitational field (this is the Riemann curvature tensor in General Relativity) and is written:

$$R_{joko} = \frac{\partial^2 \emptyset}{\partial x_j \partial x_k} \qquad (1.2)$$

The second and fourth indices may be non-zero but they will not affect the validity of the result.

Now consider the force on a test particle:

$$\underset{\sim}{F} = - m \frac{\partial \emptyset}{\partial x_j}$$

$$= - m g_j - \sum_k m R_{joko} x_k \qquad (1.3)$$

The term including R_{joko} is linearly dependent on $\underset{\sim}{x}$, it is a relative or 'tidal' force between the source and the measuring point. In his work Einstein added a gravitational wave correction to

R_{joko}.

$$R_{joko} = \frac{\partial^2 \phi}{\partial x_j \partial x_k} + R^{GW}_{joko} \qquad (1.4)$$

The form of R^{GW}_{joko} is dictated by General Relativity. A locally plane gravitational wave propagating in the z-direction has:

$$R^{GW}_{xoxo} = - R^{GW}_{yoyo} = - \frac{1}{2} \ddot{h}_+ (t-z/c) \qquad (1.5a)$$

$$R^{GW}_{xoyo} = - R^{GW}_{yoxo} = - \frac{1}{2} \ddot{h}_x (t-z/c) \qquad (1.5b)$$

Here h_+ and h_x are the arbitrary, dimensionless amplitudes of the two orthogonal polarisation states allowed, + and x. The dots denote time derivatives and c is the speed of light.

The wavelength of the propagating gravitational wave is assumed to be much less than the curvature of the space-time through which it is travelling, ie. space-time is locally flat and the gravitational wave may be understood as being composed of scalar fields of amplitude h. The propagating wave produces tidal forces perpendicular to the direction of propagation and so the waves are transverse in nature. Figure 1.1 shows the lines of force for the two polarisation states. Note that unlike electromagnetism in which the two normal polarisation states are at 90^o to each other, here the angle between them is 45^o. Rotating either polarisation state by 90^o would produce the same polarisation but 1/4 cycle out of phase.

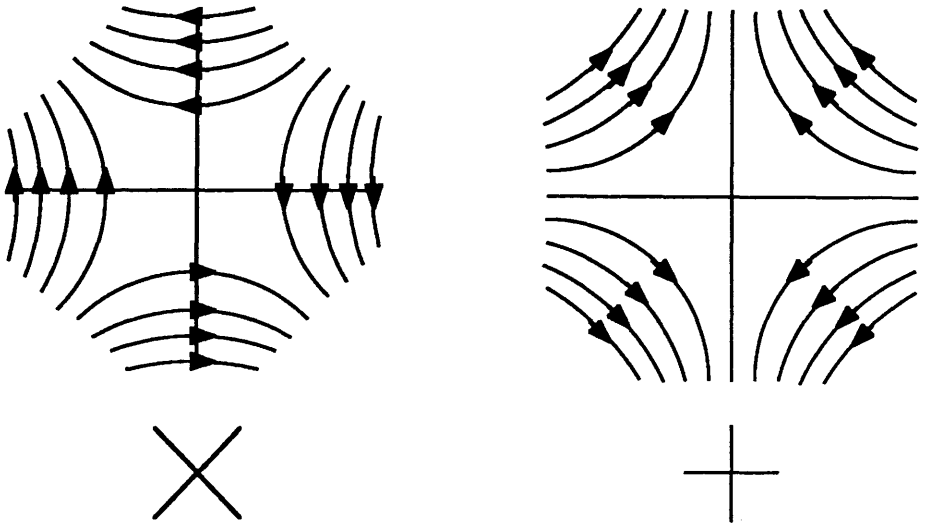

Figure 1.1 Representation of the lines of force - relative to a fiducial point at the origin of the axes - of the two polarisation states of a gravitational wave propagating in a direction perpendicular to the plane of the axes.

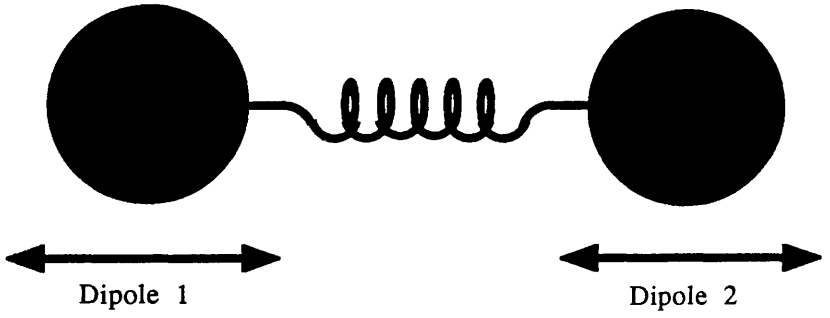

Figure 1.2 A simple generator of gravitational radiation. To first order the conservation of momentum prohibits the production of gravitational radiation. However since the field associated with each oscillating mass takes a finite time to propagate across the system there is a time-varying quadrupole moment.

1:2.1 THE GENERATION OF GRAVITATIONAL RADIATION

By analogy with electromagnetism the oscillating system of figure 1.2 might, at first sight, appear to be a good source of gravitational radiation. However, since mass only has one sign, conservation of momentum means that the centre of mass does not oscillate. There is no time-varying dipole moment. Geometrically this may be understood in terms of the difference between electromagnetism and gravitation. The electromagnetic field is a vector field and so radiation is produced by a vector dipole. However, the gravitational field is a tensor field and a tensor source is required. The simplest tensor is a conjunction of two vectors, ie. two opposed vector dipoles (a quadrupole). In the arrangement of figure 1.2 the changing field due to each oscillating mass takes a finite time to propagate across the system and so the two masses may be treated as two opposed vector dipoles and the system will be a weak source of gravitational radiation.

1:2.2 THE EFFECTS OF GRAVITATIONAL RADIATION

Consider a gravitational wave propagating perpendicular to the plane of a flexible ring. Figure 1.3 maps the cyclic distortion of the ring as the wave passes for both polarisation states. The sequence shown is for one cycle of the wave.

As in the dipole electromagnetic case any quadrupole gravitational wave configuration can be constructed from the superposition of the two polarisation states. If a phase delay of 1/4 cycle is introduced between the two polarisation states, of equal amplitude, then circular polarisaton is achieved. Figure 1.4 shows a schematic of the circularly polarised wave and its effect on

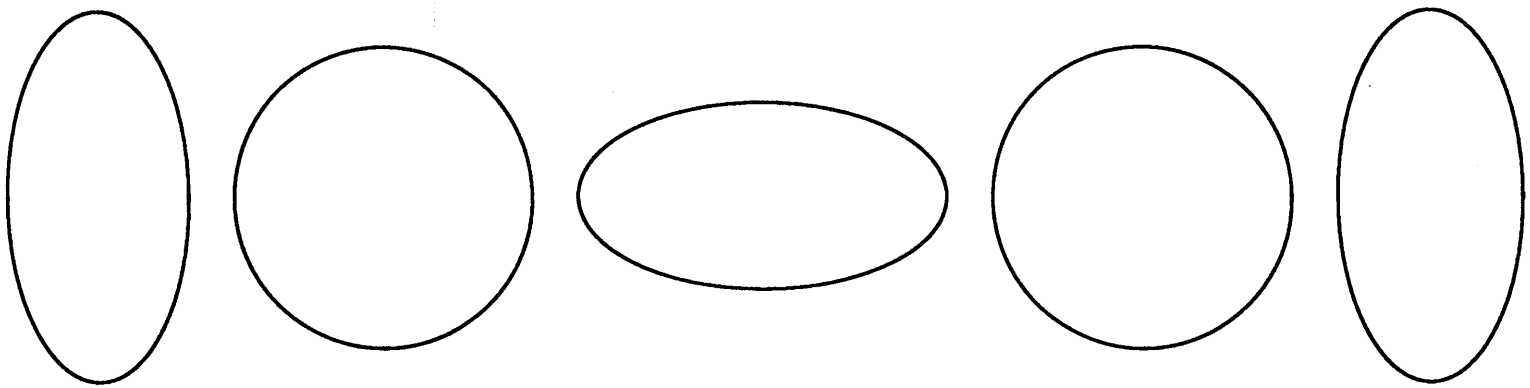

Figure 1.3a The cyclic distortion of a flexible ring when a + polarised gravitational wave propagates normal to the plane of the ring.*

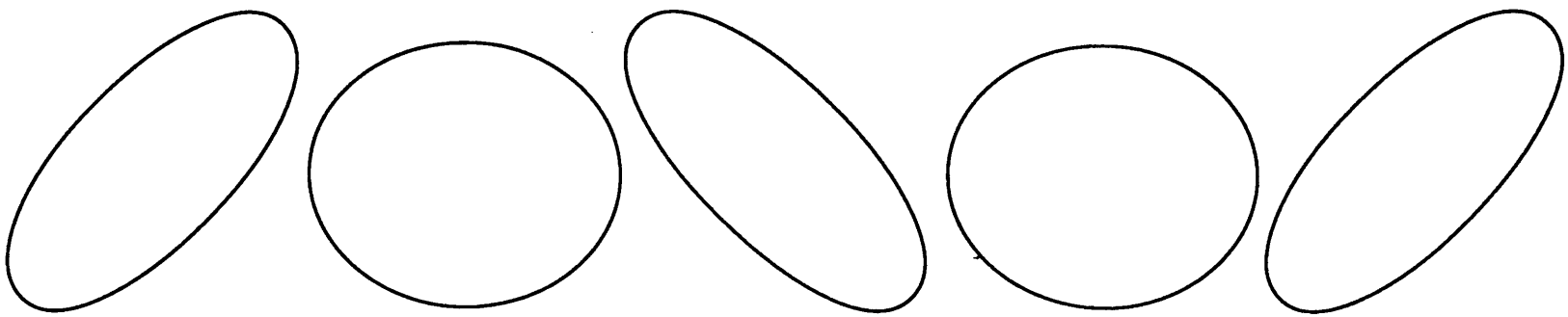

Figure 1.3b The cyclic distortion of a flexible ring when a x polarised gravitational wave propagates normal to the plane of the ring.*

* For one cycle of the wave.

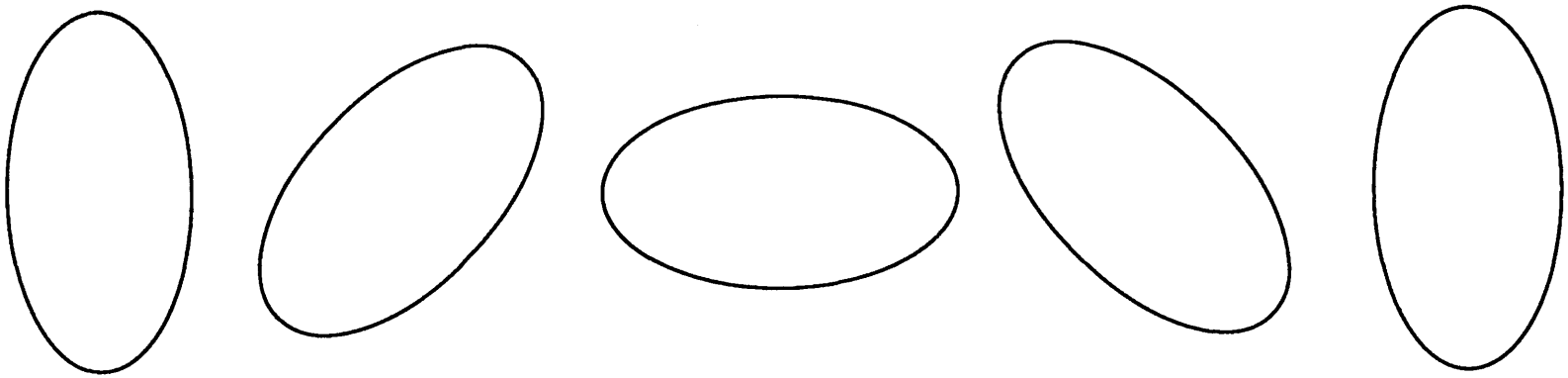

Figure 1.4A The cyclic distortion of a flexible ring when a circularly - polarised gravitational wave propagates normal to the plane of the ring. Note that the distortion only rotates through 180 degrees during one full cycle of the gravitational wave.

Figure 1.4B A schematic representation of a circularly polarised gravitational wave.

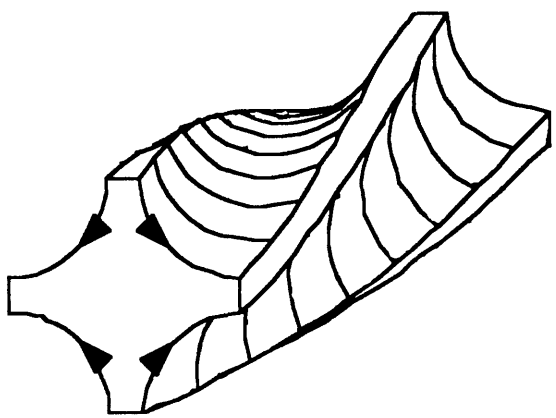

will be:

$$h_+ \sim h_x \sim h_{jk} << \frac{GM_\odot}{c^2 r} = 5*10^{-18} \qquad (1.10)$$

Summarising the above, General Relativity predicts, when large masses are accelerated to relativistic velocities in some asymmetrical manner that gravitational radiation is produced. This radiation propagates throughout space-time and is manifested in space as time-varying tidal forces whose amplitude decays as the inverse of the distance from the source and the flux decays as the inverse of the square of the distance from the source.

1:3.1 SOURCES OF GRAVITATIONAL WAVES

The first calculations of the properties of gravitational waves were performed by Einstein in 1916 involving an idealised source in a flat, empty space-time. Since then theorists have been engaged in calculating the properties of gravitational radiation from more realistic sources and describing the propagation of these waves through a curved space-time. The variety of possible sources has proliferated though the existence of some is uncertain. The possible spectrum of waves has expanded, taking in waves with frequencies of 10^{-7} - 10^{-4} Hz (wavelengths of 1 parsec - 20 A.U.) up to frequencies of 10^{8} - 10^{11} Hz (wavelengths of 3m - 3 mm).

The calculation of gravitational wave generation is simplified in most cases by the 'slow-motion' assumption which requires that the gravitational radius (GM/c^2) of the source is less than the reduced wavelength ($\lambda/2\pi$) of the waves produced. In this case, as in the 'poor antenna' in electromagnetism the lowest allowed multi-pole dominates the radiation pattern which is, in general, a series sum of

the allowed multi-poles. This means that most gravitational radiation sources will radiate most of their energy as a quadrupole wave. The luminosity of a source is determined by the third time derivative of the reduced quadrupole moment, I_{jk}.

The reduced quadrupole moment is given by:

$$I_{jk} = \int \rho \left(x_j x_k - \frac{1}{3} \delta_{jk} r^2 \right) d^3x \tag{1.11}$$

More simply the reduced quadrupole moment may be approximated by:

$$\dddot{I}_{jk} = \frac{\left[\begin{array}{c}\text{Mass of system which} \\ \text{moves non-spherically}\end{array}\right] * \left[\begin{array}{c}\text{size of} \\ \text{system}\end{array}\right]^2}{\left[\begin{array}{c}\text{time for masses to move from} \\ \text{one side of system to the other}\end{array}\right]^3}$$

$$= \frac{MR^2}{T^3} = \frac{\left[\begin{array}{c}\text{Non-spherical component} \\ \text{of kinetic energy}\end{array}\right]}{T} \tag{1.12}$$

The gravitational radiation luminosity is given by:

$$L_{GW} = \frac{1}{5} \langle \dddot{I}_{jk} \dddot{I}_{jk} \rangle \tag{1.13}$$

So from the above the reduced quadrupole moment can be equated to the internal power flow of the system which leads to:

$$\frac{L_{GW}}{L_{internal}} = \frac{L_{internal}}{L_o} \tag{1.14}$$

which may be rewritten:

$$L_{GW} \sim \left[\frac{r_g}{l} \right]^2 \left[\frac{v}{c} \right]^6 \left[\frac{c^5}{G} \right] \tag{1.15}$$

Where $r_g = 2GM/c^2$ = gravitational radius, l = size of the system and v = the velocity of the system. Clearly for a high luminosity source $l \sim r_g$ and $v \sim c$. Although the 'slow motion'

condition appears limiting, calculations show that it may be valid as an approximation for sources whose size ~ the reduced wavelength.

The range of possible sources breaks up easily into two broad categories: man-made and natural. In general waves are characterised by their amplitude, h, at the detector, and their characteristic frequency. Although several methods have been proposed for the terrestrial production of gravitational radiation[7-11] at present it is not technologically possible to produce significant levels.

Astrophysical sources fall naturally into three divisions:

a) Burst Sources; which last for only a few cycles. These may be characterised by their bandwidth, δf_g ($f_g \sim 1/\tau$, where τ is the duration of the burst).

b) Periodic sources; in which the characteristics of the waves are essentially constant for the duration of an observing run. Coalescing compact-object binaries share characteristics of (a) and (b) since they produce periodic radiation for most of their life-time and as coalescence approaches the gravitational radiation sweeps up in amplitude and frequency.

c) Stochastic; this may be a remnant of violent activity in the early universe and possibly produced by pre-galactic stars (Population III).

Figure 1.5 shows a summary of the predicted amplitudes of various sources at earth for an event rate of ~ 1/month. The topmost dotted line represents an upper limit to the amplitude of any waves reaching the earth without violating certain fundamental beliefs about the nature of the Universe, eg. conservation of energy, momentum.

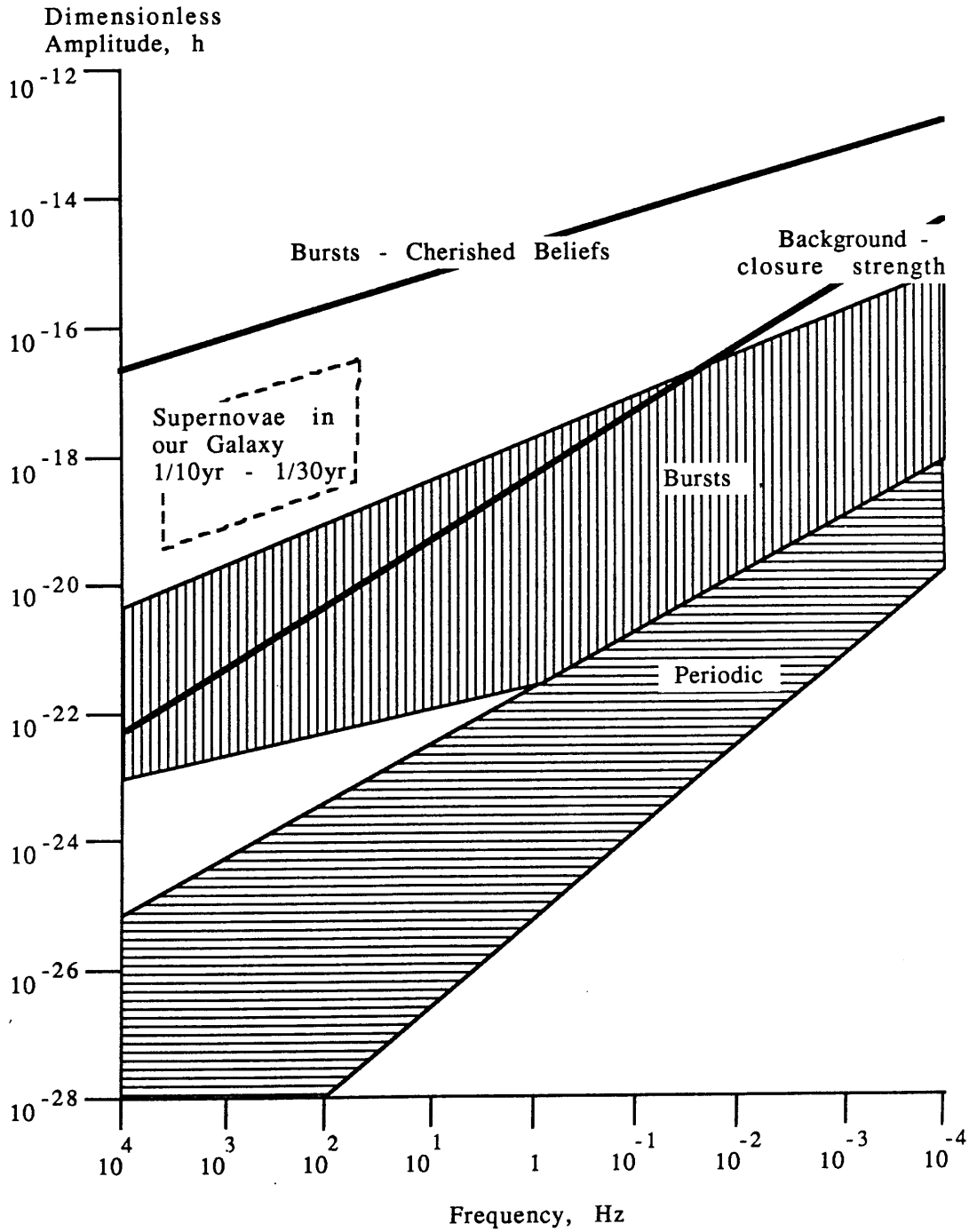

Figure 1.5 A graphical representation of the likely amplitudes, at the Earth, of some of the expected sources of gravitational radiation. (Reproduced from [5]).

1:3.2 BURST SOURCES

a) Supernovae.

These events were, until recently, considered to be the most promising sources for detection. However, calculations of the amplitude at the earth of gravitational waves from these sources vary considerably due to ignorance of the pre-supernova state. Supernovae are classed as type I or II depending on the composition of the progenitor star. Type I supernovae result from old, metal-deficient stars in which the supernova is believed to be caused by mass accretion onto a white dwarf from a companion. This may lead to nuclear detonation of the star[12-14] or the collapse of the core to form a neutron star.

Type II supernovae result from younger, massive stars which collapse to form neutron stars or black holes when their fuel is exhausted. Type II supernovae in isolation are unlikely to be good emitters of gravitational radiation since they are likely to be highly spherical.

The efficiency of production of gravitational radiation is strongly dependent on the degree of non-sphericity of the collapse. The speed of the collapse is also an important parameter. In recent years there has been a move from 'cold' collapses (nearly free-fall) to hot, slow models where the collapse is slowed by thermal pressure[15,16]

The characteristic frequency of the burst will be related to the gravitational size of the source[17]. Therefore, the characteristic frequency of the gravitational radiation from these sources is given by $f \sim 1/\tau \sim c^3/4GM$, and this gives $f \sim 10^2 - 10^5$ Hz. The duration of the burst of gravitational radiation

can be approximated by the propagation time of the radiation across the region of strong gravity, ie. twice the gravitational radius.

The lack of knowledge of the pre-collapse state means that the waves produced by these events are not well understood. In the initial collapse there will be a short-lived burst of waves followed by a 'ringing' as the core bounces or recoils from the shock of collapse. If the initial angular momentum is sufficiently high the collapsed core may form a rotating bar[18] which will produce a monochromatic signal at f ~ 1kHz. Alternatively, the core may break up and the lumps re-coalesce giving out gravitational radiation as they orbit and with each collision.

The amplitude can be described as a function of distance from the source, fraction of kinetic mass converted to gravitational radiation and the frequency and bandwidth[19]:

$$h = 5*10^{-22}\left[\frac{\Delta E/M_\odot c^2}{10^{-3}}\right]^{1/2}\left[\frac{15Mpc}{r}\right]\left[\frac{1kHz}{f}\right]\left[\frac{1ms}{\tau}\right]^{1/2} \qquad (1.16)$$

For a core of $1M_0$ the energy released as gravitational radiation can be constrained:

$$10^{-5}\ M_0c^2 < \Delta E < 0.2\ M_\odot c^2 \qquad (1.17)$$

The upper limit comes from relativistic calculations and the lower limit is obtained from the assumption that the high spatial velocities of pulsars is derived from asymmetries in the collapse processes[20]. This gives the likely amplitudes of waves (with f ~ $1/\tau$ = 1kHz) from supernovae in the Virgo cluster (~15Mpc) to be:

$$10^{-25} < h < 10^{-21} \qquad (1.18)$$

Detectors which were sensitive to this range of values could expect to see two to three supernovae/year. However, the neutron

star birthrate is believed to be three or four times greater than this which gives rise to speculation that there may be a class of optically silent supernovae[19]. Interestingly, several computer simulations of supernovae processes have produced an invisible collapse[3,21].

b) Coalescing compact-object binaries.

These events are now believed to be the most likely to be the first type of signals to be seen by a gravitational wave detector. Although the predicted event rates vary markedly the waveforms expected from such coalescences are well defined. Initially as the stars spiral in the process is well described by Newtonian physics and the slow-motion assumption. In the last seconds before coalescence the waveform will sweep up in frequency and amplitude giving a characteristic 'chirp'. The maximum frequency of the chirp is[22]:

$$f_{max} \sim 1\text{kHz} \text{ for neutron stars}$$

and $f_{max} \sim \frac{10\text{kHz}}{M_1/M_\odot}$ for black holes where M_1 is the mass of the larger hole. As the frequency of the gravitational wave reaches this maximum the calculation of the waveform requires higher order corrections until a full General Relativistic treatment is required. The detection and comparison of this waveform with that predicted by numerical calculations would provide the strongest test of General Relativity yet.

The amplitude of gravitational waves produced by a binary system is characterised by the total mass, M, the reduced mass, μ ($= M_1M_2/M$), and the distance, r. The frequency of the gravitational

radiation will be twice the orbital frequency. The amplitude of the gravitational waves at Earth is given by[19]:

$$h \sim 10^{-23}\left[\frac{100\text{Mpc}}{r}\right]\left[\frac{M}{M_\odot}\right]^{2/3}\left[\frac{\mu}{M_\odot}\right]\left[\frac{f}{100\text{Hz}}\right]^{2/3} \qquad (1.19)$$

Long before the objects are close enough to coalesce the orbits will have been circularised by gravitational back-reaction[23].

It is possible to define a parameter, τ, which will be the length of time the signal takes to double its frequency, f. This time is dependent only on the total mass of the system, the reduced mass and the frequency, f. Now the gravitational radiation output of the system is also dependent only on these parameters and it turns out that the product $h\tau$ is dependent only on distance. In the case of neutron star binary coalescences, which may have optical counterparts[24,25], the comparison of the calculated distance with the observed redshift in the electromagnetic spectrum should provide a new, and more accurate, determination of Hubble's constant.

To estimate the possible number of such sources, pulsar statistics may be used. There are ~400 known pulsars of which seven are in binary systems. One of these systems has a short period and is known as a 'binary coalescence precursor'. The birthrate of such short period systems has been calculated[26] to be ~14/year out to a distance of 200Mpc. Therefore there are expected to be a few events/year if detectors can be made sensitive enough to detect events out to ~ 100 Mpc. It is difficult to make firm predictions of the event rates from the electromagnetic data; for instance the gravitationally brightest event, two black holes coalescing, will probably be invisible. There are likely to be galactic clusters of neutron stars and black holes[27,28] and there is

observational evidence for super-massive black hole binaries[29]. Other possible sources of these events include a 'dark matter' candidate, population III black hole binary systems.

In summary, the detection of these events, by at least three detectors, would: provide a new test of General Relativity, indicate the direction of the source, inclination of the orbit (from the amplitudes of the polarisation modes), the direction of motion of the stars, the factor $(\mu^3 M^2)^{1/5}$ and the source observer distance.

c) Matter falling into black holes.

There are two possible scenarios for the infall of matter into a black hole. The first is the radial fall of matter into a non-rotating hole which is relatively inefficient in terms of gravitational wave production. The second, and more realistic, is the spiral infall of matter or the radial fall of matter into a rotating black hole.

In the case of a non-rotating hole of mass M and radially falling matter of mass m the energy released as gravitational radiation is given by:

$$\text{Energy} = 0.01 \left[\frac{m}{M} \right] mc^2$$

$$= 10^{44} * \left[\frac{m}{M_0}\right]^2 \left[\frac{M}{10^8 M_\odot}\right]^{-1} \text{ergs} \qquad (1.20)$$

For non-radial fall onto a non-rotating hole or radial fall onto a rotating hole the numerical constant may rise from 0.01 to as high as 0.05[3]. The time for the burst is determined by the gravitational radius of the hole and is given by:

$$\tau \sim 10\frac{GM}{c^2} \sim 10^4\left[\frac{M}{10^8 M_0}\right]^{-1} \text{ seconds.} \qquad (1.21)$$

As in the case of supernovae; bandwidth ~ frequency ~ $1/\tau$.

For super-massive black holes ($M \sim 10^9 M_0$) stars may plunge through the event horizon without suffering significant tidal distortion. Stars plunging into smaller holes ($M < 10^6 M_0$) will suffer tidal disruption which will reduce the levels of gravitational waves emitted[30].

For typical (non head-on) parameters the infall of a mass, M_2, into a hole, mass M_1, yields a characteristic frequency given by[31,32]:

$$f \sim 10^{-4}\left[\frac{10^8 M_\odot}{M_1}\right] \text{ Hz} \qquad (1.22)$$

and the amplitude is:

$$h \sim 2 * 10^{-21}\left[\frac{M_2}{M_0}\right]\left[\frac{10\text{Mpc}}{r_0}\right] \qquad (1.23)$$

Where r_0 is a characteristic radius which should give several events per year.

It is interesting to note that in the event of a 'near miss' of a star and a black hole the star emits gravitational brehmsstrahlung radiation similar to that produced by matter plunging into the hole. There is already observational evidence for the existence of a black hole of mass ~ $4 * 10^9$ M_0 at the centre of the galaxy M87[24].

Unfortunately due to the high levels of seismic noise at the low frequencies of these events it is highly unlikely that any terrestrial system will ever detect them. However, there are plans for space-borne detectors which will be discussed later.

1:3.3 PERIODIC SOURCES

a) Pulsars.

The efficiency of production of gravitational radiation by these sources depends on an asymmetry in the rotating neutron star. In general some asymmetry must be present due to the non-alignment of the pulsar's magnetic field with the rotational axis. However, this asymmetry is dependent on the nature of the neutron star crust which is still undetermined. Consequently estimates of the levels of radiation from such sources vary greatly.

Now, if the deformation of the neutron star is δ (= $1 - r_1/r_2$). Here r_1 and r_2 are the semi-major and minor axes respectively then the amplitude of the gravitational waves produced is[33]:

$$h = 10^{-21}\ \delta \left[\frac{f}{100\text{Hz}}\right]^2 \left[\frac{10\text{kpc}}{r}\right] \tag{1.24}$$

Where the frequency of the radiation is twice the rotational frequency of the pulsar. For comparison the amplitude of the gravitational waves from the Crab and Vela pulsars are:

$$h_{\text{Crab}} \sim 10^{-26} \left[\frac{\delta}{10^{-5}}\right] \text{ at } f=60 \text{ Hz} \tag{1.25a}$$

$$h_{\text{Vela}} \sim 10^{-27} \left[\frac{\delta}{10^{-5}}\right] \text{ at } f=22 \text{ Hz} \tag{1.25b}$$

In the cases of these two pulsars it is possible to set an upper limit to the deformation, $\delta < 10^{-3}$, by assuming that all of the rotational energy lost by the pulsar - calculated from the change of period with time - is radiated as gravitational waves.

Old neutron stars which have been spun-up through the action of accretion are likely to be poor emitters of gravitational radiation since the accretion of matter is likely to have left the star in a highly axisymmetric condition through the action of annealing processes[34].

However there is a possibility that whilst accretion is progressing the star will become unstable to a hydrodynamic oscillation of the surface[35,36]. In this scenario the crust of the neutron star supports a travelling wave. This gives the appearance of a non-spherical star rotating with a velocity equal to the sum of the wave velocity and the star's rotational velocity. In this case the star may be a good emitter of gravitational radiation. The effect of this instability should also be seen as an intensity modulation of the X-ray output from the star but no search of sufficient sensitivity has yet been carried out.

In this scenario of a rotating hydrodynamic instability the energy emitted is proportional to the mass accretion and so the gravitational wave amplitude can be calculated from the X-ray flux, F_x[37]:

$$h \sim 2 * 10^{-27}\left[\frac{300Hz}{f}\right]\left[\frac{F_x}{10^{-8}erg/cm^2sec}\right] \qquad (1.26)$$

Where $f = 1 * v_p/(2\pi R)$, 1 is the spherical harmonic of the hydrodynamic wave (1 = 3,4,5,....) and v_p is the pattern speed of the wave in the observer's reference frame. If the deformation of the crust is supported by the rigidity of the crust or arises from the magnetic field then the emission will be largely quadrupolar, 1=2.

In all these cases the slow-motion formalism is adequate for the calculation of the resultant gravitational waves.

b) Binary systems.

These are the best understood of all probable sources of gravitational radiation. From the mass of the components, the orbit and the distance of the system it is possible to calculate the precise nature of the waves which would bathe the Earth. This is because the weak internal fields of these systems allow high accuracy in calculations.

The radiation is most strongly emitted at periastron, which will tend to make the orbits circular and reduce the levels of gravitational waves emitted[22].

Only a few binary systems have been discovered with P<1Hr[38]. Therefore, in general, the frequency of the waves bathing the Earth will be, $f<10^{-3}$Hz. Due to the effects of seismic noise at these frequencies on terrestrial detectors it is unlikely that such sources will be detected on Earth, though space-borne detectors are in the planning stages.

The gravitational waves emitted by these systems will have $f_{GW} = 2 * f_{orbit}$ + harmonics, but if the ellipticity of the orbit, $\varepsilon<0.2$, then the lowest frequency is dominant. In this case the amplitude of the gravitational waves is given by[22]:

$$h \sim 8.7*10^{-21}\left[\frac{\mu}{M_\odot}\right]\left[\frac{M}{M_\odot}\right]^{2/3}\left[\frac{100pc}{r}\right]\left[\frac{f}{10^{-3}Hz}\right]^{2/3} \qquad (1.27)$$

The highest frequency to be expected is 0.06Hz from a white dwarf binary since the onset of mass transfer occurs at higher frequencies, which would complicate the waveform. There may also be mass loss to infinity as a result of these interactions. For a neutron star binary system the highest frequency is 0.007Hz since frequencies higher than this would result in an excessively high rate

of coalescence.

1:3.4 STOCHASTIC SOURCES

Signals from such sources would appear as a random background and might be attributed to density fluctuations in the early universe, cosmic strings or population III supernovae[39] for instance. However any 'thermal' gravitational waves from the big bang, analagous to the 3K microwave background, will be too small to be detected[40]. It is possible that chaos in the early universe gave rise to large amplitude gravitational wave modes but in this epoch they will have been red-shifted to indetectability[41].

By convention the possible energy density in gravitational radiation is referred to as a fraction of the energy density required for closure of the universe, in a bandwidth, $\delta f \sim f$, about a frequency, f. The mean amplitude, dependent on the fraction of the closure density at a frequency, f, will then be[19]:

$$\langle h \rangle = f^{1/2} h_f \sim 6*10^{-26} \left[\frac{\Omega_{GW}}{10^{-10}}\right]^{1/2} \left[\frac{100Hz}{f}\right] \qquad (1.28)$$

Where h_f is the root spectral density. Observations have already placed a typical limit of $\Omega_{GW} < 10^{-4}$, for periods ~ 10^7 seconds[42]. Current string theories of galaxy formation require $\Omega_{GW} \sim 10^{-7}$[43].

In summary, many possible sources have been conceived of which only the most likely have been introduced here. When the next generation of gravitational antennae become operational there may well be sources which were never predicted, as has been the case in other areas of astronomy. The doubt which surrounds the amplitudes and

waveforms which a particular source may produce or the rate at which events are expected is due to the lack of detailed information for modelling purposes, and in some cases the non-detection of the predicted radiation would be as interesting and informative as detection.

1:4 DETECTORS OF GRAVITATIONAL RADIATION

1:4.1 INTRODUCTION

The spectrum of radiation from the possible astrophysical sources of gravitational radiation spans a range of frequencies from 10^{-4}Hz for large black hole interactions up to several kilo-Hertz for stellar collapses. It is clearly unrealistic to expect any one detector system to be capable of functioning across such a range. Earth-based detectors, for instance, are likely to be limited to signals above a few tens of Hertz due to seismic noise. Lower frequencies down to a few milli-Hertz may be detected by the Doppler tracking of spacecraft or fully space-borne systems. Frequencies below this may be investigated through their effect on pulsar rotation[42,44].

1:4.2 HISTORICAL DEVELOPMENT

In 1960[45] Professor Joseph Weber of the University of Maryland started work on the first gravitational wave detector. He used a large, resonant aluminium bar with piezo-electric crystals bonded around the girth to detect any disturbances. After almost a decade of development work Weber announced that he was detecting events which he believed were due to gravitational radiation[46].

Weber compared the output of two detectors separated by 1000Km and found coincident pulses above the level expected from purely random fluctuations at the rate of about one per day. By studying how the event rate varied with time Weber deduced that these pulses were arriving from the centre of the galaxy.

The exciting results of Weber's work stimulated several groups around the world, including one at Glasgow University, to build their own detectors. In the main these new detectors were essentially the same as Weber's original bars although in Moscow capacitive sensing was used and in Glasgow split mass detectors were used with the piezo-electric crystals sandwiched between the two masses. However, despite the fact that some of the new bars were more sensitive than the originals no other group reported the detection of any signals apart from one possible event at Glasgow[47].

The predictions of the levels of gravitational radiation expected at the Earth were very uncertain at the time but even so the levels which Weber's detector seemed to be sensing were unexpectedly high. His observations suggested an enormous loss of mass from the galaxy in the form of gravitational radiation which was incompatible with any theories of galactic evolution[3]. Further calculations on likely source strengths suggest that Weber's events were almost certainly not due to gravitational waves.

The lack of positive results and the expected levels of gravitational radiation discouraged several groups who then left the field. However several groups continued their efforts to develop detectors which would have sufficient sensitivity to detect the predicted levels of gravitational radiation.

1:4.3 BAR DETECTORS

It was this type of detector which Weber developed in the 1960's. The differing tidal forces acting between particles in the bar as a gravitational wave passes set up stresses within the bar. If a gravitational wave passes through the bar in a direction with a component perpendicular to the axis of the bar then the resulting stresses excite the normal longitudinal mode of the bar.

The detector is analogous to the generator of Figure 1.2. The two halves of the bar act as two masses connected by a spring, the spring constant of the aluminium. Normally, forces other than those associated with the passage of a gravitational wave will be responsible for any disturbances of the bar, eg. thermal fluctuations or seismic effects. Weber reduced the effects of these sources of noise by suspending his bar by a single wire in a vacuum. He detected small movements by bonding piezo-electric crystals round the girth of the bar. Information about the gravitational wave is contained in the amplitude and phase of the signal from the piezoelectric sensors.

The resonant nature of the bar system has the advantage of increasing the sensitivity of the bar to continuous radiation at the resonant frequency and of extending the duration of the signal from a burst of radiation. In the latter case the bar 'rings' and the signal decays with a time related to the quality factor, Q, of the bar. The disadvantage of the bar is that it is relatively insensitive to continuous radiation at other frequencies and the reduced bandwidth of the pulse detection means that information on the phase and duration of the pulse is limited.

The limit to sensitivity of the early bars was the motion due to the temperature of the bar. The bar can be treated as a simple oscillator. The energy contained in the fundamental mode of

the bar is then:

$$E \sim M\omega_o^2 \delta x^2 \sim kT \tag{1.29}$$

Where k is Boltzmann's constant, T is the temperature of the bar, ω_o is the bar's resonant frequency, M is the mass of the bar and δx is the displacement of the end of the bar. It would seem, at first sight, that this is the smallest energy which must be deposited for a signal to be detectable. However in the case when the measuring time, τ_{meas}, is less than the storage, or 'ringing', time of the bar the smallest detectable energy change is:

$$\delta E \sim kT(\tau_{meas}/\tau) \tag{1.30}$$

Combining equations 1.29 and 1.30 gives the minimum detectable displacement:

$$\delta x \sim \left[\frac{kT\tau_{meas}}{M\omega^2} \right]^{1/2} \tag{1.31}$$

But the storage time, τ, of the bar is related to the quality factor, Q:

$$\tau = \frac{Q}{\omega_o} \tag{1.32a}$$

and,

$$\omega_o L = \pi v_s \tag{1.32b}$$

Where L is the length of the bar and v_s is the velocity of sound in the bar material. Now from equation 1.6 the amplitude of the signal is related to a strain, $\delta l/l$. Therefore, the minimum detectable strain in a thermally limited bar is given by:

$$\frac{\delta x}{L} = \left[\frac{\tau_{meas}}{M\omega_0 L^2 Q}\right]^{1/2} \qquad (1.33)$$

The amplitude sensitivity of a bar can be written:

$$h \sim 2*10^{-19}\left[\frac{T}{300K}\right]^{1/2}\left[\frac{\tau}{10^{-3}s}\right]^{1/2}\left[\frac{1m}{L}\right]\left[\frac{10^3 kg}{M}\right]^{1/2}\left[\frac{1kHz}{\omega/2\pi}\right]^{1/2}\left[\frac{10^7}{Q}\right]^{1/2} \qquad (1.34)$$

Clearly, to improve the sensitivity of the bar there are four alternatives:

a) Lowering the temperature of the bar to a few Kelvin or fractions of a Kelvin.

b) Increasing the length of the bar.

c) Increasing the mass of the bar.

d) Increasing the Q of the bar.

In principle it is possible to increase the sensitivity by reducing τ_{meas} but this is constrained by other factors which will be discussed later. With regard to the above, all of the 'second generation' bars are cooled to around 4K. Increasing the length of the bar reduces the resonant frequency of the bar but since the operational frequency range of terrestrial detectors is in the range of a few hundreds of Hertz to a few kiloHertz this is undesirable.

In practice it has proved difficult to produce large, ~10^3kg, masses with very high Q. In this respect groups have diverged. For instance in Moscow the group have chosen to work with low masses, ~30kg, and high Q, ~10^9, materials (initially sapphire and later silicon). In Stanford and elsewhere the move has been towards higher masses, ~5000kg, and medium Q, ~ 10^6 - 10^7.

However, even when the thermal noise problem has been overcome there still remains the problem of noise in the amplifier system.

This noise has two manifestations. Firstly, the actual noise of the detection and amplifying system, the 'series' noise, which increases as the measuring time decreases (ie. measurement bandwidth increases). The second problem is due to 'back-action', the effect the measurement has on the bar. This is called the 'parallel' noise and increases as the measurement time is increased (ie. measurement bandwidth decreases). Clearly for efficient operation of the bar the measurement time will be constrained by a combination of the parallel noise and thermal noise at one extreme and by the series noise at the other.

These noise sources can be reduced in importance by various techniques, However there is a more fundamental problem due to the Heisenberg Uncertainty Principle. In the limit the bar's quantum nature must be taken into account. The smallest displacement which may be detected is given by[48]:

$$\delta x = \left[\frac{2\hbar}{M\omega} \right]^{1/2} \tag{1.35}$$

Obviously for a bar detection system limited by the Uncertainty Principle a large mass will be an advantage. Surprisingly, it appears that it may be possible to circumvent this limit to some extent through what have become known as Quantum Non-Demolition techniques[49,50]. In the case of a bar for instance, the measuring system would be designed to measure one phase of the bar's complex amplitude, composed of the relative position and momentum of the bar's ends, and so the error from the measurement would enter the orthogonal phase. Work is also proceeding on systems which reduce the back-action.

1:4.4 LASER INTERFEROMETRY

An alternative method of detection is to use nearly free test masses and sense the displacement caused by a gravitational wave using optical interferometry. The technique was first implemented by R. Forward in 1971[51,52]. The interferometric detector has the advantage that the masses may be separated by any distance up to the limit that the light transit time is equal to one half of the gravitational wave period.

Two implementations of the technique are currently showing most promise, see Figures 1.6, 1.7. In both cases the beam path is folded to reduce the actual separation of the masses required. In one type of detector the path of the beam on each pass follows a different course to form an optical delay line. In the second version the beams are collapsed to give a single spot on each mirror and an optical cavity is formed between the test masses. Both of these techniques use two orthogonal arm lengths to allow a search for a differential signal. The light from each arm may be interfered coherently and in the event of some relative change in the arm lengths the output light will be intensity modulated.

In these systems the masses are isolated from seismic disturbances by suspending them as pendulums. The pendulum suspension points are isolated from seismic noise by lead and rubber stacks. When the frequency of the gravity wave is much greater than the pendulum frequency then the masses are essentially free. The Fabry-Perot technique has been developed at Glasgow[53] and subsequently at the California Institute of Technology[54] and will be discussed in more detail in the next chapter. The delay line technique has been developed at the Max Planck Institute, Germany[55] and at the Massachusetts Institute of Technology[56].

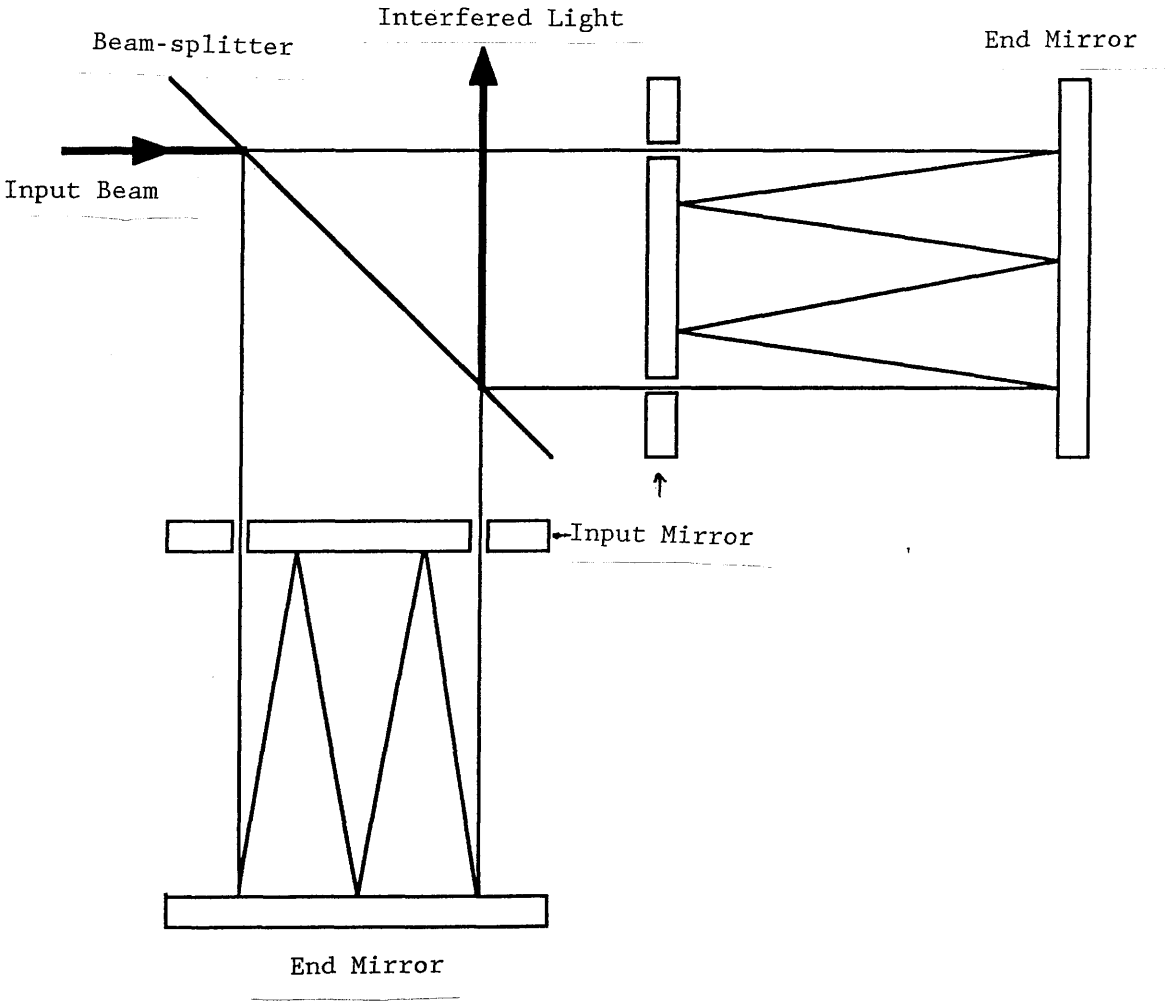

Figure 1.6 Schematic of the delay line type of interferometer. The light traverses each arm of the interferometer (n+1) times and the output light recombines to give fringes.

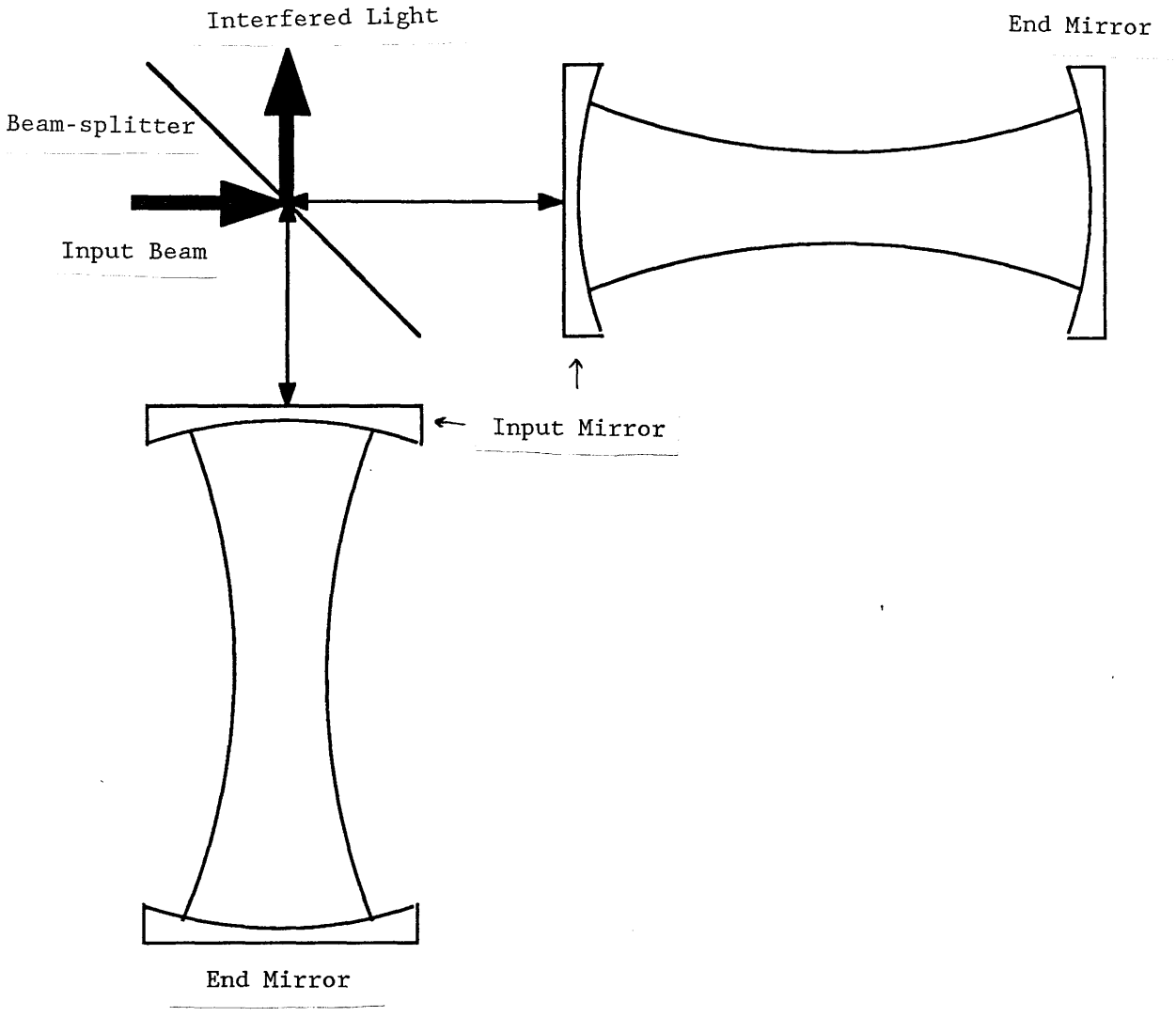

Figure 1.7 Highly schematic representation of a Fabry - Perot interferometer. Light is split into each of the orthogonal optical cavities by a beam splitter which also acts to recombine the light leaving the two resonant optical cavities. The effective optical length of each cavity is determined by the reflectivities of its two mirrors. This has the advantage over Michelson systems of using smaller mirrors and therefore requiring smaller vacuum tubes.

Consider the schematic diagram in Figure 1.6. Let n be the total number of reflections of the beam in the delay line. Now, assuming that the mirrors are lossless the intensity of the recombined light will be:

$$I = \frac{I_o}{2} (1 - \cos \phi) \qquad (1.36)$$

where the difference in phase of the two beams is defined to be $\pi-\phi$, ie. the interferometer is adjusted to a dark fringe, and I_o is the total intensity of light entering the interferometer. In practice the mirrors will not be lossless but will have a reflectivity, R~1. Therefore the number of photons detected at the output of the cavities is given by:

$$N = \frac{I_o R^n \tau}{2hf} (1 - \cos \phi) \qquad (1.37)$$

Where h is Planck's constant, f is the frequency of the input light and τ is the counting time. Differentiating the above with respect to ϕ relates the change in the output photons to a change in the phase of the recombining beams, ie:

$$\delta N = \frac{I_o R^n \tau}{2hf} \sin \phi \, \delta\phi \qquad (1.38)$$

Now consider the light in the cavity. The total optical path length is (n+1)*L, where L is the cavity length. Therefore the change in phase of the recombining beams, $\delta\phi$, is equivalent to a change in cavity length:

$$\delta\phi = \frac{2\pi(n+1)\delta l}{\lambda} \qquad (1.39)$$

Combining 1.38 and 1.39 relates the detected photons to a

relative change in the length of the cavities:

$$\delta N = \frac{I_o R^n \tau \pi}{hc}(n+1)\sin \emptyset \; \delta l \qquad (1.40)$$

Now in the absence of external perturbations, eg. cavity vibration, the photons in laser light obey Poisson statistics. This is usually true at spectral frequencies of a few MegaHertz and measurements are made in this region through the use of modulation techniques. These modulation systems give the best results when the cavities are operated on a dark fringe, ie $\emptyset = \pi/2$. Hence from 1.37 and 1.40 the smallest detectable displacement is:

$$\delta l > \left[\frac{hc\lambda}{4\pi^2 \varepsilon I_o R^n (n+1)^2 \tau \cos^2 \emptyset/2}\right]^{1/2} \qquad (1.41)$$

Where ε is the photo-diode efficiency, typically 30 - 50%. This expression will be true when $\delta\emptyset << \emptyset$.

Now consider the term $R^n(n+1)^2$. As n increases the total loss of light due to reflections from the mirrors will reduce the sensitivity (expression 1.38). However each additional reflection increases the path length by L and increases the sensitivity up to the limit $(n+1)*L = \lambda_g/2$. To optimise the function use the relation, $R^n = \exp(n \log_e R)$ and differentiate the term above with respect to n and set it to zero. Then using the approximation $\log_e R \sim 1 - R$ gives:

$$(n + 1) = \frac{2}{1 - R} \qquad (1.42)$$

And so equation 1.41 becomes:

$$\delta l > \left[\frac{hc\lambda(1 - R)^2}{16\pi^2 \varepsilon I_o e^{-2\tau}}\right]^{1/2} \tag{1.43}$$

Assuming that $\emptyset \sim 0$ and $1 - R << 1$. Now if $\lambda = 514.5$ nm and $\varepsilon = 0.5$ then:

$$\delta l \sim 10^{-16} \left[\frac{(1 - R)^2}{I_o \tau}\right]^{1/2} \tag{1.44}$$

Usually the significance of a noise source is described in terms of the apparent displacement. By convention it is measured as the square root of the spectral density. Using the relation $\delta f = 1/2\tau$.

$$\delta l \sim 1.4 * 10^{-16} \frac{1 - R}{I_o^{1/2}} \text{ m/Hz}^{1/2} \tag{1.45}$$

The present generation of detectors is approaching this limit with the power currently available. The prototype detector at Garching, Germany, currently has the best sensitivity in the world for this system.

It would seem from equation 1.45 that given sufficient isolation from other noise sources the sensitivity may be increased to any desired level by increasing the intensity of the input laser light. However there is a fundamental limitation to the sensitivity of any measurement, which is given by the Heisenberg Uncertainty Principle. This limit will be treated later since there are other limiting factors which will become important before the Uncertainty Principle becomes dominant.

One of these factors which must be taken into account is the time which the light will spend in traversing the cavity, the 'light storage time'. If the storage time exceeds half of the gravitational

wave period then the signal will gradually be cancelled out by the change in phase of the gravitational radiation. In delay line interferometers the storage time is controlled by changing the number of reflections of the laser light. In Fabry-Perot systems the storage time is controlled by altering the transmissivity of the input mirror in each cavity.

It is likely that the next generation of interferometric gravitational radiation detectors will achieve photon shot noise limited sensitivity in storage time limited operation.

However, it has been suggested that the photon shot noise limit may be reduced to some extent. One proposal[57] - for use in the case where the number of reflections of the beams in the arms is limited by the storage time requirement and the mirrors are very low loss - involves the recirculation of the light leaving the detector which effectively increases the intensity of the input light, this is the 'standard' recycling.

In another form of recycling, resonant recycling, the light in the cavities is effectively transferred from one arm to another on a timescale of half the period of the gravity wave being searched for. The detector in this instance is somewhat analagous to the resonant bar, sacrificing bandwidth for sensitivity.

The technique of 'squeezing the vacuum'[58] - which allows measurements to be made below the level of photon shot noise - is promising but appears to hold some problems in its execution although it has been demonstrated recently[59] to be feasible.

However, as in the case of the bars, the fundamental limit to the sensitivity of the system comes from quantum mechanics. It has been calculated[60] that the smallest detectable differential change in the lengths of two cavities is given by:

$$\delta l^2 = \frac{4\hbar\delta f}{M\omega^2} \qquad (1.46)$$

when the measurement is made at a frequency, ω, far above the resonant frequency of the test mass suspension over a bandwidth, δf.

This corresponds to an amplitude sensitivity,

$$h = \frac{\delta l}{l} = \left[\frac{4\hbar\delta f}{M\omega^2 l^2} \right]^{1/2} \qquad (1.47)$$

The limit to sensitivity, dictated by the quantum limit, can be written:

$$h \sim 10^{-23} \left[\frac{100\text{kg}}{M}\right]^{1/2} \left[\frac{2\pi 10^3}{\omega}\right] \left[\frac{1\text{km}}{l}\right] \qquad (1.48)$$

It should be noted however that the levels at which the quantum limit becomes important for interferometric systems with kilometre baselines is very much lower than in the case of resonant Weber bars.

1:4.5 DOPPLER TRACKING OF SPACECRAFT

At frequencies below a few Hertz the seismic noise and fluctuating gravity gradients of a terrestrial environment prohibit the development of a gravitational radiation detector. At these frequencies space-borne systems become necessary. The effect of low frequency gravitational radiation on the separation between a satellite and the Earth may be measured to high precision. The technique was first suggested in 1967[61] and analysis was made of pre-existing data in 1971[62].

The system requires a stable oscillator ('master clock') on

Earth which transmits to the spacecraft. The spacecraft then amplifies and retransmits the signal. The frequency of the signal received at the Earth is then compared to the master clock. A gravity wave will cause small Doppler shifts in the frequency of the received signal, $\delta f/f \sim h$. Searches have already been carried out with a sensitivity, $h \sim 3 * 10^{-14}$[63], to pulses of gravitational radiation in the frequency range $10^{-2} - 10^{-4}$ Hertz. No signals were detected though the system could be improved. The main limitations were in clock stability and fluctuations in refractive index of the earth - spacecraft medium. In future missions these effects may be reduced by using more than one tracking frequency, or by including a stable clock on the spacecraft. This latter scheme[64] would allow measurements to be made of other paths than the simple Earth - spacecraft - Earth link.

A more complex system with greater sensitivity involves the use of three, or more, satellites. These satellites would employ laser tracking, effectively an interferometer with arm lengths of 10^6 kilometres[65]. However this scheme is many years away at present.

1:4.6 OTHER DETECTORS

Many alternative systems have been proposed[3,22] and only the most promising have been touched upon here. In the event of a confirmed detection of gravitational radiation these alternative systems may be developed and provide new information.

The element of risk in the search for gravitational radiation cannot be ignored. However the uncertainty in predicted amplitudes and event rates is due to the paucity of information available from the electromagnetic spectrum. This is the value of searching for

gravitational radiation. Searches for radiation at the levels described in this chapter will revolutionise our understanding of the universe. Gravitational waves offer the chance to probe General Relativity to its limits, to obtain information on the mechanisms of star development and to examine the earliest eras of the universe.

CHAPTER 2

A FABRY-PEROT INTERFEROMETRIC GRAVITATIONAL WAVE DETECTOR

2:1 INTRODUCTION

Chapter one presented a review of the most likely astrophysical sources of gravitational radiation and the amplitudes expected on Earth. It also described the main detection techniques currently being developed. This chapter opens with a brief description of the current configuration and sensitivity of the prototype detector at Glasgow. It then proceeds with an introduction to the major sources of noise in an interferometric gravitational wave detector and the levels at which they may become important.

After the growth of the gravitational radiation detection effort in the wake of Weber's results the groups remaining in the field had to decide between the construction of more sensitive, 'second generation' bars or the development of new and potentially more versatile techniques. The work of theoreticians suggested that for a reasonable event rate a terrestrial detector would need a sensitivity of $h \sim 10^{-22}$ over a bandwidth of a few hundred Hertz. In Glasgow, work began on a small-scale, separated-mass detector employing optical interferometry to sense small displacements.

After several years of development work a larger, 10 metre baseline system was constructed as a prototype for a gravitational radiation observatory with a baseline of around 1km. After some initial work with three-mirror ring cavities it was decided to operate the system with two-mirror, resonant Fabry-Perot

cavities.

The use of Fabry-Perot cavities has the advantage of requiring smaller mirrors and vacuum pipes. It should be noted that the vacuum system is a major cost item in the proposed large extensions of such detectors. It is also believed that an interferometric detector based on resonant cavities is intrinsically less sensitive to the effects of light scattered within the cavities than the delay line system.

Each mass is suspended from a pendulum whose resonant frequency (~ 1Hz) is very much lower than the frequencies of the gravitational radiation being searched for. In this regime the masses are essentially free to respond to the stresses induced by the passing wave. During the passage of a gravitational wave of suitable orientation the distance between each pair of masses will undergo differential expansion and contraction.

These detectors are essentially broadband in nature, unlike the Weber bars, which means that, in principal, more information is available about the arrival times of pulses and the waveforms of the gravitational radiation.

2:2 THE PROTOTYPE DETECTOR AT GLASGOW

The prototype detector is housed in a vacuum system comprising four tanks, one at each corner of a ten metre square, linked by vacuum pipes. The whole system is supported by a rigid frame which has only four points of contact with the ground through lead and rubber stacks to provide isolation from seismic disturbances.

The masses are suspended in the vacuum tanks at three corners of the square (see Figure 2.1). Each suspension point is further isolated from the tanks by lead and rubber stacks. To maintain the

PBS = POLARISING BEAM SPLITTERS
POL = POLARISER
PD = PHOTODIODE & PREAMP
PC = POCKELS CELL
Q = QUARTER WAVELENGTH PLATE

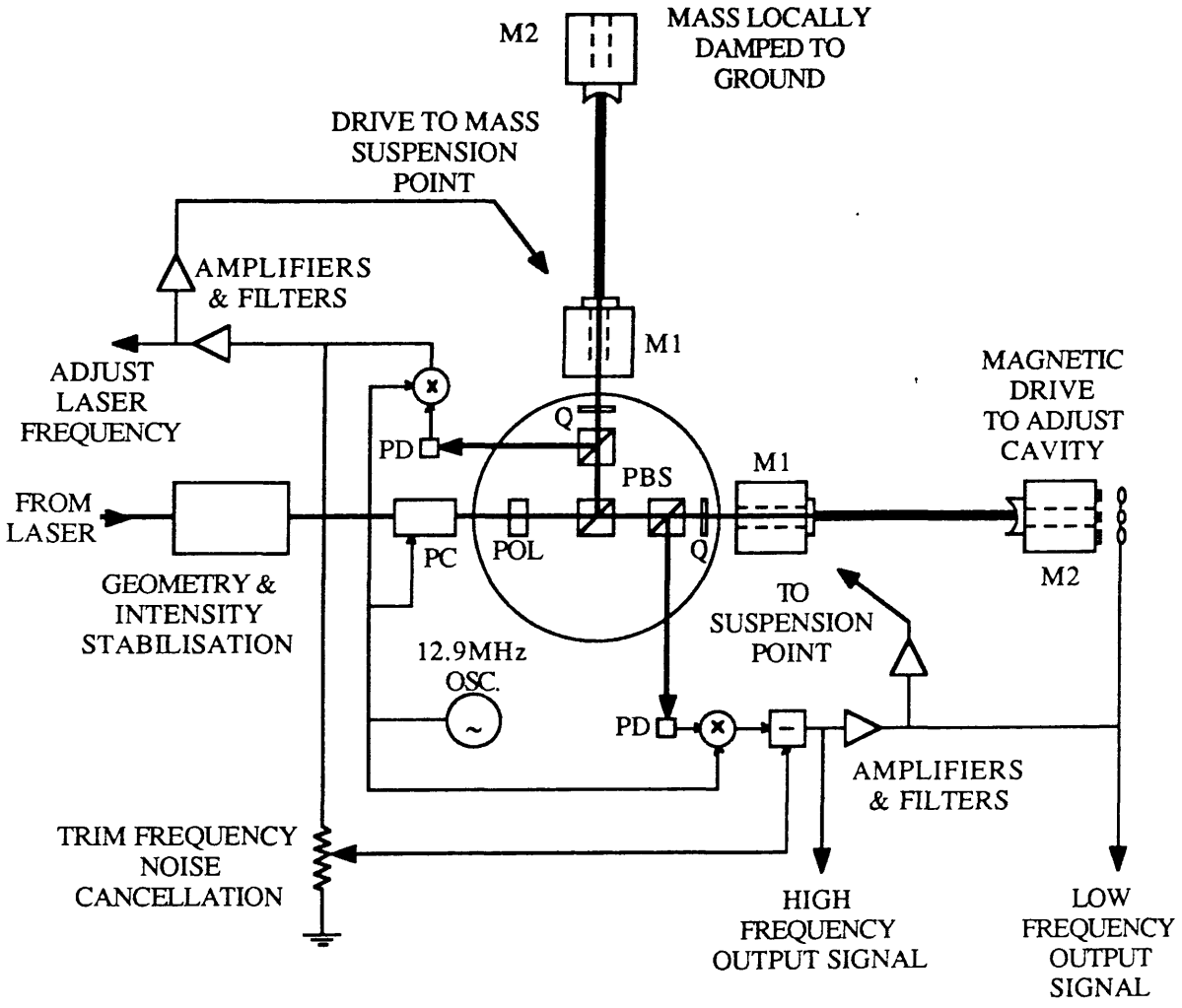

Figure 2.1 An outline of the recent configuration of the 10m prototype gravitational wave detector at Glasgow.

cavities on resonance the orientation of each mass must be controlled. One of the end test masses is held in the correct orientation by a magnetic drive system which acts directly on the mass. The error signal is obtained from shadow-meters which are incorporated into the driving coils.

The central tank contains three masses two of which incorporate the input mirrors for the two orthogonal cavities. The third mass holds various optical components associated with injecting light into the cavities and splitting off the output light.

The central masses are oriented by feeding back to their respective suspension points. In this case the error signals are derived from a subsidiary system of Helium-Neon lasers and position-sensitive photodiodes.

The end mass mentioned above, and one of the central masses, form the primary cavity, which acts as a stable frequency reference for the illuminating Argon Ion laser. The r.f. sideband reflection technique[66] is used to frequency stabilise the laser to this cavity by altering the effective length of the laser cavity. This alteration is achieved by mounting one of the laser mirrors on a piezo-electric transducer; high frequency changes are achieved through an electro-optic modulator within the laser cavity.

The remaining centre mass and the second end mass form the secondary cavity which is orthogonal to the primary cavity. The second end mass is controlled by a number of systems. The orientation is controlled by a system of Helium-Neon lasers and position-sensitive diodes which produces an error signal which is applied to the suspension point of the mass. The cavity length is also monitored by a Helium-Neon laser which feeds back through a magnetic drive system to reduce the large, low frequency fluctuations in the cavity length which would otherwise prevent the cavity

remaining on resonance.

In this system the second cavity has to track the changes in frequency of the input light (or the change in length of the primary cavity). The fine control of the secondary cavity length is also carried out through the magnetic drive system which attempts to maintain the cavity on resonance. With this arrangement the effect of a gravitational wave can be monitored at points within the servosystem which maintains the secondary cavity on resonance as an alternative to interfering the output light.

2:3 SOME LIMITATIONS TO SENSITIVITY

2:3.1 PHOTON SHOT NOISE

Consider a lossless, single-pass interferometer; from equation 1.37 the number of photons detected by a photo-diode at the output is given by:

$$N = \frac{I_o \tau \varepsilon}{2hf} (1 - \cos \emptyset) \qquad (2.1)$$

Where the symbols are as designated in the previous chapter. A change in the relative lengths of the arms of the interferometer, δl, will produce a change in the relative phase of the output light, $\delta\emptyset$, where $\delta\emptyset = k\delta l$ and k is a constant of proportionality. Therefore rewriting 2.1 in the presence of some disturbance:

$$\delta N = \frac{I_o \tau \varepsilon}{2hf} \sin \emptyset \; k\delta l \qquad (2.2)$$

As in the case of the delay-line interferometer, discussed in the previous chapter, the Fabry-Perot interferometer is arranged to lie on a dark fringe for optimum sensitivity and the

out-going laser light is assumed to obey Poisson statistics. The detection condition is then given by:

$$\delta l > \left[\frac{2hf\delta f}{I_o \varepsilon k^2} \right]^{1/2} \qquad (2.3)$$

Where f is the frequency of the input light and $\delta f = 1/2\tau$, the observational bandwidth of the measurement. Referring to Figure 2.1 let R_1 and R_2 be the intensity reflection coefficients of mirrors M_1 and M_2 respectively. The finesse, F, of the cavity is defined to be:

$$F = \frac{\pi (R_1 R_2)^{1/4}}{1-(R_1 R_2)^{1/2}} \qquad (2.4)$$

Now when the light storage time is less than or close to the gravitational wave period the shot noise limit may be shown to be[48]:

$$\delta l > \left[\frac{hc\lambda\delta f}{8\varepsilon F^2 I_o} \right]^{1/2} \qquad (2.5)$$

The light storage time is related to finesse by:

$$F = \frac{c\pi\tau_s}{2l} \qquad (2.6)$$

and so for pulses of order 1msec and an arm length of 1km the finesse should be ~ 500. Therefore the shot noise limit for a lossless, storage time limited detector is:

$$h \sim \frac{\delta l}{l} \sim 10^{-20} \left[\frac{100W}{I_o} \right]^{1/2} \left[\frac{0.5}{\varepsilon} \right]^{1/2} \left[\frac{1km}{l} \right] /Hz^{1/2} \qquad (2.7)$$

In practice there will always be some losses in the mirrors

and these losses affect the contrast of the fringes. The sensitivity is then modified by a factor dependent on the visibility of the fringes and the depth of phase modulation achieved in the laser frequency stabilisation system[67]. This factor is typically ~3-5 but may approach unity for very low loss mirrors (ie. less than one part in ten thousand).

The foregoing treatment assumes that the output beams interfere but in the case where each cavity is monitored separately the sensitivity limit will be raised by a factor $2^{1/2}$. It should be noted that the light levels required for these sensitivities may be lowered by the use of 'squeezing' and recycling techniques.

2:3.2 RADIATION PRESSURE

In the case where the sensitivity of a detector is limited only by photon shot noise this limit may be lowered by increasing the intensity of the light illuminating the interferometer. However as photon shot noise falls with increasing power the positional fluctuations of the test masses caused by radiation pressure increases. These fluctuations, caused by the statistics of photon recoil from each mass, will limit the sensitivity of the detector at some new level. Caves has calculated[58] that the optimum laser power is given by:

$$I_{opt} = \frac{mc\lambda\pi}{4F^2\tau^2} \qquad (2.8)$$

Where m is the mass of each test particle and τ is the duration of the measurement. Substituting for a mass of 10kg, a finesse of 500 and a 1msec bandwidth gives an optimum light intensity of ~ 5kW. Clearly this will only be of importance for future, very

high power, detectors.

2:3.3 THERMAL NOISE

There are two major possible components of thermal noise in an interferometric detector. One arises from motions of the pendulums which support the test masses and the second from vibrations within the masses themselves.

Consideration of the transfer function of a pendulum[19] indicates that the displacement of the test mass due to thermal excitation of the normal mode far from resonance is:

$$\delta l = \left[\frac{4kTf_o}{8\pi^3 f^4 mQ} \right]^{1/2} \quad m/Hz^{1/2} \qquad (2.9)$$

Where kT is the thermal energy associated with the resonance of frequency, f_o, and quality factor, Q, of the pendulum and m is the test mass. Therefore the limit to sensitivity for pulses of length τ with a detection bandwidth $1/2\tau$ centred about a frequency $1/\tau$ is given by[19]:

$$h \sim 10^{-22} \left[\frac{1km}{1}\right]\left[\frac{\tau^3}{10^{-3}s}\right]^{1/2}\left[\frac{10^6}{Q}\right]^{1/2}\left[\frac{f_o}{1Hz}\right]^{1/2}\left[\frac{10kg}{m}\right]^{1/2} \qquad (2.10)$$

To reduce the coupling of vibrations of the resonant modes of the test masses into the displacement sensitivity of the interferometer the lowest normal mode is chosen to be much higher than the upper limit of the gravitational radiation observation 'window'. For a material of density, ρ, velocity of sound, v, and quality factor, Q the limit to sensitivity is[19]:

$$h \sim 10^{-21}\left[\frac{1KM}{1}\right]\left[\frac{10^6}{Q}\right]^{1/2}\left[\frac{10^3 m^3/s^3}{v^3}\right]^{1/2}\left[\frac{10^3 kg/m^3}{\rho}\right]^{1/2}\left[\frac{10^{-3}s}{\tau}\right]^{1/2} \qquad (2.11)$$

Reasonable values for Aluminium are: $v \sim 3*10^3 m/s$, $\rho \sim 3*10^3 kg/m^3$ and $Q \sim 10^6$ which gives a limit to gravitational wave sensitivity of:

$$h \sim 10^{-22}\left[\frac{1km}{1}\right] \qquad (2.12)$$

2:3.4 SEISMIC NOISE

For a pendulum with a high quality factor, Q, and a resonant frequency, ω_o, a ground motion, δx_o, produces a displacement, δx_1, of the mass at a frequency, ω, which is given by:

$$\frac{\delta x_1}{\delta x_o} = \left[\frac{\omega_o}{\omega}\right]^2 \qquad (2.13)$$

until $f = \omega_o Q$ after which the transfer function falls off as $1/\omega$.

Figure 2.2[68] shows a composite of measurements of the spectral density of ground displacement against frequency. The source of each curve is identified in the footnote. Curve J represents data collected at Glasgow by the author with a seismometer employing a piezo-electric transducer to measure spectral density of acceleration. This is then converted into a ground displacement curve by using the relationship $\ddot{X} = -(2\pi f)^2 X$ at each frequency f. This curve may be approximated by $(10^{-7}/f^2)$ $m/Hz^{1/2}$ in the region from 300 - 700Hz although it rises more sharply at lower frequencies. Measurements taken by the author at Tentsmuir Forest, a likely site for a long baseline detector, gave similar results although there was slightly less activity below 300Hz.

By combining this figure with the degree of isolation obtained

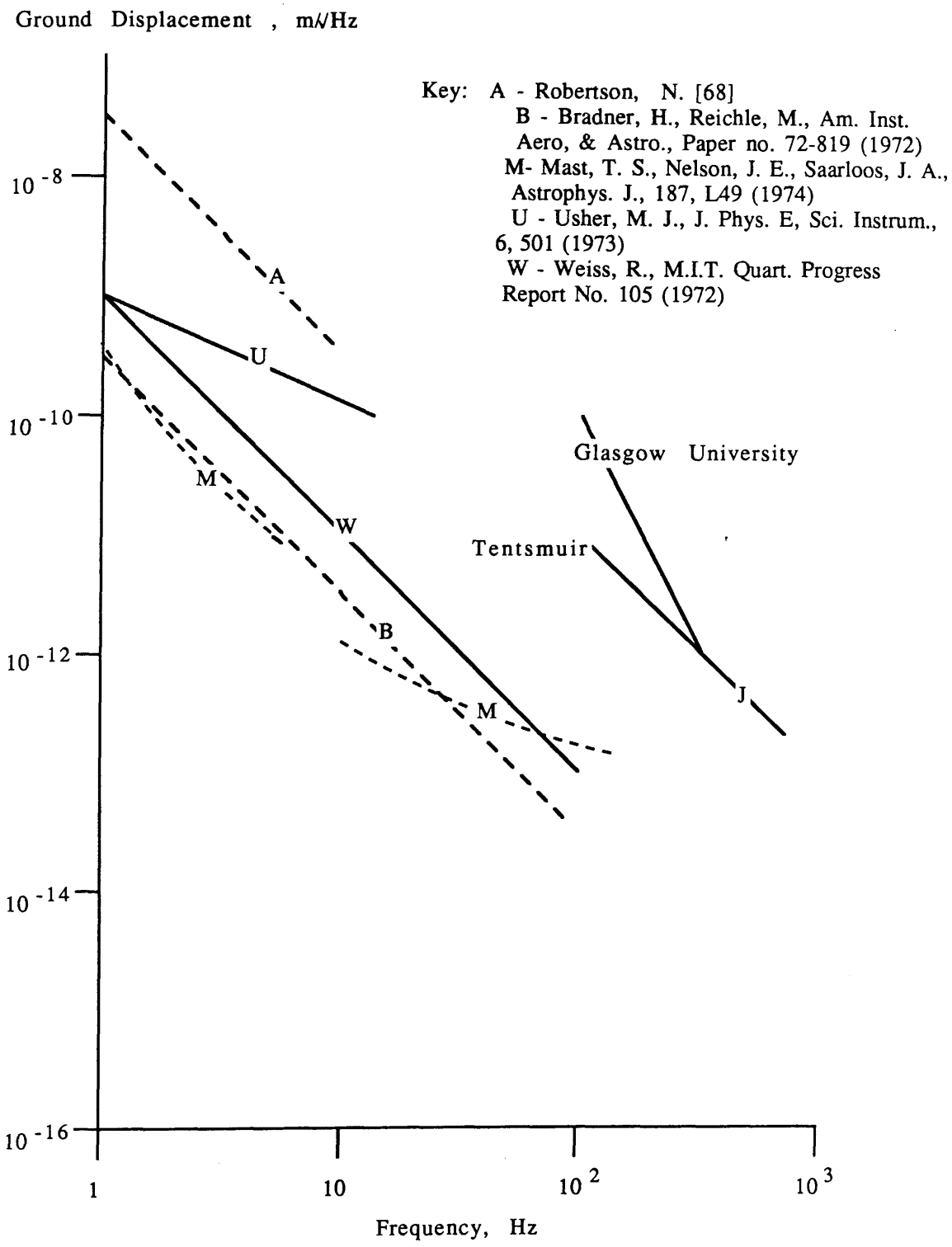

Figure 2.2 Several measurements of spectral density of ground displacement against frequency. This graph has been reproduced from [68] with the addition of recent data collected at Glasgow and in the Tentsmuir forest (J, see text).

by a simple pendulum the limit to sensitivity is given by[19]:

$$h \sim 6*10^{-21} \left[\frac{1km}{1} \right] \left[\frac{\tau}{10^{-3}sec} \right]^{7/2} \qquad (2.14)$$

when f_o=1Hz. To achieve a strain sensitivity of $h \sim 10^{-22}$ the suspension points will clearly require further isolation, possibly by the use of passive filters such as lead and rubber stacks and/or active systems which stabilise the pendulum suspensions to some reference point.

2:3.5 FREQUENCY NOISE

Frequency fluctuations in the light illuminating the interferometer will appear as a displacement of the test masses if the optical lengths of the cavities are not identical, ie. for a residual difference in length, Δl, between the two cavities[67]:

$$h = \frac{\delta l}{l} = \frac{\Delta l}{l} \cdot \frac{\Delta f}{f} \qquad (2.15)$$

The main factor in determining the optical length is the finesse. Hence

$$h = \frac{\Delta F}{F} \cdot \frac{\Delta f}{f} \qquad (2.16)$$

So if the cavities are matched in finesse to ~ 1% then the frequency fluctuations are constrained, $\Delta f < 10^{-5}$ for $h \sim 10^{-22}$. This figure assumes that the output light from the cavities is interfered.

When the output of each cavity is monitored separately common components may be subtracted electronically. Typically the system at Glasgow achieves ~ 12dB of subtraction.

2:3.6 INTENSITY NOISE

The intensity fluctuations in the light from an Argon Ion laser are many orders of magnitude above shot noise at low spectral frequencies. In general these fluctuations are cancelled out by interfering the outputs of two ideal, identical cavities. In practice this is not the case though the use of modulation techniques means that the light is sampled at higher spectral frequencies where intensity noise is essentially due to photon shot noise. However the residual intensity fluctuations will couple to the sensitivity through a static offset in the feedback null of the servo which maintains the cavities on resonance[67].

If Δl is the path length difference when the servosystem is open-loop then:

$$h = \frac{\delta l}{l} = \frac{l}{l} \cdot \frac{\delta I}{I} \cdot \frac{\Delta l}{G} \qquad (2.17)$$

Where G is the open-loop gain of the servosystem. Clearly to reduce the effect of intensity fluctuations on the sensitivity of the detector requires very high open-loop gain. The fluctuations may also be reduced at source by passive systems, ie. rebuilding the laser resonator, or active systems such as that described in chapter three.

2:3.7 BEAM POSITION-GEOMETRY FLUCTUATIONS

It has been shown that fluctuations in beam position, angle and diameter can couple into detector sensitivity as phase noise if the wavefronts of the output beams are not perfectly matched[69]. In fact it has been demonstrated that the geometry fluctuations in the

beam from a free-running Argon Ion laser could limit the sensitivity of an interferometer at a level of[67]:

$$h = \frac{\delta l}{l} \sim 10^{-18} \left[\frac{1km}{l} \right] m/Hz^{1/2} \qquad (2.18)$$

The significance of these fluctuations may be reduced by passing the light through mode-cleaning cavities or optical fibres or by the use of servo-controlled mirrors to stabilise the beam's position. The fluctuations in the light emitted by the laser may be reduced by, for example, rebuilding the laser resonator. Chapter five describes the investigation of the possible uses of optical fibres.

2:3.8 SCATTERED LIGHT

One of the reasons that the Glasgow group opted for Fabry-Perot cavities in their prototype detector was the belief that this type of system is inherently less sensitive to scattered light than the optical delay line. Light will be scattered by imperfections in the mirrors of each cavity and so the fluctuations in scattered light in each cavity will be uncorrelated. Therefore these fluctuations will appear as phase noise in the interfered light.

If a fractional amplitude, σ, of scattered light impinges on the monitoring photo-diode with a phase variation, θ, then this will give rise to phase fluctuations in the observed output:

$$\Delta\phi = \sigma \sin \theta \qquad (2.19)$$

Variations in σ or θ (frequency fluctuations) will limit the sensitivity of an interferometer.

In fact the sensitivity will be limited to[67]:

$$h = 2\sigma\,(\Delta f/f) \qquad (2.20)$$

And assuming a reasonable value, $\sigma_{max} = 0.01$, then again the frequency stability is constrained to $\Delta f < 10^{-5}$ for $h \sim 10^{-22}$.

2:3.9 RESIDUAL GAS NOISE

Residual gas in the vacuum enclosure may affect sensitivity in two ways:

Pressure fluctuations in the beam path will cause variations in refractive index which will appear as phase noise in the light detected at the output of the interferometer.

Secondly, the statistical fluctuations of the residual gas molecules recoiling from the test masses will contribute to their thermal motion. This has the effect of reducing the quality factor of the pendulum. To avoid these effects limiting the sensitivity of a long baseline Fabry-Perot interferometer a pressure of 10^{-8} torr is required[19].

CHAPTER 3

THE INTENSITY STABILISATION OF AN ARGON ION LASER

3:1 THE REASONS FOR INTENSITY STABILISATION

In an ideal interferometric gravitational radiation detector the two orthogonal cavities would be identical in all respects apart from that of orientation. In such a symmetric system when the cavities were resonating, any noise introduced equally to the cavities, for example laser intensity noise, would be transmitted equally to and reflected from each cavity. At the point of recombination of the light from each cavity any such intensity fluctuations would be cancelled out leaving the asymmetric signal which is expected to be produced by the passage of a gravitational wave.

In the Glasgow gravitational radiation detector the cavities are kept on resonance by a servosystem utilising a reflection r.f. sideband technique developed at Glasgow[66]. The laser is frequency locked to one of the 10m long cavities which acts as a reference. The second cavity is locked to the stabilised laser light and any disturbance is, in principle, monitored at the point of recombination of the beams. When locking on the feedback null there should be complete cancellation of any low frequency, excess intensity noise on the coherently detected output light. However, intensity noise can couple into the detected signal through a static offset error in the locking point of the feedback loop.

A spectrum of the natural intensity fluctuations of an Argon Ion laser is shown in Figure 3.1 the level of intensity fluctuations

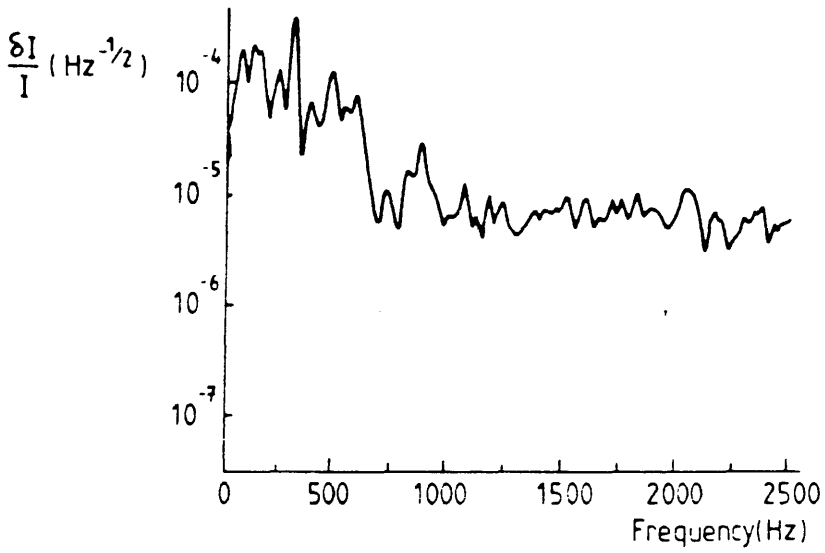

Figure 3.1 Typical Fourier spectrum of the natural intensity fluctuations of an argon ion laser*. In a gravitational wave detector employing laser interferometry such fluctuations could be a serious limitation to the sensitivity achieved.

* Spectra Physics 164 Argon Ion Laser.

at 1kHz is approximately:

$$\frac{\delta I}{I} \sim 10^{-5} \ /Hz^{1/2} \tag{3.1}$$

The level at which this noise then couples into the signal locking the second arm is equivalent to a displacement signal given by[48]:

$$\delta l = \frac{\delta I}{I} \cdot \frac{\Delta l}{G} \tag{3.2}$$

Where δl is the displacement noise, Δl the offset in the cavity length with the loop open and G is the open loop gain.

Inserting typical figures of $\Delta l = 10^{-6}$m and $G = 10^{7}$ gives a displacement, $\delta l = 10^{-18}$ m/Hz$^{1/2}$, which may be a serious limitation to an operational detector.

If the incident laser intensity noise can be reduced to the level of photon shot noise and the other servosystem loops for laser frequency and cavity length control are also limited by shot noise then the associated displacement noise is given by[19]:

$$\delta l = \frac{1}{l_{eff}} \cdot \left[\frac{\lambda \hbar c}{2\pi I_o \varepsilon \tau} \right]^{1/2} \tag{3.3}$$

Where the symbols have their usual meanings and ε is a factor to account for the efficiency of the photo-diode (~ 50%), l_{eff} is the effective length of the cavities given by $l_{eff} = 2lF/\pi$. τ is the light storage time, l is the separation of the mirrors and F is the finesse of the Fabry-Perot cavities. The two cavities are matched in finesse to reduce the coupling of the frequency noise of the laser light into the detector sensitivity[67].

Typical figures of λ = 514.5 nm, F ~ 3000, l = 10m, τ ~ 60μs and I_o ~ 30 mW give a displacement sensitivity of $\delta l \sim 2*10^{-19}$

$m/Hz^{1/2}$ in a 1kHz bandwidth around 1kHz.

It is this potential for allowing high sensitivity to be achieved, particularly as higher laser power becomes available, that provides the incentive for developing a laser intensity stabilisation system.

3:2 DESIGNS FOR A LASER INTENSITY STABILISATION SYSTEM.

Laser interferometric gravitational radiation detectors are not alone in requiring laser illumination which is stabilised to a high degree, eg: some applications in Spectroscopy and Holography, and there are several techniques which have been implemented with good results.

One method is to utilise an acousto-optic modulator as the control element[70,71]. An acousto-optic device may be composed of any material displaying the photo-elastic effect coupled to a strain-inducing transducer, usually a piezo-electric ceramic, which produces a travelling sound wave within the material. Light travelling through the crystal is scattered from the travelling acoustic disturbance by Bragg diffraction and frequency shifted by an amount δf, where δf is equal to the frequency of the sound wave. Varying the power to the transducer varies the ratio of the light power in each of the diffracted output beams and the undiffracted beam. The angle of diffraction may be controlled by varying the frequency of the sound wave which is usually of the order of a few tens of Megahertz. A schematic of the system is shown in Figure 3.2. The photo-diode samples a fraction of the beam and the photo-current is compared to a stable reference. The difference signal is amplified and fed back to a variable r.f. amplifier thereby modulating the intensity of the through beam. With care up to 85% of

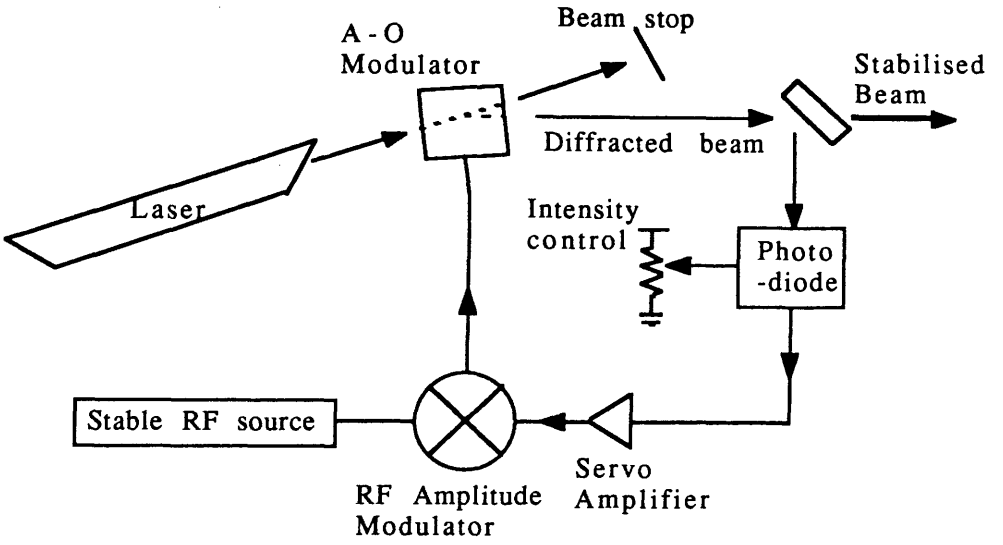

Figure 3.2 A schematic representation of a laser intensity stabilisation system utilising an acousto - optic modulator as the control element.

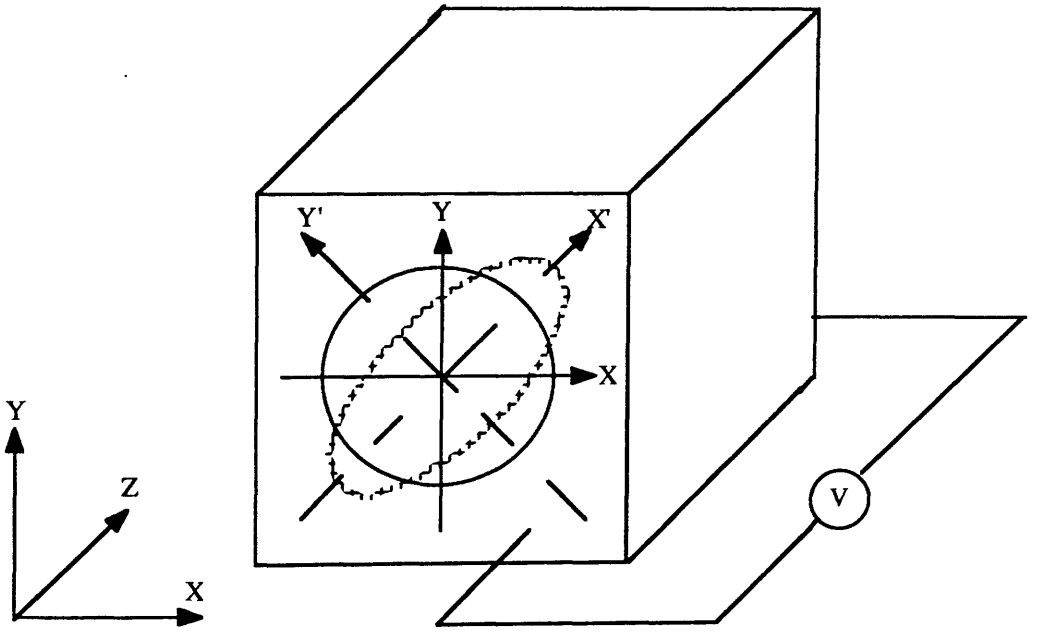

Fig.3.3 Longitudinal mode Pockels cell. The solid curve is the projection of the index ellipsoid onto the x-y plane with no applied field. The broken line indicates the index ellipsoid in the presence of an applied voltage, V.

the light power may be scattered into the first sideband although a stabilisation system must be biased lower than this for operation. Loop gains of up to 80dB at low frequencies have been reported in amplitude stabilisation systems of this sort[70]. In experiments where light reflected back into the laser is a problem due to frequency 'pulling', the first diffraction beam may be selected for stabilisation to provide some degree of isolation. The retro-reflected beam will be frequency shifted to $f + 2\delta f$ or $f - 2\delta f$ and this can be arranged to lie outside the gain profile of the laser medium. An alternative scheme of isolation is to arrange that δf be equal to an odd multiple of one quarter of the laser free spectral range; in this case the frequency of the return beam will lie half-way between two axial modes where the gain medium will be effectively transparent.

A second method of intensity stabilisation which is in use in high power commercial Argon Ion lasers is the modulation of the tube current to compensate for fluctuations in output. Typically these systems have a bandwidth of a few kHz and a gain of a few times ten. Recently at Orsay in France, work has been in progress on a similar system with wider bandwidth and higher gain. Suppression factors of ~ 40dB at around 1kHz have been achieved although there are associated problems of induced beam position or geometry fluctuations which may be due to inhomogeneities in the plasma induced by current transients.

In this chapter the results of experiments using an electro-optic control element are presented and discussed. There are several commercial intensity stabilisers available which utilise electro-optic modulators. One type used at Glasgow, the Coherent model 307 noise-eater, did not give sufficient improvement in the level of intensity noise.

Examination of the specifications of the device indicates that all of the gain is not being seen and this is a further reason for investigating what limitations there may be for such a system.

The electro-optic effect is found in crystals which display an electrical anisotropy, that is the polarisation vector produced by an applied field is dependent on the direction of that field with respect to the crystal lattice. This is generally true of crystal structures which do not have inversion symmetry. One of the consequences of this is that light transmitted through such a crystal will encounter varying refractive indices as it varies in orientation or polarisation. The crystal has three principal dielectric axes; x, y, z[72]. A commonly used crystal is Ammonium Dihydrogen Phosphate (ADP) which has a four-fold axis of symmetry which by convention is taken to be the z, or optic, axis. The optic axis is that direction in the crystal in which, in the absence of an electric field, unpolarised light incident on the crystal will undergo no relative phase-shift of its polarisation components.

The index ellipsoid is a useful representation of the effects of the electrical anisotropy of the crystal on unpolarised light. This is an ellipse of revolution around the optic axis. The radius at an angle, θ, is proportional to the inverse of the refractive index in that polarisation direction. For example, for a perfect crystal in the absence of any applied field the projection of the index ellipsoid on to a plane perpendicular to the optic axis would be a circle - all polarisations propagate at the same velocity. When a field is applied parallel to the optic axis the projection becomes an ellipse with the major and minor, (x' and y'), axes at 45^{o} to the principal dielectric axes; cf. Figure 3.3. If plane polarised light is now incident on the crystal and the plane of polarisation is parallel to one of the principal axes, eg. x, then the light can be

resolved into two orthogonal polarisation components parallel to the ellipsoid axes x' and y'. These components will be subject to different indices of refraction and will propagate through the crystal at different velocities.

Therefore given an incident field plane polarised in the x direction:

$$E_x = E_o \cos(\omega t + \phi_o) \tag{3.4}$$

Then the two orthogonal polarisation components will be:

$$E_{x'} = \frac{E_o}{2^{1/2}} \cos(\omega t + \phi_o) \tag{3.5a}$$

$$E_{y'} = \frac{E_o}{2^{1/2}} \cos(\omega t + \phi_o) \tag{3.5b}$$

Then after traversing the crystal the two components will have undergone a phase shift $\delta x'$ and $\delta y'$ respectively. This phase shift is given by:

$$\delta x' = \frac{2\pi n_{x'} L}{\lambda} \tag{3.6}$$

Where $n_{x'}$ is the refractive index appropriate to light polarised in the direction of the x' axis and is given by:

$$n_{x'} = n_o + \frac{1}{2} r n_o^3 E_z \tag{3.7}$$

Where r is the linear electro-optic coefficient appropriate to the axis of propagation and the direction of the applied field and n_o is the index of refraction in the absence of any field. The value of $n_{y'}$ is given by a similar expression:

$$n_{y'} = n_o - \frac{1}{2} r n_o^3 E_z \qquad (3.8)$$

Therefore the two components will undergo a differential phase change:

$$\delta x' = \phi_o + \Delta\phi \qquad (3.9a)$$

$$\delta y' = \phi_o - \Delta\phi \qquad (3.9b)$$

and

$$\Delta\phi = \frac{\pi r n_o^3 V}{\lambda} \qquad (3.10)$$

The emerging beams will then be of the form:

$$E_{x'} = \frac{E_o}{2^{1/2}} \cos(\omega t + \phi_o + \Delta\phi) \qquad (3.11a)$$

$$E_{y'} = \frac{E_o}{2^{1/2}} \cos(\omega t + \phi_o - \Delta\phi) \qquad (3.11b)$$

If a polarisation analyser is now placed after the crystal with its orientation orthogonal to the incident wave of equation 3.4 then the transmitted beam will be the sum of two components:

$$E_1 = \frac{E_{x'}}{2^{1/2}} \qquad (3.12a)$$

and

$$E_2 = -\frac{E_{y'}}{2^{1/2}} \qquad (3.12b)$$

$E_{x'}$ and $E_{y'}$ are as given in equations 3.11a and 3.11b and it can be seen that the output intensity, I, will be:

$$I = I_o \sin^2(\Delta\phi) \qquad (3.13)$$

Where I_o is the intensity of the input light of equation 3.4.

It is useful to define a half-wave voltage, V_π, which is the voltage that will produce a relative phase shift of $2\Delta\emptyset = \pi$ or $\lambda/2$. This represents a rotation of the plane of polarisation of the input beam of 90^o. In the system described above with crossed polarisers the output beam would be equal in intensity to the input beam neglecting reflection losses.

From equation 3.10:

$$V_\pi = \frac{\lambda}{2rn_o^3} \tag{3.14}$$

And so equation 3.13 becomes:

$$I = I_o \sin^2 \left[\frac{\pi}{2} \frac{V}{V_\pi} \right] \tag{3.15}$$

Where, $V = V_o +/- V_{sig}$. V_o is the biasing voltage which determines the percentage of light transmitted and V_{sig} is a modulation signal applied to the crystal.

This arrangement, together with a feedback servosystem of suitable design, will form the basis of an electro-optic intensity stabiliser. By applying a suitable bias voltage to the Pockels cell any required fraction of light can be transmitted. Sampling some portion of this transmitted light and comparing the signal to a stable reference provides information for a feedback loop. There are two main disadvantages to the arrangement as outlined above.

Firstly, the $\sin^2$ dependence of the transmitted light intensity will reduce the loop gain of the servosystem to zero as the bias voltage, V_o, approaches V_π. Large intensity excursions will also cause the servosystem to overshoot the top of the transmission curve and enter a region where the feedback becomes positive and will cause the amplifiers to saturate.

The second disadvantage is related to the choice of axes in the crystal. The requirement that the applied field be parallel to the z axis means that the electrodes must cover the input and output faces of the crystal. This is usually achieved with thin metal or metal oxide films. For greater transmission and higher power capacity it is possible to compromise with the requirement for field uniformity by using ring electrodes[73].

The transverse effect Pockels cell is more useful in this case because the electrodes will not interfere with the transmission of the beam. There is a second advantage in that the retardation in a transverse effect crystal is proportional to the length of the crystal, cf. equation 3.16a, and so the voltage may be reduced by selecting larger crystals. As with the longitudinal effect the field is applied along the z axis, although the light is transmitted along the y' axis. The principal axes of the index ellipsoid in the presence of an applied field are now x' and z. Thus the retardation in this case will be:

$$\delta x' = \phi_o + \frac{2\pi}{\lambda} r n_o^3 \frac{VL}{D} \qquad (3.16a)$$

and

$$\delta z = \phi_o + \frac{2\pi n_z}{\lambda} \qquad (3.16b)$$

D is the electrode spacing and L is the crystal length. And by combining equations 3.16a and 3.16b it can be shown that:

$$\Delta\phi = \frac{2\pi}{\lambda} (n_o - n_z)L - \frac{2\pi}{\lambda} r n_o^3 \frac{VL}{D} \qquad (3.17)$$

The voltage-independent term will bias the transmission curve. However, since L and D are constants of the crystal it can be seen

that equation 3.15 is still valid.

A further option which will improve the relative phase change, $\emptyset$, per volt is to use a 45^{o}-cut transverse crystal[74,75]. For instance, in a 45^{o} x-cut transverse crystal the bias voltage is applied parallel to the x axis. The incident beam is arranged to be orthogonal to this axis and at 45^{o} to the y and z axes. When a voltage is applied then the axes rotate by 45^{o} about the x axis. The index ellipsoid is then determined by the voltage independent x term and the varying z' term. The voltage dependent term is of the same form as in equation 3.17. The appropriate linear electro-optic coefficient, r, is more than a factor of three larger for this arrangement than for the longitudinal or transverse mode.

An advantage of the static birefringence, which arises in equation 3.17, is that it can be used to align the Pockels cell correctly. The polarisers are arranged to be parallel (in the absence of the Pockels cell) and then the orientation of the Pockels cell between the polarisers is adjusted to give a transmission maximum. At this point the plane of polarisation is parallel to one of the principal axes since no polarisation rotation is taking place. The Pockels cell is then rotated by 45^{o}. The output polariser may then be orientated either parallel, or orthogonal, to the orientation of the input polariser depending on the requirements of the particular experiment. The choice of parallel polarisers will give rise to a constant phase term of $\pi/2$ in the bias curve and the transmission now takes on a $\cos^{2}$ dependence.

The initial static birefringence of the crystal is temperature dependent and this will lead to variations in the biasing of the intensity modulator unless some compensation is provided. There are two methods by which this can be achieved passively[76], both involving a second crystal equal in length to

the first. In the Pockels cell utilised for these experiments the second, compensating, crystal is rotated by 90° about the axis of beam propagation and the voltage is applied to the second crystal in the opposite sense to the first. Therefore the y' component of the first crystal will be the x' component of the second crystal and there will be no net change with temperature of the perceived static birefringence. Conversely, since the voltage is reversed in the second crystal the phase change due to the applied voltage will be complementary.

If a 45° x-cut crystal is used then the problem of beam 'walk-off' must also be considered. Since the incident beam is neither parallel, or perpendicular, to the optic axis then one of the polarisation components will be deviated in passing through the crystal - the so-called extra-ordinary ray. If two crystals are used as above to correct for the temperature dependence of the static birefringence then the divergence will be present in two dimensions. To prevent beam divergence and reduce the effect of temperature fluctuations a set of four crystals is used. The first pair will deviate and then correct one of the polarisation components. A pair may be composed of two x-cut or two y-cut crystals with the voltage applied in the opposite sense to the second crystal of the pair. Alternatively, one x-cut and one y-cut crystal may be used to form a pair. The advantage of this second arrangement is that the voltage is applied in the same sense to both crystals and so the crystals may be in contact. The second crystal pair will be rotated by 90° about the axis of beam propagation and will perform the same function for the second polarisation component. Alternate crystals in the arrangement will compensate for the temperature dependence of the static birefringence.

3:3 CONSTRUCTION OF AN INTENSITY STABILISATION SERVOSYSTEM.

The primary design aim of the proposed intensity stabilisation system was to achieve photon-noise limited performance in the laser light at low (<few kHz) frequencies. A small sample, nominally 1mW, of light would be split off from the main beam on to a low-noise photo-diode and the photo-current compared to a constant reference. The resultant signal would be amplified and filtered and fedback to an electro-optic modulator to attain photon-noise limited stability in the sample. The control element was chosen to be a 4-crystal 45^{o}-transverse-cut ADP Pockels cell with a half-wave voltage, V_{π}, of 280V. This may be compared with a typical half-wave voltage of 10kV for a single-crystal, longitudinal mode ADP Pockels cell.

Starting with this information it is possible to calculate some of the necessary system parameters which the design will have to satisfy.

The requirement is for photon-noise limited performance in 1mW which is at the level:

$$\frac{\delta I}{I} \sim 7 * 10^{-8} /Hz^{1/2} \qquad (3.18)$$

Laser intensity fluctuations at low frequencies (2-300 Hz) have been found to be as large as:

$$\frac{\delta I}{I} \sim 7 * 10^{-5} /Hz^{1/2} \qquad (3.19)$$

At d.c. the variation in intensity may be of the order of 1 - 3%. Therefore, the system will need to have a closed loop gain greater than 10^{4} at low frequencies. It is important, however, that the system does not disturb the photon-noise limited characteristics

of the laser output at higher frequencies where radio frequency servosystems are in use and to comply with these high frequency requirements the unity gain point was chosen to be at 100kHz.

To satisfy these requirements will require a circuit with a high d.c. gain which will roll off steeply to the unity gain crossover point without loss of stability. A circuit of 'bypass' design was proposed as being most suitable for this application.

The circuit is constructed on a copper-plated plastic board which provides a good earth plane and facilitates shielding of the components from power line noise which could affect the performance of such a high gain circuit.

The signal from a photo-diode is compared to a stable d.c. reference at the input of a high gain, wide bandwidth AD-50J operational amplifier. The output is then split into two branches. One part of the signal is further amplified by a fast operational amplifier (OEI 9826) and applied to one side of the modulator through a resistor. This resistor in series with the capacitance of the Pockels cell determines the high frequency roll-off of the system gain. The upper corner frequency is ~ 70kHz.

The second branch of the circuit amplifies and filters the low frequency signal and applies it differentially to both sides of the modulator via high voltage operational amplifiers (Burr Brown 3583) arranged to have a total output swing of +/- 200V. In early experiments the d.c. bias point of the modulator was set by a large bank of batteries in series with the output of one side of the high voltage amplifier. Small corrections to the biasing point were made with a variable d.c. supply summed with the input to one of the high voltage amplifiers. In later experiments a variable d.c. supply was amplified and summed with the input to one of the high voltage amplifiers to achieve biasing. The final circuit configuration is

shown in Figure 3.4.

The calculated open loop gain of the circuit, shown in Figure 3.5, has a d.c. gain of around 90dB falling off steeply above a few hundred Hertz to around 10kHz approaching ~ 18dB/octave between 1 and 3 kHz. Above 10kHz the roll-off is approximately 6dB/octave through the unity gain point at around 100kHz. A more complete circuit analysis is presented in Chapter 4.

3:4 OPERATION OF AND RESULTS FROM THE SYSTEM.

The light source to have its intensity stabilised was a Spectra Physics model 165 Argon Ion laser with a typical output of 500mW on a single longitudinal mode of the green line. For an approximately linear response and for largest closed-loop gain, the intensity modulation system should be biased at $V_o=V_\pi/2$. This condition is not desirable because it requires that 50% of the laser output be rejected. However at high V_o the circuit will lose lock more often - due to the large, low frequency laser intensity excursions - and suffer a reduction in closed-loop gain.

In normal operation the stabilisation system is biased to allow 70% of the light to be transmitted as a compromise between high transmitted intensity and dynamic range.

To test the effectiveness of the servosystem the optical layout of Figure 3.6 was used. The input polariser is optional since the Argon Ion laser output is highly polarised. A second 'monitor' photo-diode sampled the light downstream of the Pockels cell/polarisers combination and was typically placed at the same distance from the laser as the feedback photo-diode. The level of noise in the output from this photo-diode should reveal the intensity noise which will be 'seen' by any experiment illuminated by

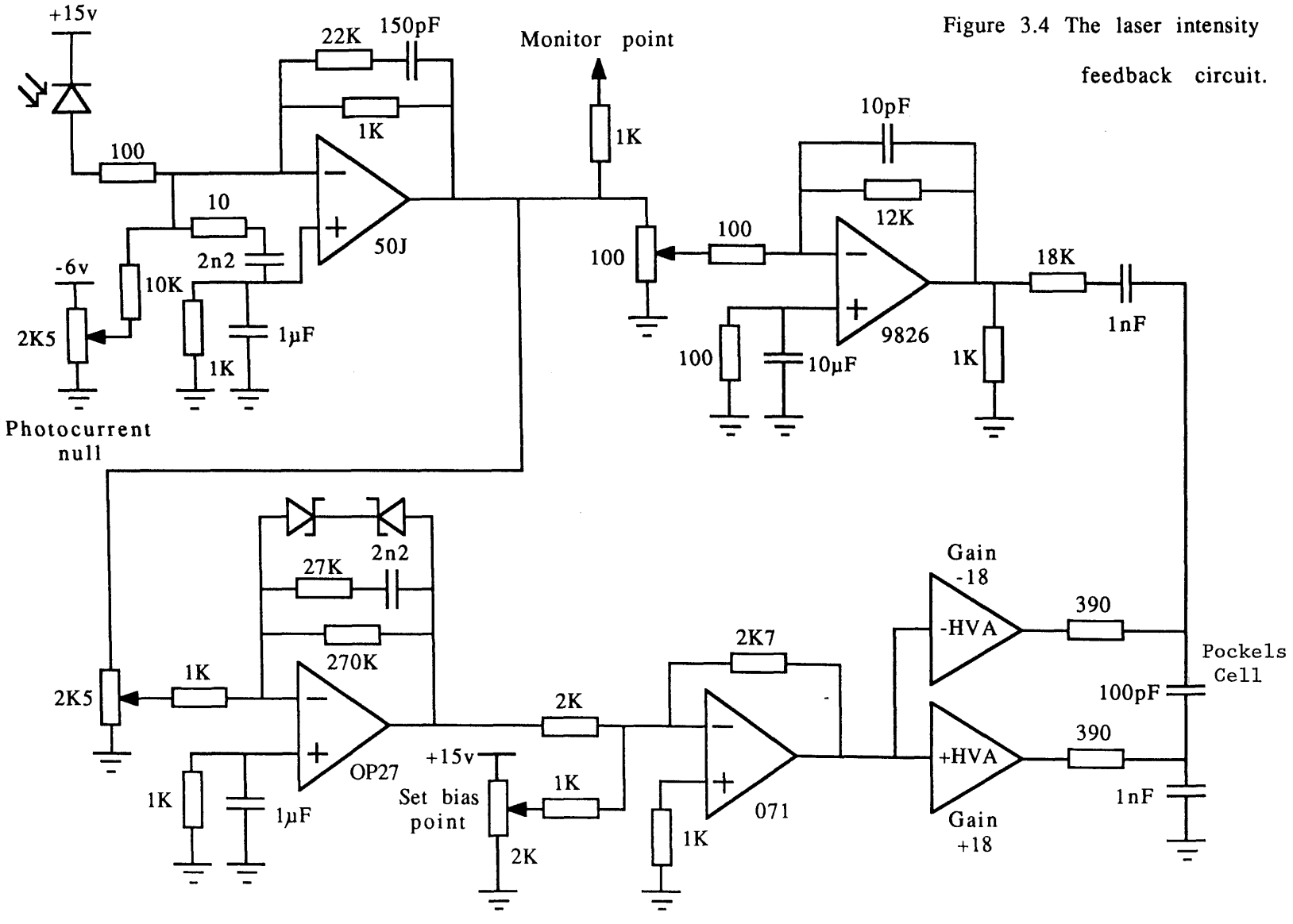

Figure 3.4 The laser intensity feedback circuit.

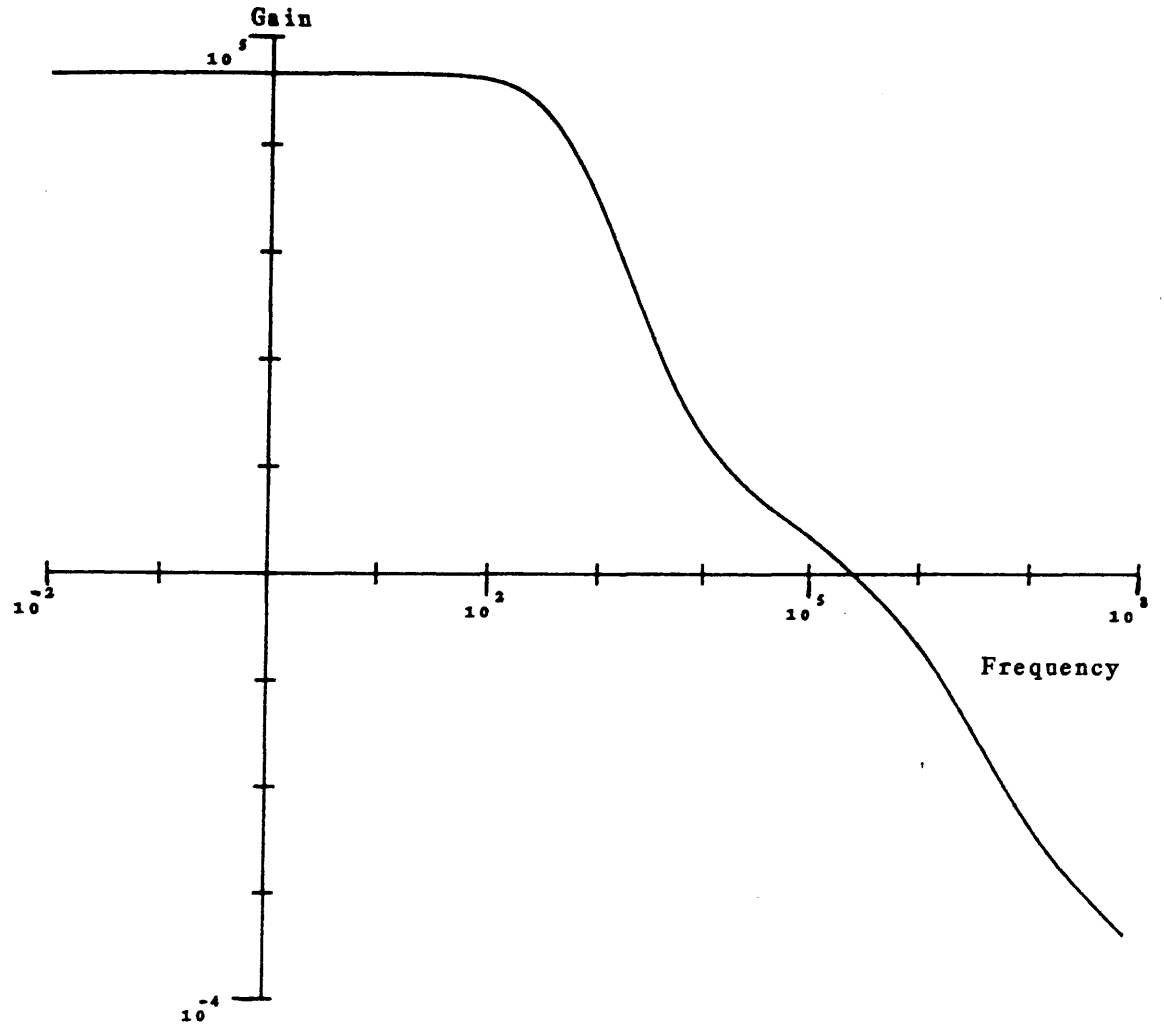

Figure 3.5 The calculated open-loop gain of the intensity stabilisation system when $V_o = V_\pi * 0.7$. Note that the available gain exceeds 80dB at low frequencies but falls away rapidly to the unity gain point at around 100kHz.

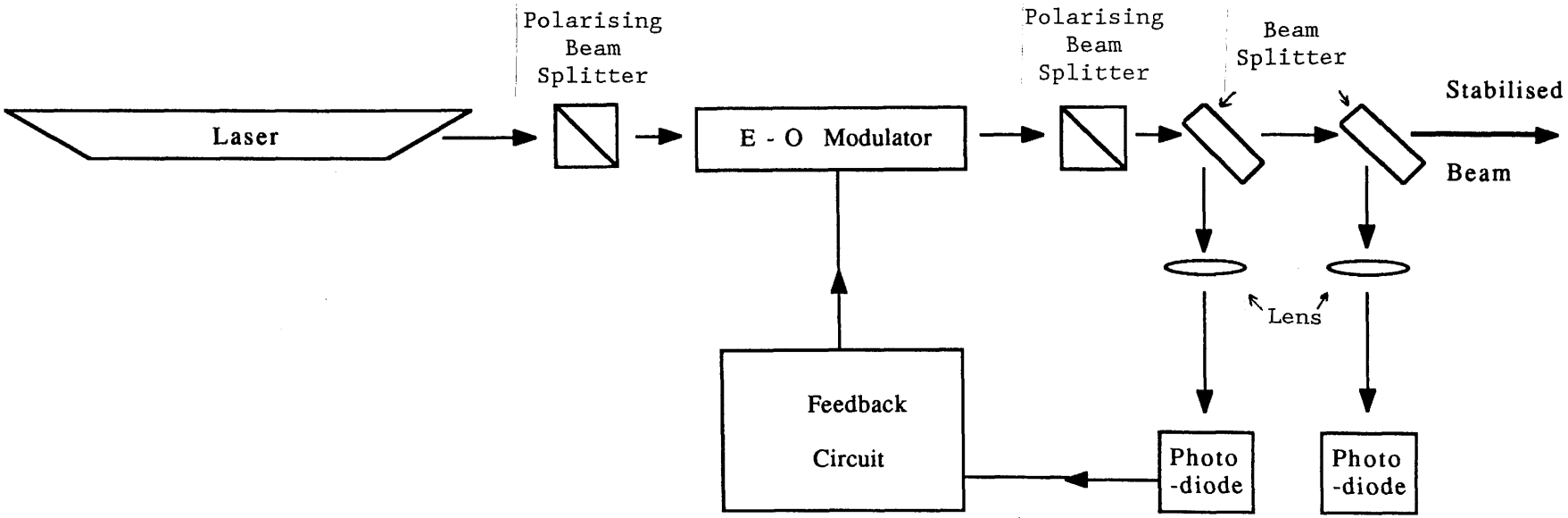

Figure 3.6 A schematic of the experimental arrangement used to operate the laser intensity stabilisation system. A sample of light is split off by the first beam splitter onto a photo - diode which provides a measure of the intensity fluctuations present A second beam splitter allows the use of a second, independent photo - diode to observe the reduction in intensity fluctuations which would be seen by an experiment illuminated by the stabilised light.

the full intensity stabilised laser output provided that the intrinsic electronic noise of the photo-diode does not dominate. To calibrate the system a battery torch was used to produce the same d.c. output from the photo-diodes as a known intensity of laser light. These signals were compared with the electronic noise produced by the photo-diodes when screened from any source. The torch reproduced a photon-noise signal of 2.4mW and demonstrated the level of electronic noise of the two photo-diodes in terms of a photon shot-noise intensity.

An EGG SGD-200 photo-diode was chosen to sample the beam because of its low intrinsic electronic noise. The photo-diode and 50J pre-amplifier combination have a noise level equivalent to the photon-noise of an incident light intensity of 0.3mW.

A UDT Pin 10D photo-diode was selected as the second photo-diode since it, like the SGD-200, was shown to have a low intrinsic electronic noise and a relative insensitivity to beam movements. This second diode has an intrinsic electronic noise level equivalent to the shot-noise in approximately 0.7mW of incident laser light. The apparatus was usually set up such that 2-3mW of light were incident on this second 'monitor' photo-diode. It should be noted that when observing results from this second photo-diode with the system in operation and with photon-noise limited stability in the amount of light sampled by the loop photo-diode the minimum noise level will be determined by the sum, in quadrature, of the noise levels appropriate to the two photo-diodes.

There is a second useful monitoring point within the circuit itself which provides information on the servosystem performance. Comparing the output of the 50J operational amplifier with the circuit both open- and closed-loop gives a direct measure of the circuit gain.

Since the low frequency closed-loop gain of the system is of the order of 10^4 and photon-noise limited stability is being sought it is important to ensure that the two photo-diodes are shielded from the 100Hz intensity fluctuations of the fluorescent room lighting and from scattered light from the laser. During experiments all the components of the system following the Pockels cell and its associated polarisers were encased by an opaque cover with suitable holes to allow entrance and egress of the laser beam.

Shown in Figure 3.7 are typical results from the system as perceived by the monitoring photo-diode. Above ~ 1kHz the output level is consistent with being photon-noise limited. However, below this frequency the gain is typically ~ 40dB. Figure 3.8 shows the output from the first-stage amplifier when the system is: a) Open loop and b) Locking. It is seen from the output of the 50J preamplifier that the circuit has a loop gain of ~ 90dB near d.c. falling to ~ 35dB at 2.5kHz and to ~ 15dB at 25kHz as required by the high frequency constraints. This shows that there is sufficient gain available to achieve photon-noise limited performance down to ~ 100Hz but since this is not achieved there must be other limiting factors.

It is perhaps an obvious point, but worth noting nonetheless, that if the two diodes were identical in every respect and sampled the same portion of light at the same distance from the laser then the residual intensity fluctuations detected by the monitor photo-diode would be identical to those seen by the loop photo-diode down to the limit of photon shot-noise in the sampled light. This is clearly not possible since, for example, it requires the two photo-diodes to occupy the same position in space. It can be seen that if the loop photo-diode perceives non-intensity noise as fluctuations in the laser output the feedback servosystem will impose

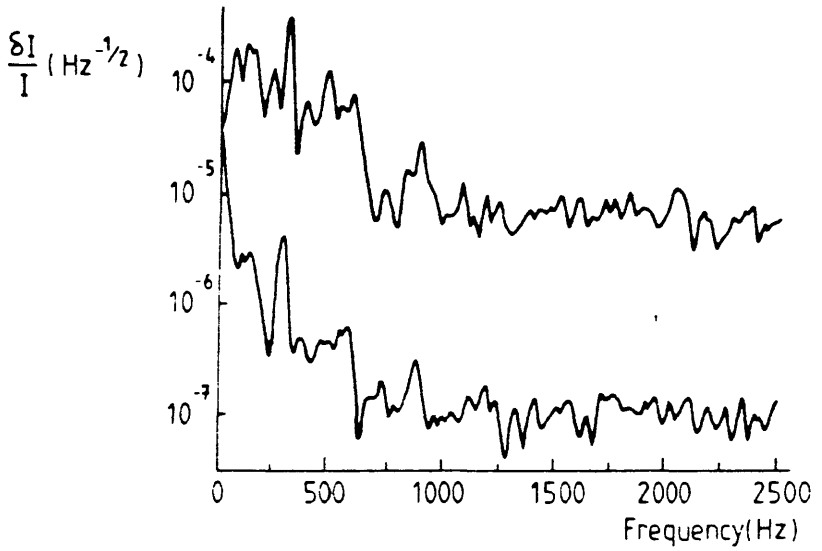

Figure 3.7 Typical Fourier spectra of the intensity fluctuations of the laser light. The upper curve shows the natural intensity fluctuations, and the lower curve shows the residual fluctuations with the stabilisation system in operation.

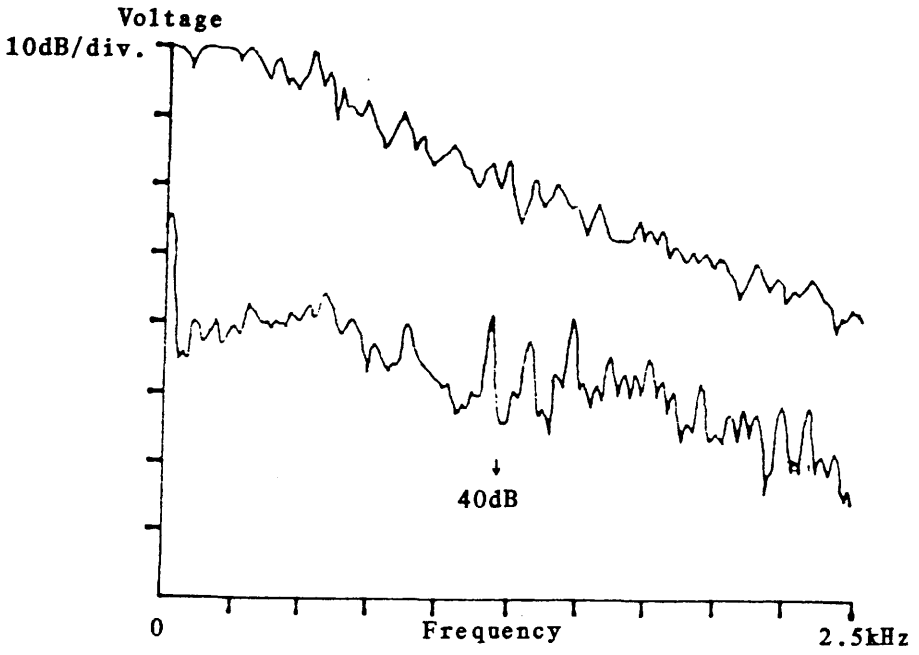

Figure 3.8 Fourier spectrum of the output of the 50J amplifier. The vertical axis is in arbitrary decibel units. The lower trace shows the voltage fluctuations when the servosystem is operating and it has been raised by 40dB to fit both traces onto the same graph. It can be seen that the gain follows the calculated profile quite closely.

these signals on the transmitted light at some level. It is also possible that the monitor photo-diode perceives other laser beam fluctuations as intensity noise thus concealing the level of stability actually achieved by the servosystem.

It should be noted that small changes in the positions and orientations of optical components could alter the shape and significance of low frequency peaks in the Fourier spectrum of the stabilised light.

Mains pickup could be a problem but this seems unlikely because of the irregular character of the signal at low frequencies. Argon Ion laser power supplies characteristically produce a regular series of peaks at 100Hz intervals which decrease in amplitude with increasing frequency.

There are three possible mechanisms by which intensity noise could be, or appear to be, imposed on the transmitted light. Firstly, it is possible that beam position or geometry fluctuations could couple into the intensity spectrum in several ways. Variations in the path of light through the Pockels cell will cause intensity fluctuations at some level; variations in sensitivity across the face of a photo-diode will produce apparent intensity fluctuations as the beam changes in size or shape or moves across the diode; small particles of dust on, or other imperfections in, the beam-splitters or the photo-diode windows will produce a similar effect. Secondly, it is possible that the higher feedback voltages required to correct for the larger fluctuations at low frequencies cause the Pockels cell to impose beam position or geometry fluctuations which are then coupled into the intensity spectrum as above.

A third possibility is that laser frequency fluctuations may couple into the intensity spectrum through the interference of two beams differing slightly in optical path and therefore in phase.

Before investigating the factors which might be limiting the performance of the system it is worth noting that the system was tested for biases of 50-80% of the input light transmitted with no significant variation in performance. The system also performed well at a bias point of 90% transmission though with some degradation in the quality of stabilisation achieved.

The monitor photo-diode and an associated focussing lens were used to investigate how much degradation there was in performance at a distance from the laser. The stability appeared to be unaffected up to six metres from the intensity stabilisation optics, see Figure 3.9.

3:5 INVESTIGATIONS OF THE FACTORS LIMITING THE ACHIEVED INTENSITY STABILISATION OF AN ARGON ION LASER

3:5.1 LASER BEAM POSITION OR GEOMETRY FLUCTUATIONS

Position or geometry fluctuations in laser light may be produced by inhomogeneities in the laser medium or vibrations in the mirror mounts which alter the mode structure within the resonator. Figure 3.10 shows the optical arrangement used to observe the beam positional fluctuations and investigate whether these might be limiting the achieved stability in the transmitted light. The level of beam positional fluctuations were observed using a quadrant photo-diode. Observing the difference currents from opposite quadrants produces two orthogonal components of positional fluctuations. If the spot is well centred on the diode then this sensor becomes relatively insensitive to intensity fluctuations. This holds true so long as the beam movements are a small fraction of the spot size.

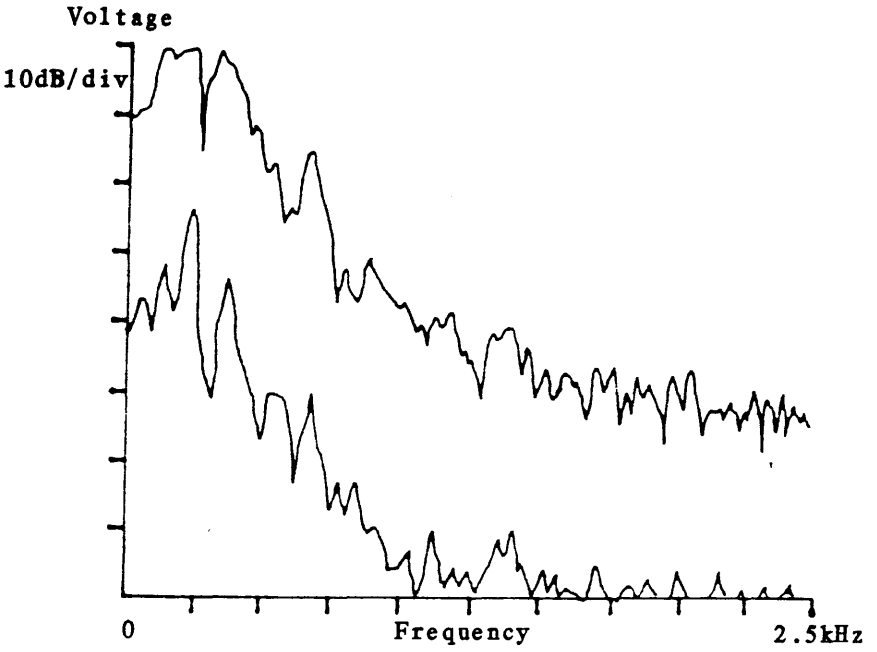

Figure 3.9 Fourier spectra of the fluctuations in intensity observed by a monitoring photodiode when separated by 5.47 metres from the intensity stabilisation system. The lower trace shows the improvement in intensity fluctuations when the system is in operation, compared to the upper trace when the system is not operating. In this case $V_o = 0.85 * V_\pi$.

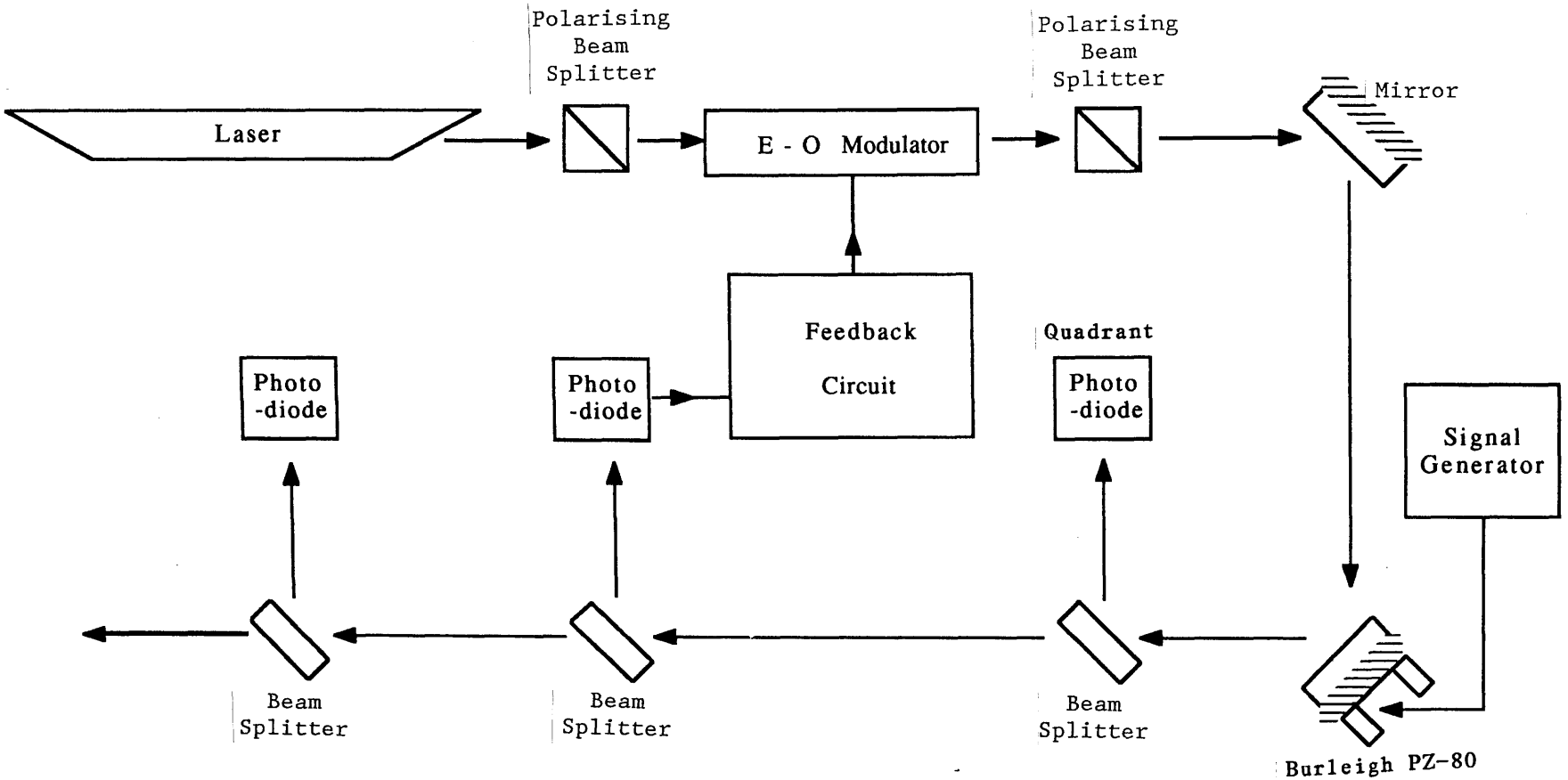

Figure 3.10 A schematic of the experimental layout used to examine the contribution of laser beam positional fluctuations to the factors limiting the performance of the laser intensity stabilisation system. A mirror mounted on PZT actuators was used to calibrate the natural level of laser beam fluctuations.

To determine the level of positional fluctuations produced by the laser a Burleigh PZ-80 was used to produce a calibration signal. This unit consisted of a mirror (diameter = 2.54 cm) mounted on three piezo-electric transducers so that the mirror could be tilted or moved to and fro. For simplicity of comparison only one of these transducers was employed at any one time. The mount provided an angular tilt of the mirror of 0.06 arcsec/V when a single transducer was used. Since the incident beam was not certain to be coincident with the mirror's axis of rotation there was also a transverse shift in the reflected beam. However, it was comparatively simple to calculate the relative magnitudes of the two components in terms of a beam displacement.

Consider a ray incident at some angle, $\emptyset$, on the mirror at a distance, r, from the axis of rotation. Now if the mirror moves by some small angle, θ, then the reflected beam will experience a transverse shift of $r * \theta * 2 \sin(\emptyset)$. The beam will also experience an angular deviation of $2 * \theta$. The shift in beam position due to the angular movement will clearly dominate the transverse shift at some distance, d, from the mirror. From the above for the angular component to dominate then $d > r * \sin(\emptyset)$; ie. within one mirror radius from the point of reflection, see Figure 3.11. Therefore, the imposed signal may be regarded as being a purely angular beam motion.

Beam position fluctuations may be reduced substantially by decoupling the resonator mirrors from the laser tube mounting. The water which acts as a coolant in Argon Ion lasers has a tendency to vibrate the entire resonator structure which leads to excess beam position and geometry fluctuations. The mirrors were removed from the resonator structure for some experiments but as it was difficult to maintain the rigidity of the resonator in these circumstances little

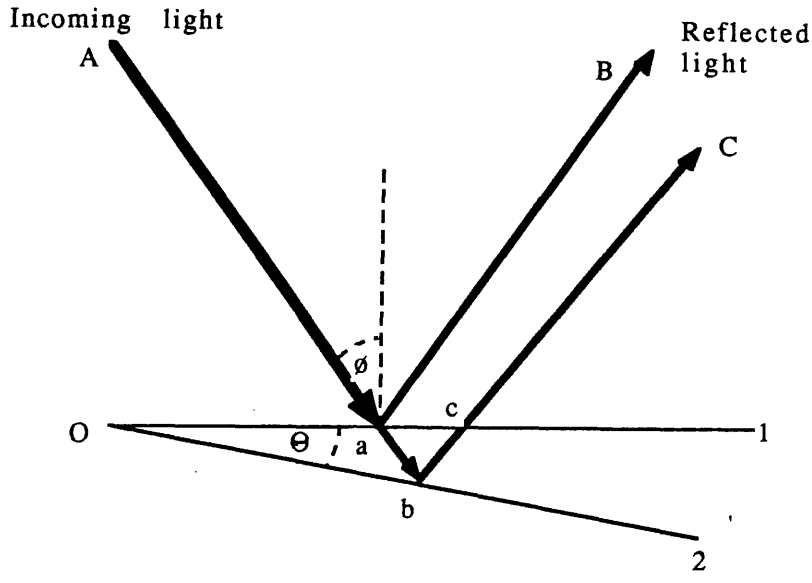

Figure 3.11 In the above arrangement consider an observer who detects the light reflected from point a at B. Now if the mirror is rotated through an angle, Θ, then there are two effects:

a) There is a transverse shift of the beam, ie. it now appears to the observer to emanate from c.

b) The direction of travel of the reflected beam has been rotated by $2 * \Theta$.

Now if the angle of incidence of the original beam was ø then the translation may be approximated by taking the bisector of angle abc. If the bisector is extended to line ac then, because Θ is small, it will have length r * Θ and will bisect line ac. The distance ac/2 is then given by r * Θ * sin ø.

new information was obtained. In fact the laser frequency noise became more prominent and the laser intensity was very sensitive to acoustic pick-up. However, it should be noted that a laser has been successfully rebuilt at Glasgow with a separate, rigid resonator and utilising feedback techniques to reduce frequency noise[77].

To check for the importance of beam positional fluctuations the intensity noise spectrum with the loop closed was compared with the beam positional fluctuation spectrum from the quadrant photo-diode. It can be seen in Figure 3.12 that there are several features which appear in both spectra and have the same relative significance with respect to the applied test peak. This indicates that beam movements may well be coupling into the perceived intensity noise at such a level as to limit the intensity stabilisation achieved. However, it is possible to adjust the orientation of the monitoring photo-diode so that the relative significance of the test peak varies by several dBs with respect to the laser-originated background. This could be explained by the difference between the beam movement due to the test signal and the natural beam movement. The Burleigh mirror was vibrated in one axis only while the laser produced random motion of the beam position over the plane of the diode face. It is possible that a particular orientation of the diode might be more or less sensitive to beam movement in a particular dimension, however it will still be susceptible to the sum of the laser-originated movements in all other directions and therefore the perceived background level will change much less.

Inspection of the beam positional fluctuations under conditions of the intensity stabilisation loop open and closed shows that the beam is well centred on the quadrant photo-diode if the spectrum remains constant. This observation is also evidence that the Pockels cell control element is not imposing position or geometry

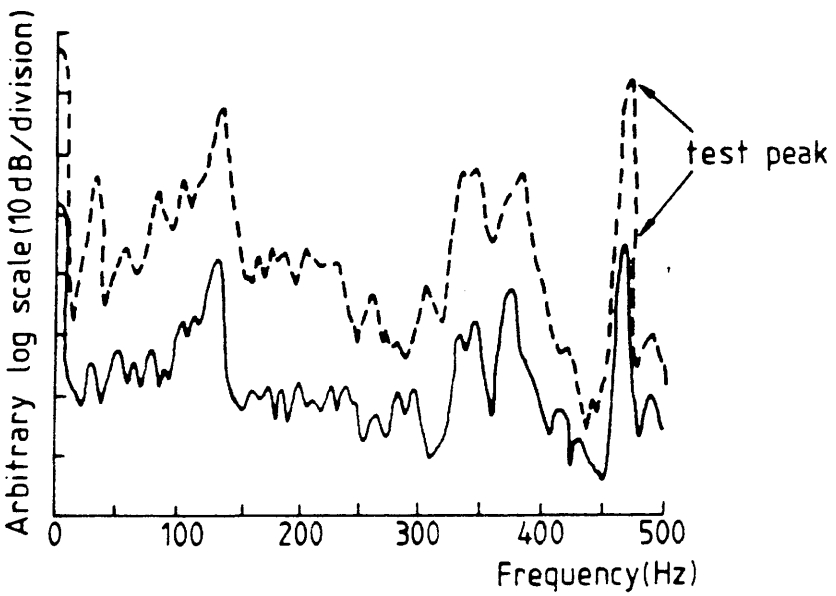

Figure 3.12 Comparison of Fourier spectra of laser-beam-position fluctuations (dotted curve) and residual laser-intensity fluctuations with the stabilisation system in operation (solid curve).

fluctuations on to the transmitted light at any significant level. However to investigate this further an intensity peak was imposed on the light before the Pockels cell control element. To do this a half-wave plate and a second Pockels cell were introduced to the beam path before the first of the polarisation analysers. The half-wave plate, the added Pockels cell and the first analyser are equivalent optically to the transducer of the intensity stabilising system since the laser output is highly polarised. The added Pockels cell was biased to allow 80% transmission and a sinusoidal signal of ~ 500Hz was applied to it. The relative level of the test peak was observed on the monitor photo-diode with the loop open and closed. The output of the error point of the stabilising loop demonstrates the available gain at the frequency of the test peak; and all of the available gain is not seen as a reduction in the test peak. A spectrum from the quadrant photo-diode confirms that the Pockels cell is producing a psuedo-intensity peak while compensating for the imposed peak. However, the level of beam position and geometry fluctuations imposed by the Pockels cell is at too low a level to limit the system in its present configuration.

3:5.2 LASER BEAM FREQUENCY FLUCTUATIONS

To measure the intrinsic frequency noise of the laser a tuneable Fabry-Perot cavity (Coherent Tropel) is used in the arrangement shown in Figure 3.13. The intensity of light transmitted by the test cavity is dependent on how close the cavity resonant frequency and the input laser light frequency are in the frequency domain. The transmitted light is incident on a photo-diode and the output is passed to a differential amplifier which also receives a signal from the monitoring photo-diode. The system is arranged so

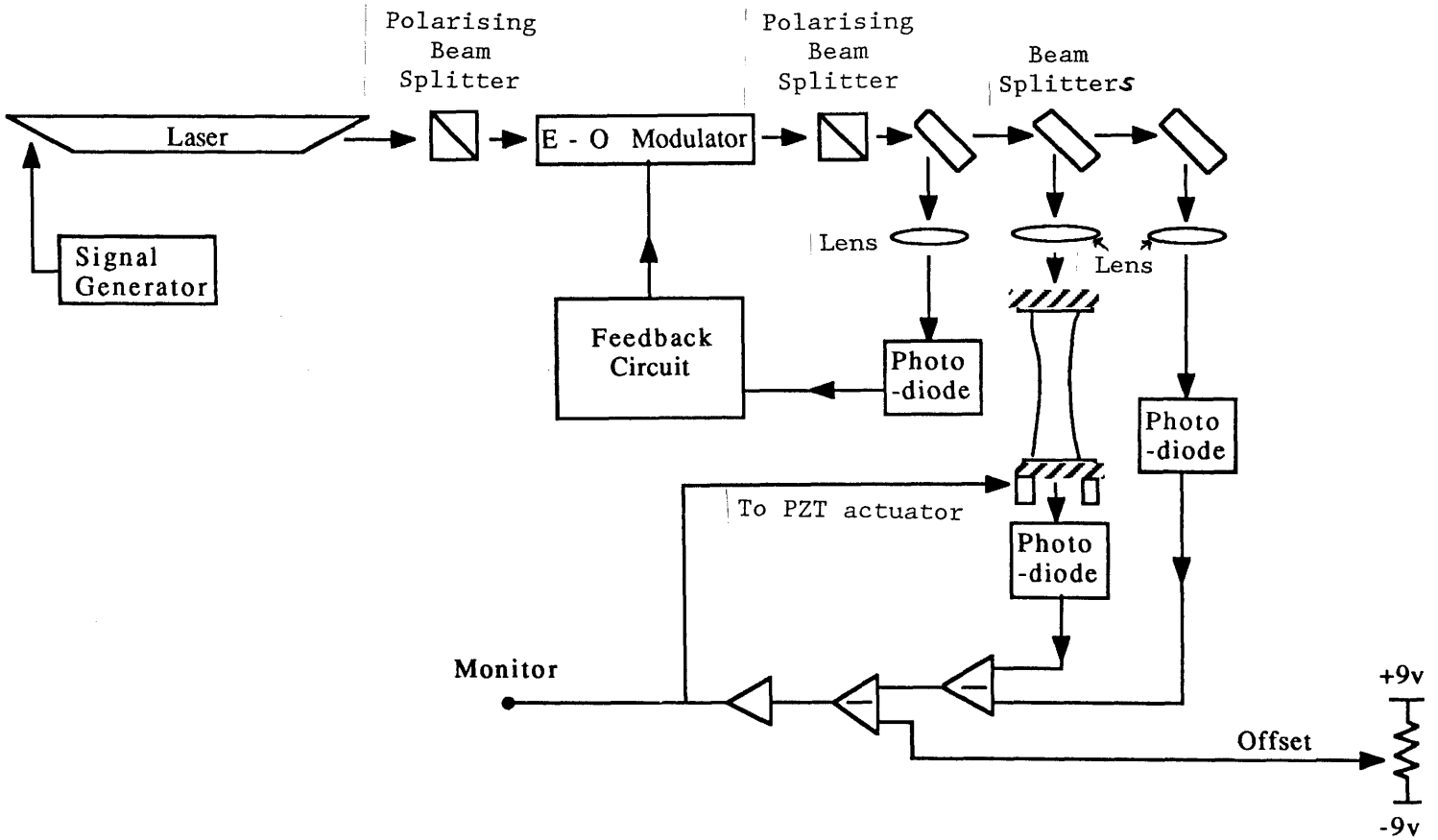

Figure 3.13 A schematic representation of the experimental arrangement used to measure the frequency fluctuations of the laser light and to determine whether or not this was a factor limiting the degree of intensity stabilisation achieved. The rear mirror in the laser cavity was mounted on a PZT transducer to provide a calibration peak.

that the output from the differential amplifier is zero when the laser light is resonating at the half-power point of the cavity transmission curve. It should be noted that the input from the second photo-diode makes the system relatively insensitive to intensity fluctuations. The amplitude of the signal from the differential amplifier is proportional to how closely the cavity follows the laser frequency fluctuations. The output of the differential amplifier is filtered and amplified and transferred to the piezo-electric transducer which alters the length of the tuneable cavity to keep it in resonance at the half-power point. This signal is a measure of the laser frequency fluctuations and is monitored by a spectrum analyser. An air-spaced etalon is positioned within the laser cavity to make the laser operate in single longitudinal mode and so reduce the laser frequency fluctuations to a level at which they can be measured.

To calibrate the level of frequency fluctuations observed and to investigate how frequency noise coupled into the intensity spectra the back mirror of the laser resonator was mounted on a piezo-electric transducer which allowed the laser cavity length to be altered thus introducing a frequency fluctuation of known origin and amplitude.

The piezo-electric transducer within the laser moved the mirror $6 * 10^{-10}$ m/V. The applied signal was $24V_{pp}$ and this produced a frequency fluctuation of ~ 2.7MHz rms. Comparing this to the test peak displayed on the Tropel output shows that the intrinsic laser frequency fluctuations are on average at a level of ~ 1 $MHz/Hz^{1/2}$ below ~ 500Hz. The frequency noise falls rapidly above ~ 500Hz. Comparison of the shape and significance of the frequency test peak on the locked intensity noise spectrum and the frequency spectrum (Figure 3.14) shows that the level is consistent with

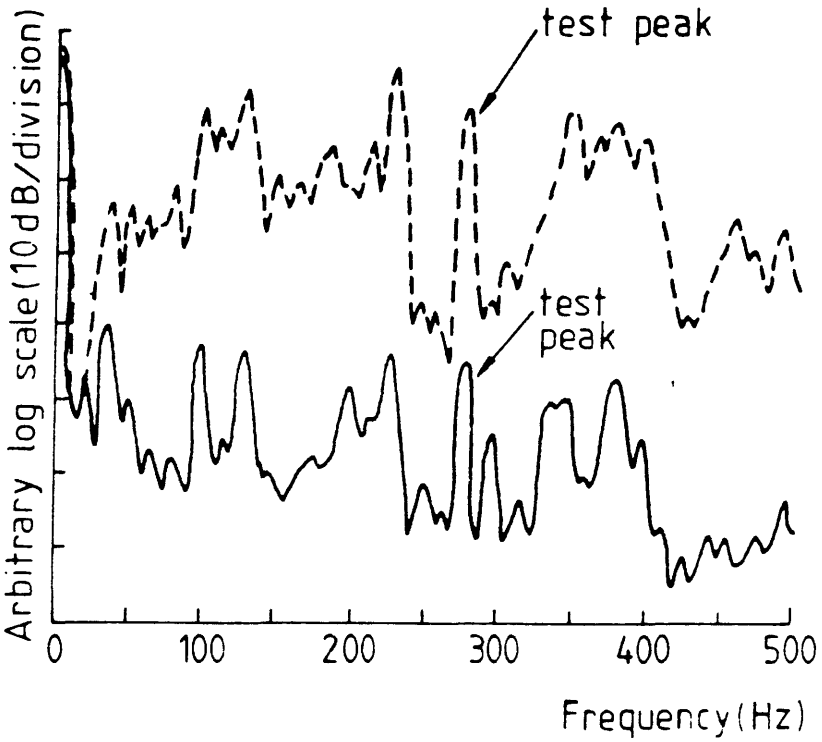

Figure 3.14 Comparison of Fourier spectra of laser-frequency noise (dotted curve), and the residual laser-intensity fluctuations with the stabilisation system in operation (solid curve).

frequency noise limiting the system performance below ~ 500Hz. However, there is no indication that this can account for all of the excess noise in the locked intensity noise spectrum. It was also noted that the apparent level of intensity stability achieved varied with the removal or replacement of the focussing lens associated with the monitoring photo-diode. The frequency spectrum showed no corresponding change. It is possible that the laser mirror does not just move to and fro but may in fact produce laser beam position or geometry fluctuations. If this is the case then the presence or absence of the lens may alter the sensitivity of the monitoring photo-diode to these motions. In fact the output of the quadrant photo-diode does reveal a component of laser beam position fluctuations which correspond to the induced frequency peak. The frequency peak also appears on the closed-loop intensity spectrum.

3:6 CONCLUSIONS AND FINAL REMARKS

To summarise the above results: an intensity stabilisation system utilising an electro-optic modulator has been constructed and tested for quality of performance. The system has been shown to have sufficient loop gain to achieve photon shot-noise limited performance in 1mW of sampled light down to ~ 1 kHz. It has been found that the intrinsic position, geometry and frequency fluctuations of the laser used are the major limiting factors in the performance of the stabilisation system. To achieve photon-noise limited performance below 1kHz it will be necessary to employ passive, or active, beam position and frequency stabilisation systems. Spatial filtering techniques may also prove useful[78,79].

A further test of the system and the experimental conclusions was carried out using approximately 1.5 metres of mono-mode

stepped-index optical fibre placed in the beam path after the Pockels cell and polarisation analysers but before the sample for the loop photo-diode is split off, as in Figure 3.15. The monitoring photo-diode sampled light leaving the fibre and revealed a much improved performance in the level of stability achieved. The output light shows intensity fluctuations at a level consistent with photon shot-noise above 400Hz in the 7mW of detected light, Figure 3.16, as a result of the fibre's beam cleaning action. This is consistent with the results above. The fibre should reduce significantly the level of beam position and geometry fluctuations since it will only transmit the fundamental mode of the laser beam. The frequency noise of the transmitted light will be relatively unaffected by passing through the fibre although there will be some reduction in the amount of scattered light reaching the photo-diodes.

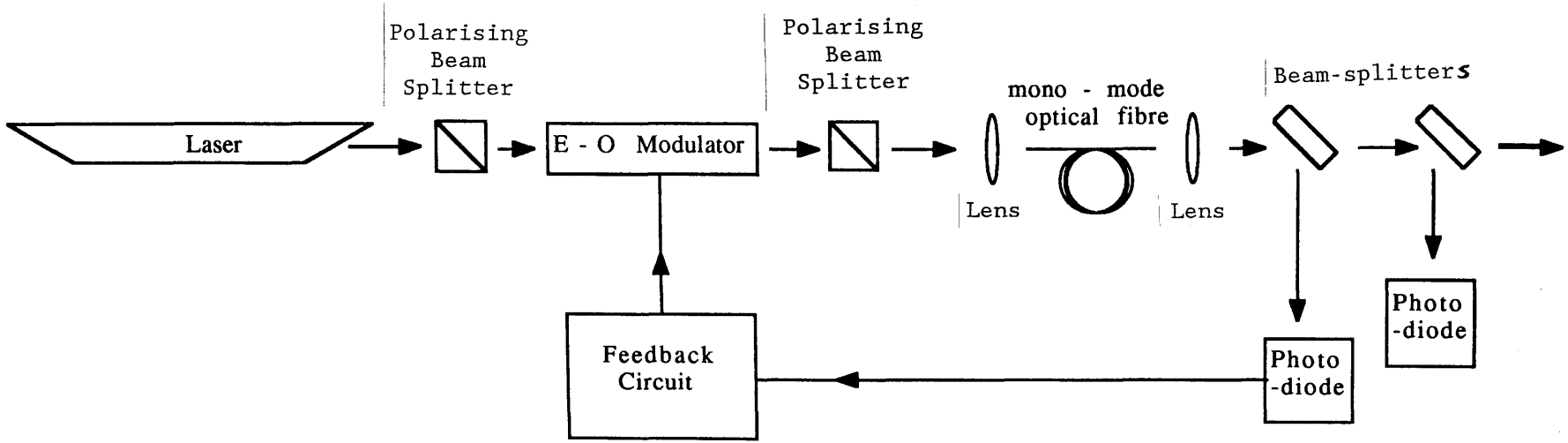

Figure 3.15 The experimental arrangement used to demonstrate the possible improvement in the observed performance of the laser intensity stabilisation system when a length of mono - mode optical fibre is used to reduce beam geometry fluctuations.

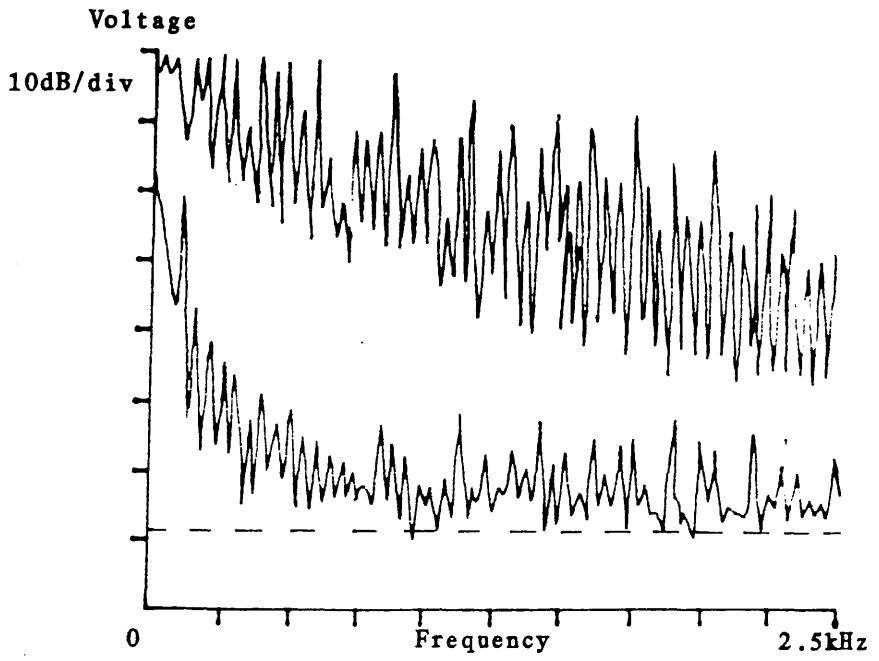

Figure 3.16 Fourier spectra of the relative intensity fluctuations observed by a monitoring photo-diode under conditions of the servosystem open(top) and closed(bottom) loop. In this case $V_o = 0.85 * V_\pi$ and the light has been passed through a mono-mode optical fibre prior to sampling. The dashed line indicates the approximate level of photon shot noise fluctuations.

CHAPTER 4

AN ANALYSIS OF TWO FEEDBACK CIRCUITS

4:1 PRINCIPLES OF FEEDBACK SYSTEMS

The prototype gravitational radiation detector being developed at Glasgow makes extensive use of feedback systems to reduce the effects of otherwise seriously limiting noise sources and to hold the Fabry-Perot cavities on resonance. These feedback systems are of novel design and frequently incorporate several stages of amplification and filtering to achieve the desired response. It is helpful when designing such circuits to be aware of the possible problems encountered with feedback systems and some of the inherent limitations. This chapter presents an analysis of two such circuits constructed by the author and considers design aims and stability criteria.

Any negative feedback system may be depicted schematically as below:

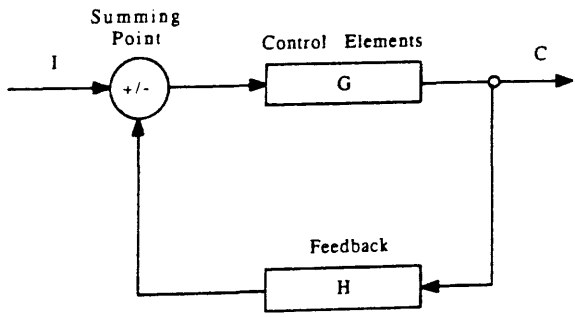

Figure 4.1

Where I is the input.

G is the forward transfer function.

H is the feedback transfer function.

ε is the sum of the input and feedback signals.

Other useful definitions are:

$F/\varepsilon = GH$ = Open-loop transfer function.

C/I = Closed-loop transfer function.

ε/I = Error ratio.

F/I = Primary feedback ratio.

These quantities are related simply by the following equations:

$$\frac{C}{I} = \frac{G}{1 + GH} \tag{4.1}$$

$$\frac{\varepsilon}{I} = \frac{1}{1 + GH} \tag{4.2}$$

$$\frac{F}{I} = \frac{GH}{1 + GH} \tag{4.3}$$

The primary requirements of a feedback system are high gain coupled with stable operation. A simple definition of stability is that the system response to a bounded input is bounded. A common problem with high gain negative feedback systems is a tendency to enter a region of oscillation which is self-sustaining. Many systems are designed to be unconditionally stable, that is the gain may be varied continuously from a low value up to the maximum point at which the system is still stable. In some cases unconditional stability is not an important requirement and the system may be designed to give higher maximum gain with the loss of stable operation at low gain.

Calculation of the stability of a particular system is usually achieved by consideration of the circuit response to an impulse in the complex s-domain. The technique used to transform time functions

to frequency dependent functions of a complex variable is the Laplace transform. So, given a function f(t) where f is a real function of a real variable, t, the complex function F(s) is given by:

$$F(s) = L[f(t)] = \int f(t)e^{-st}dt \qquad (4.4)$$

In the above s is a complex variable, $s = \sigma + i\omega$ where σ and ω are real and $i=(-1)^{1/2}$.

The transfer function T(s) in the s-domain is given by:

$$T(s) = \frac{L[r(t)]}{L[e(t)]} = \frac{R(s)}{E(s)} \qquad (4.5)$$

Where r(t) and R(s) are the responses in the time- and s-domain respectively and e(t) and E(s) are the excitation functions in the time- and s-domains.

Thus the response in the s-domain is:

$$R(s) = T(s).E(s) \qquad (4.6)$$

Now instability will be caused when the response is infinite. These values of the response are called poles and are equivalent to:

$$T(s)^{-1} = 0 \qquad (4.7a)$$

or $$E(s)^{-1} = 0 \qquad (4.7b)$$

e(t) can be a unit impulse of infinite magnitude and zero width and when Fourier transformed this is an input in which all frequency components are present. The Laplace transform of such an input is unity.

So, the response in the time domain will be given by:

$$r(t) = L^{-1}T(s) \qquad (4.8)$$

Where L^{-1} is the inverse Laplace transform. T(s) may have several poles and therefore may be written as:

$$T(s) = \frac{1}{(s_1+a_1)} \cdot \frac{1}{(s_2+a_2)} \cdot \cdots\cdots \frac{K}{M} \qquad (4.9)$$

$-a_1$, $-a_2$, ... are the values of the poles in the complex s-plane, K is the gain factor and M represents those elements which are not poles.

Thus the time-dependent response will be composed of products of the form:

$$f(t) = L^{-1}\left[\frac{1}{s + a_i}\right] = \exp(-a_i t) \qquad (4.10)$$

Where $s_i = -a_i = \sigma_i + i\omega_i$; σ and ω are real.

And therefore:

$$f(t) = A \exp(s_i t) \qquad (4.11)$$

Now if σ_i is positive then the response will be unbounded. If σ_i is zero then the system will oscillate with constant amplitude. Only in the case of σ_i being negative will the time dependent response decay away exponentially.

The transfer function T(s) is a complex function of a complex variable and two two-dimensional graphs are required for displaying it.

The first is a plot of σ against $i\omega$ in the complex s-plane. The Nyquist Path is a construction which encloses the entire Right-Half Plane of the complex s-plane. It does not include singularities at the origin or on the $i\omega$ axis. The Nyquist Path therefore encloses all the poles of the transfer equation which have $\sigma > 0$.

The second graph is a mapping of s onto the complex T(s) plane. That is T(s) is plotted with ω as a parameter where $-\infty \leq \omega \leq \infty$ and forms a closed contour. The plot for $0 \leq \omega \leq \infty$ is a mirror image about the Real T(s) axis of the plot for $-\infty \leq \omega \leq 0$.

In the special case of $\sigma = 0$ the s-plane degenerates into a straight line $s = i\omega$. The locus of $T(i\omega)$ then defines the boundary between the area of positive σ and negative σ and is known as a Polar, or Nyquist, plot.

Using the properties of the mapping it can be shown that the area to the right of the $T(i\omega)$ locus has $\sigma > 0$, where positive direction is along the line of increasing frequency. The area to the right of the locus is said to be enclosed.

The stability of a servosystem is determined by the closed-loop transfer function. From equation 4.1 it can be seen that the equation which defines the poles of the closed-loop transfer function, ie. the characteristic equation, is:

$$1 + GH(s) = 0 \tag{4.12}$$

Now if the servosystem is not to become unstable then $\sigma < 0$ for the pole of the closed-loop transfer function. Poles and zeros of $1 + GH(s)$ enclosed by the Nyquist Path map onto the GH(s) plane as clockwise and counter-clockwise encirclements respectively of the (-1,0) point. A clockwise encirclement means that the (-1,0) point is enclosed and so $\sigma > 0$. Therefore, the Nyquist stability criterion may be stated thus: the closed-loop control system whose open-loop transfer function is GH(s) is stable if and only if:

$$N = -P_o \leq 0 \tag{4.13}$$

Where P_o is the number of poles enclosed by the Nyquist Path and N is the number of clockwise encirclements of the (-1,0)

point in the GH(s) plane. Thus for stability the point (-1,0) must not be enclosed by the locus of GH(iw).

Assuming that the servosystem satisfies the above criterion there is a further consideration. Although the system may be shown to be mathematically stable it is important to have some knowledge of the degree of stability, ie. how easily the system may be made unstable. Nyquist plots and the closely related Bode plots allow the relative stability of a system to be calculated. This information allows trade-offs to be made between gain and bandwidth as requirements vary with applications. Bode plots are composed of two graphs both with frequency as the horizontal axis. One of the plots is of the magnitude of $GH(i\omega)$ and the other of the phase angle of $GH(i\omega)$ [or $\arg(GH(i\omega))$].

Now, consider a simple first order system. The response of the system to a transient will be damped with a time constant, τ, where $\tau = 1/\sigma$. However, GH(s) is typically a second or third order function.

The transient response of a second, or higher, order system can be characterised to good approximation by a linear, constant coefficient, second order differential equation of the form[80]:

$$\frac{d^2y}{dt^2} + 2\xi\omega_n \frac{dy}{dt} + \omega_n^2 y = \omega_n^2 x \qquad (4.14)$$

Where x is the input, e(t), and the forced response of this equation represents the transient response of the higher order system.

The coefficient, ξ, is called the damping ratio and is defined as σ/ω_n. ω_n is the undamped natural frequency and is related to ω_d, the damped natural frequency by:

$$\omega_d = \omega_n (1 - \xi^2)^{1/2} \qquad (4.15)$$

The damped natural frequency is the frequency at which $|GH(i\omega)|=1$. The undamped natural frequency is that frequency at which the locus of $GH(i\omega)$ intersects the point $(-1,0)$, ie. the phase lag is 180^{o} at the unity gain point with no damping.

$\xi=1$ corresponds to a critically damped system and optimum stability. As ξ becomes smaller transient overshoot occurs and stability is reduced. As a rule of thumb, assuming that the response function satisfies the criterion for stability, ie. that the $(-1,0)$ point is to the left of the $GH(i\omega)$ locus, then the further the locus of $GH(i\omega)$ crosses the negative real axis from $(-1,0)$ the closer ξ approximates to 1. As the crossing point approaches $(-1,0)$ $\xi \longrightarrow 0$ and the system becomes unstable.

There are two useful quantities which may be determined from either Nyquist or Bode plots which will give a measure of a system's stability.

The first, Gain Margin, is defined as the magnitude of the reciprocal of the open-loop transfer function at the frequency, ω_{π} (equation 4.16). ω_{π} is that frequency at which the phase angle of the open-loop transfer function is -180^{o} and is known as the phase crossover frequency. On a Bode plot the gain margin is the number of dB below zero of the $|GH(i\omega)|$ plot at ω_{π}.

$$Gm = \frac{1}{|GH(i\omega_{\pi})|} \tag{4.16}$$

The second useful indicator of stability commonly extracted from these plots is the Phase Margin. The phase margin is defined as -180^{o} plus the phase angle of the open loop transfer function at the frequency of unity gain, ω_{1}, the gain crossover frequency. That is:

$$\phi_{PM} = [\ 180 + \arg GH(i\omega)\ ] \text{ degrees} \tag{4.17}$$

On a Nyquist plot the phase margin is the angle through which the $GH(i\omega)$ locus must be rotated to cross the negative real axis at the $(-1,0)$ point. When critical damping is a requirement then $\xi \sim 1$, and by reference to the second order system described by equation 4.14 the phase margin is constrained to be $\sim 70^{o}$.

This is not an exhaustive treatment of methods of feedback analysis. There are several methods available for investigating the properties of complex feedback circuits[80,81] but the Nyquist and Bode plots have been used in this treatment because of the wealth of information which may be extracted for a modest computational effort.

4:2.1 AN ACTIVE FREQUENCY STABILISATION SYSTEM

The first circuit to be considered in this chapter was designed as a high-gain wide bandwidth amplifier for a laser frequency stabilisation system. The frequency stability of the illuminating light is an important consideration for interferometric gravitational radiation detectors and, for example, in high resolution atomic spectroscopy. In the prototype Glasgow detector frequency noise can couple in through imbalances in the characteristics of the cavities and may prevent the detector reaching photon shot-noise limited sensitivity.

There are several techniques currently in use to actively reduce laser frequency fluctuations. The laser frequency is compared to a frequency reference and a control signal derived which is fed back to a transducer to control the laser frequency. A commonly used feedback element is an intra-cavity Pockels cell.

The frequency of the laser light was compared to a stable reference cavity (Tropel 216) and the error signal produced by

application of the reflection r.f. sideband technique developed at Glasgow[66]. The system discussed here was initially designed to apply the correcting signals to an intra-cavity Pockels cell. In the first experiments the signal was amplified and fed back to a transverse-cut ADP Pockels cell fitted with Brewster cut windows. The overall aim was for a system with high gain, low power loss and wide (>2MHz) bandwidth. The fundamental limitation, assuming that sufficient gain is provided by the servosystem, is the photon shot-noise in the detected light. If the gain is sufficiently high the servosystem will impose frequency fluctuations on the transmitted light at this level. The system is shown schematically in Figure 4.2.

4:2.2 THE CIRCUIT DESIGN AND ANALYSIS

The system was required to give very high gain in the kHz band where the gravitational radiation detector operates. Hence the unity gain point was designed to be at high frequency (~2MHz) and the gain increased steeply at low frequencies to achieve a smooth gain profile. To achieve stable locking of the servosystem the fast signals must be able to propagate even when the low frequency signals are at saturation level. To achieve these capabilities the circuit is of 'bypass' design and is shown in Figure 4.3.

Referring back to Figure 4.1 it is possible to characterise the servosystem as below:

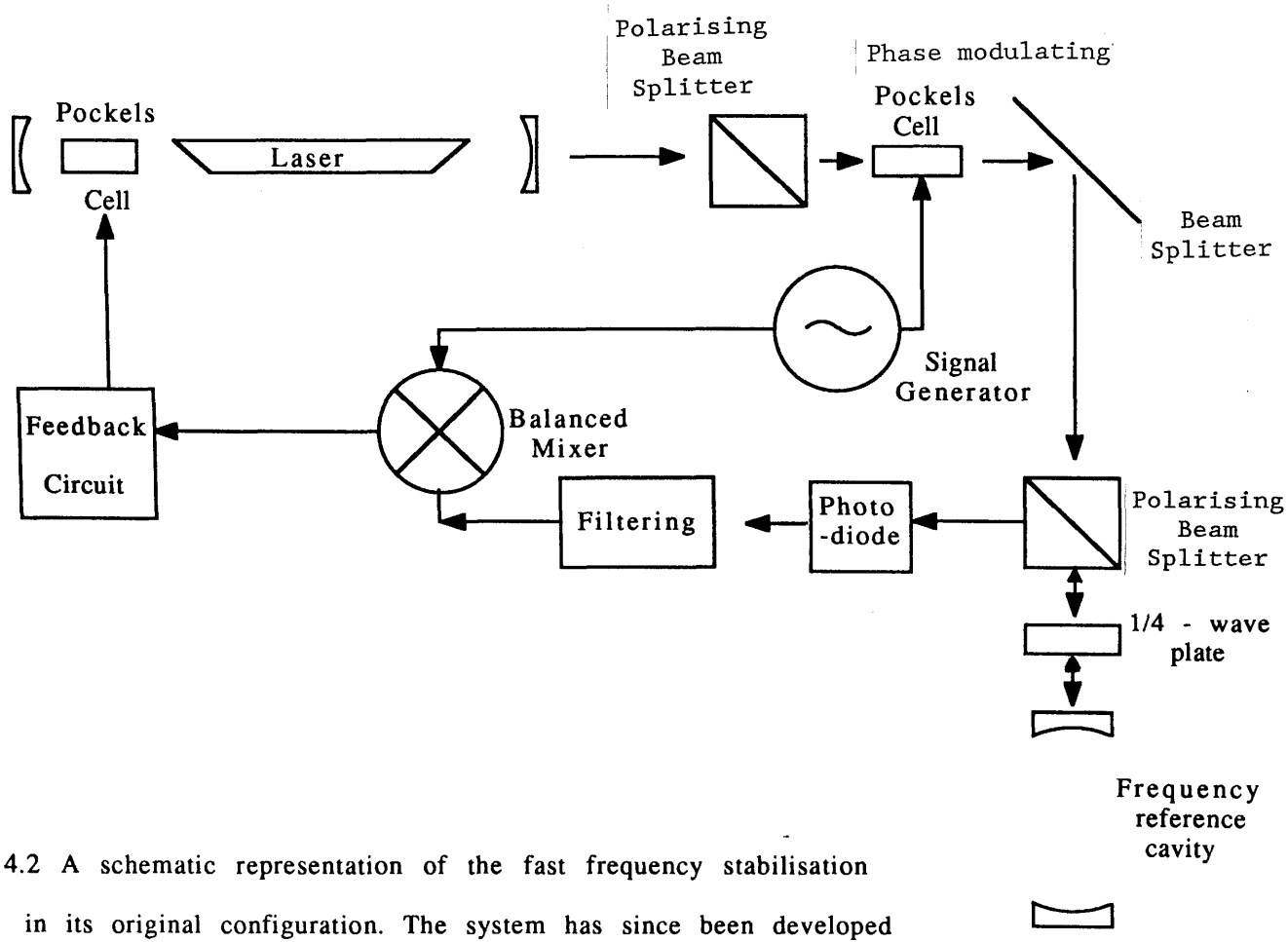

Figure 4.2 A schematic representation of the fast frequency stabilisation system in its original configuration. The system has since been developed to operate with one external Pockels cell and a PZT - mounted laser - cavity mirror.

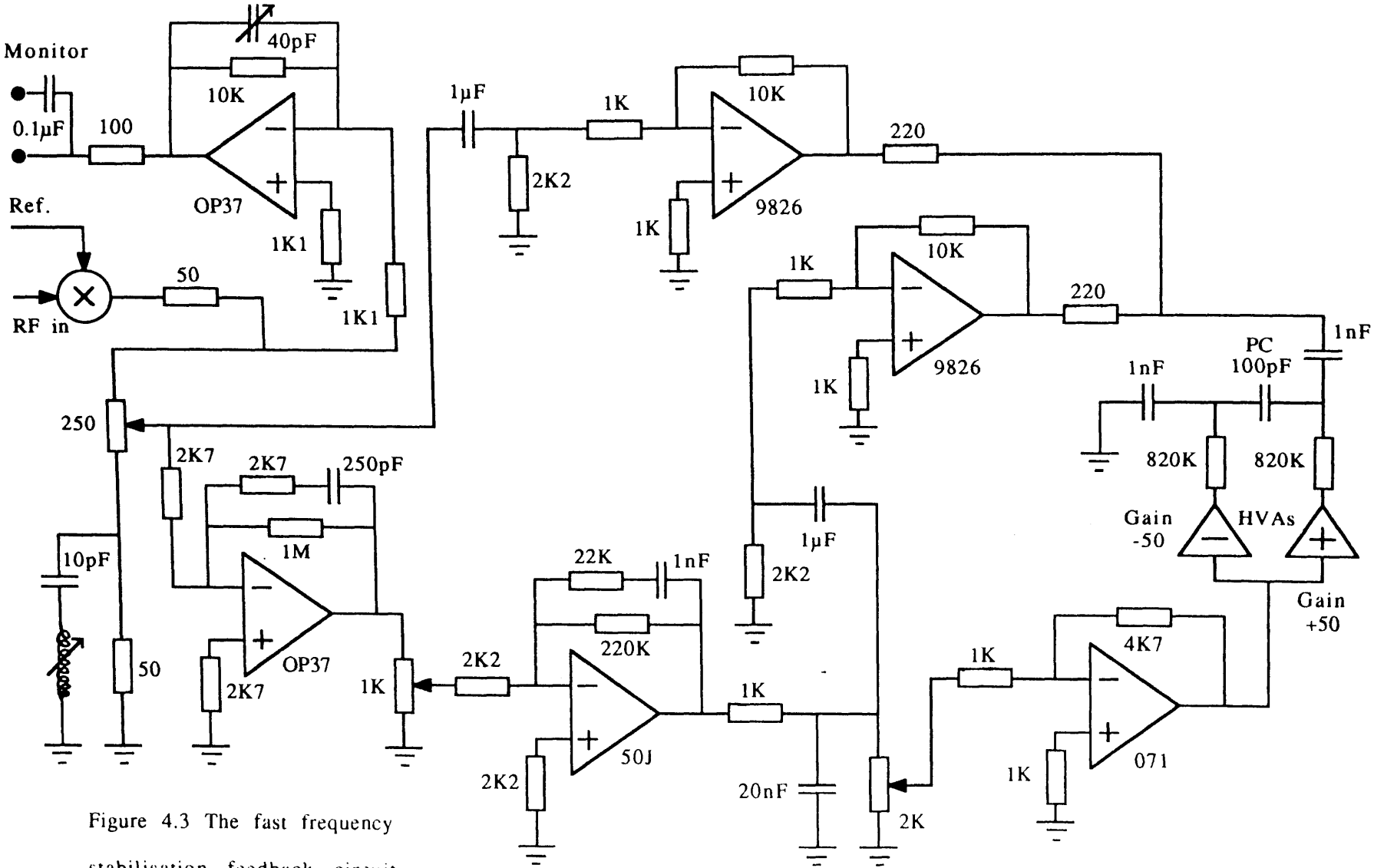

Figure 4.3 The fast frequency stabilisation feedback circuit.

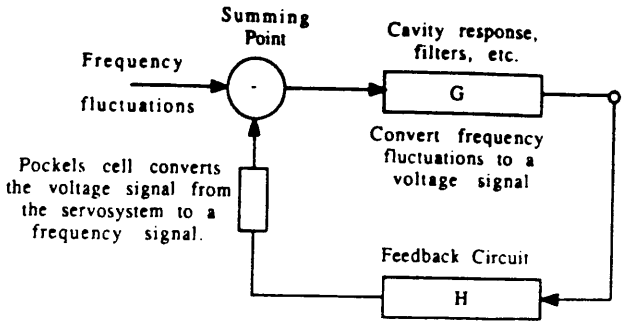

Figure 4.4

The open-loop transfer function, $GH(i\omega)$, includes several components. Apart from the response of the circuit itself there is the response of the photo-diode and of the reference cavity. After the amplification of the control signal there is a further conversion from the signal applied to the Pockels cell to a frequency change in the laser output. The output from the detecting photo-diode after suitable filtering is bipolar and the cavity bandwidth divided by the peak to peak voltage (for example 1 Volt is a typical value) yields the conversion factor for frequency noise to voltage signal. However the relationship is not truly linear and the ratio is larger by a factor two for small ($<<1.5$MHz) fluctuations which will be the case when the loop is closed. The relation is:

$$\delta V = \frac{2}{1.5*10^6} * \delta f \qquad (4.18)$$

The detection of frequency noise on the sampled light will be limited by the bandwidth of the reference cavity. In this case the reference cavity has a bandwidth of 1.5MHz. This implies that at the upper limits of the servosystem's operation the cavity will be acting as an integrator of frequency fluctuations. The time constant, τ, of the cavity is given by $2/\delta\omega$, where $\delta\omega$ is the cavity bandwidth. Therefore the cavity frequency response is:

$$\frac{f_o}{f_i} = \frac{1}{1+i\omega\tau} \tag{4.19}$$

Which can be rewritten as:

$$\frac{f_o}{f_i} = \frac{1-i\omega\tau}{1+\omega^2\tau^2} \tag{4.20}$$

Therefore the forward transfer function is given by:

$$G(i\omega) = \frac{\delta f}{7.5*10^5}\left[\frac{1-i\omega\tau}{1+\omega^2\tau^2}\right] \tag{4.21}$$

The feedback function is complicated by the presence of several 'branches' of the circuit and is consequently too long to present here other than as $H(i\omega)$ although the method of calculation is presented in Appendix A. The transfer function is:

$$GH(i\omega) = \frac{\delta f H(i\omega)}{7.5*10^5}\left[\frac{1-i\omega\tau}{1+\omega^2\tau^2}\right] \tag{4.22}$$

This function must also be multiplied by the factor which relates the voltage applied to the Pockels cell to the change in frequency of the laser output. Firstly, within a laser cavity:

$$\frac{\delta f}{f} = \frac{\delta l}{l} \tag{4.23}$$

Where l is the length of the laser cavity, 1.8 metres in this case.

The Pockels cell has a half-wave voltage of 800V at 514.5nm. So $\delta l = (514.5*10^{-9})/2$ when V = 800 volts. Therefore equation 4.23 may be rewritten:

$$\frac{\delta f}{f} = \frac{514.5*10^{-9}}{2 * 1.8}\frac{\delta V}{V_{1/2}} \tag{4.24}$$

And:

$$\delta f = 8.3 * 10^7 \frac{\delta V}{V_{1/2}} \qquad (4.25)$$

Which means that the open-loop gain is given by:

$$GH(i\omega) = 0.14 * H(i\omega) * \left[\frac{1 - i\omega\tau}{1 + \omega^2\tau^2} \right] \qquad (4.26)$$

This function is plotted in Figure 4.5 as Re[GH(iω)] against Im[GH(iω)]. It can be seen that the system satisfies the Nyquist criterion for stability. However, at high frequencies the locus of GH tends towards the negative real axis (-180°) asymptotically. Hence the Gain Margin is infinite which seems to imply that the gain may be increased without limit, without the system becoming unstable. This apparent lack of limits is caused by the simplicity of the circuit modelling. Each element in the circuit is treated as having no delay in its reaction to an input. In practice, of course, there will be propagation delays associated with each part of the circuit. The use of the 'bypass' design minimises the effects of these delays. At higher frequencies these delays will become significant and will eventually limit the gain of the system since they introduce a further phase shift. The magnitude of these propagation delays is not modelled but for stable operation it is usual to allow a phase margin of 45°. This corresponds to a maximum roll-off through the unity gain point on a Bode plot of 9dB/octave.

It is also clear from Figure 4.5 that if the gain is reduced then the servosystem will eventually become unstable when the unity gain point is at ~ 3kHz. This does not represent a real problem since in practice locking can be achieved without reducing the gain.

The computed Bode plots of the system response shown in Figure 4.6 serve to show how the stability of the servosystem will

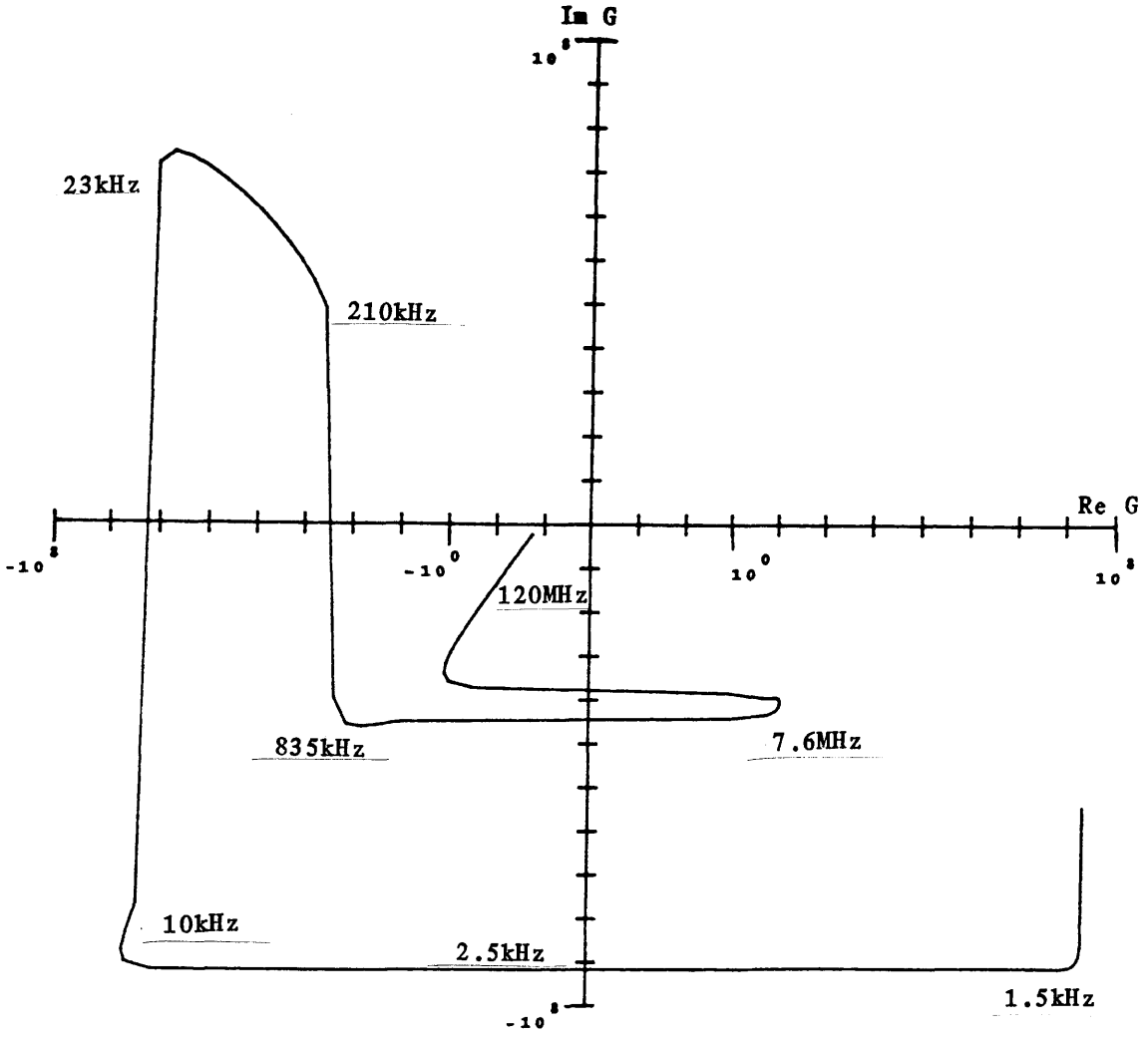

Figure 4.5 A Nyquist plot of the transfer function of the fast frequency stabilisation system indicating the situation of conditional stability.

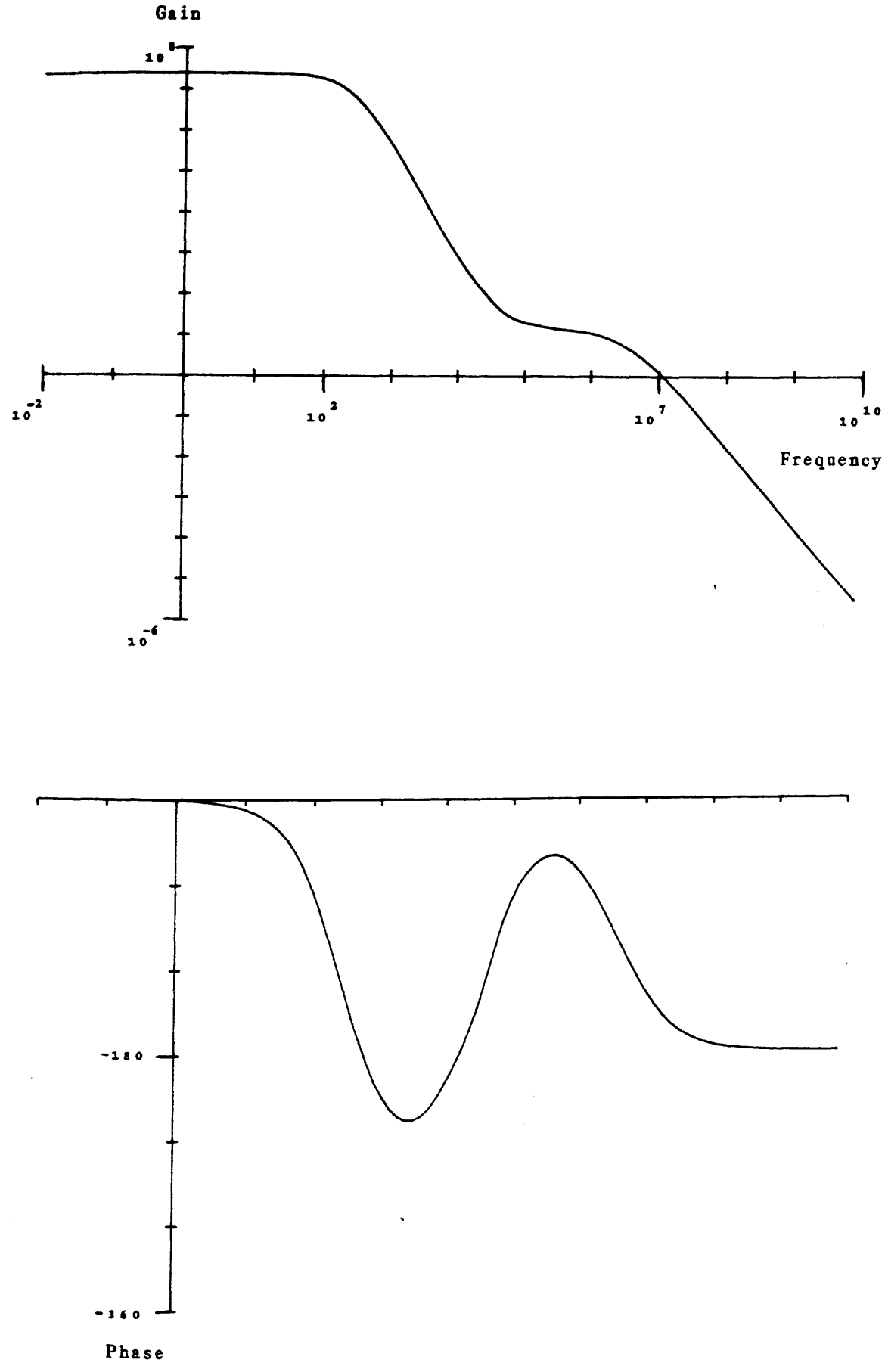

Figure 4.6 Bode plots of the transfer function of the fast frequency stabilisation system.

vary as the fraction of signal fed into the circuit is varied. It can be seen that the unity gain point (or damped natural frequency) is 12.6MHz. The roll-off through the unity gain point is 9dB/octave which corresponds to a phase margin of 45^{o}. By referring to the characteristics of a second order system this yields a damping ratio, $\xi = 0.4$[82], which allows a short ringing in the system response. The d.c. gain is $2.4*10^{7}$ and rolls off from around 100Hz. The roll-off reaches a maximum of about 15dB/octave at ~ 2.5kHz. The high frequency branch of the circuit dominates above ~ 120kHz.

For comparison consider the case where only one quarter of the detected signal is fed into the circuit. Now the d.c. gain is $6.1*10^{6}$ and the unity gain point is at ~ 5 MHz. The phase margin is now 70^{o}, ie. a roll-off of ~ 7dB/octave, which corresponds to $\xi = 0.8$[82]; the system is very near critical damping.

From the above it is clear that the system can be run with high gain and wide bandwidth and that it will be stable as required. The gain at which the system will actually become unstable is uncertain because of the uncertain nature of the limiting delays but this limit can be determined experimentally and it is clear that there is a wide range of gain over which the system will behave satisfactorily.

The system was used by Mr. G. Kerr and Dr. N. Robertson to stabilise a high power Argon Ion laser in a rebuilt cavity. Frequency noise in the stabilised laser light was reduced to a level of ~ $0.45Hz/Hz^{1/2}$ at 1kHz in preliminary trials.

The servosystem has since been developed by Mr. Kerr and Dr. Robertson to stabilise the same laser by using a slightly modified version of the circuit to drive a piezo-electrically controlled rear mirror. The higher frequency fluctuations were controlled by an extra-cavity electro-optic modulator. This overcame

the problem of power loss associated with intra-cavity Pockels cells and reduced the possibility of causing serious damage to the Pockels cell. This work has been published in reference [77].

4:3 A LASER INTENSITY STABILISATION SERVOSYSTEM

The second circuit to be considered was designed for the laser intensity stabilisation system described in the previous chapter. The circuit, shown in Figure 3.4, is slightly simpler than the previous example. For this particular application the bandwidth was dictated by external requirements rather than by the circuit design.

As noted in Chapter 3 the servosystem was required to stabilise the output intensity of a high power Argon Ion laser by varying the transmission of the laser output through an arrangement of two crossed polarisers and a four-crystal, transverse cut, ADP Pockels cell with a half-wave voltage of 280 Volts. The error signal was derived from a small sample (nominally 1mW) of the laser output. The intensity fluctuations of the Argon Ion laser required an open-loop gain of ~ 10^3 in the kHz region rising to greater than 10^4 at d.c.

Referring once more to Figure 4.1 the intensity stabilisation servosystem may be depicted schematically as in Figure 4.7 below.

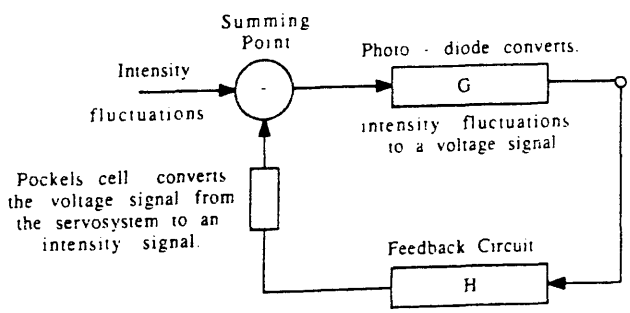

Figure 4.7

The sampled light is some constant fraction of the total output power of the laser and so it is easiest to consider only this sample which is incident on the photo-diode. The effect of the servosystem will then scale to the full laser output.

Consider I_o Watts of light incident on the photo-diode when the Pockels cell is biassed to maximum transmission ie. V_o = 280 Volts. If V_o = 0 Volts then the incident light intensity will fall to 0 Watts. It is possible to take a linear approximation $\delta I/\delta V = I_o/V_{1/2}$. Now when light is incident on the photo-diode a current flows into the inverting input of the 50J pre-amplifier. An intensity of I Watts causes a current of 0.25*I Amps to flow into the 100 Ohm resistor giving a voltage drop of 25*I Volts. Therefore the signal applied to the Pockels cell is $25*I*G(i\omega)$ Volts, where $G(i\omega)$ is the frequency dependent voltage gain of the feedback circuit. So, if the output intensity changes by I_o Watts then the voltage applied to the Pockels cell will be $25*I_o*G(i\omega)$. The loop gain is then given by:

$$GH(i\omega) = \frac{\text{Volts produced by change } I_o}{\text{Volts to produce a change } I_o} \qquad (4.27)$$

Or:

$$GH(i\omega) = 25*G(i\omega)* \frac{I_o}{V_{1/2}} \qquad (4.28)$$

However, the transmission curve is not a linear function of voltage. Referring to equation 3:15 the voltage varies as:

$$I = I_o \sin^2 \left[\frac{\pi}{2} \frac{V_o}{V_{1/2}} \right] \qquad (4.29)$$

And so differentiating:

$$\frac{\delta I}{\delta V} = 2*I_o*k*\sin(kV_o)*\cos(kV_o) \qquad (4.30)$$

Where $k=\pi/(2*V_{1/2})$. Comparing this to the linear approximation of $\delta I/\delta V$ above gives the correction factor, $\pi*\sin(kV_o)*\cos(kV_o)$. Therefore, the Open Loop Gain is given by:

$$GH(i\omega) = \frac{25*I_o G(i\omega)}{V_{1/2}} *\pi*\sin(kV_o)*\cos(kV_o) \qquad (4.31)$$

The open loop gain is linearly dependent on the intensity of the sampled light. The choice of the biasing voltage, V_o, is of great importance. V_o determines the power being discarded by the system and the gain varies with V_o as in Figure 4.8. In practice the low values of loop gain which result in setting $V_o \sim V_{1/2}$ will not be the main limitation because as V_o approaches $V_{1/2}$ the servosystem loses dynamic range and so will lose lock readily.

In Figure 4.9 the computed Bode plots of the open loop gain of the system shows that the gain rolls off from about 200Hz at 6dBV/octave rising to greater than 12dBV/octave around 2kHz. The unity gain point varies from a maximum of 400kHz when $V_o = 0.5*V_{1/2}$ to 79.5kHz when $V_o = 0.9*V_{1/2}$ which corresponds to the maximum practicable transmission of the system for short timescales. For the same values of V_o the d.c. gain is 95dBV and 85dBV respectively. In normal operation the system was operated at a biasing voltage of $0.7*V_{1/2}$ which gives a d.c. gain of 93dBV and the unity gain point at 316kHz. The phase margin is $\sim 80^o$ ($\xi \sim 1$)[82] which could allow the gain to be increased if required although this would cause the unity gain point to rise above its design value.

The Nyquist plot shows that if the gain is reduced the system will operate stably until the crossing point at 3kHz reaches the

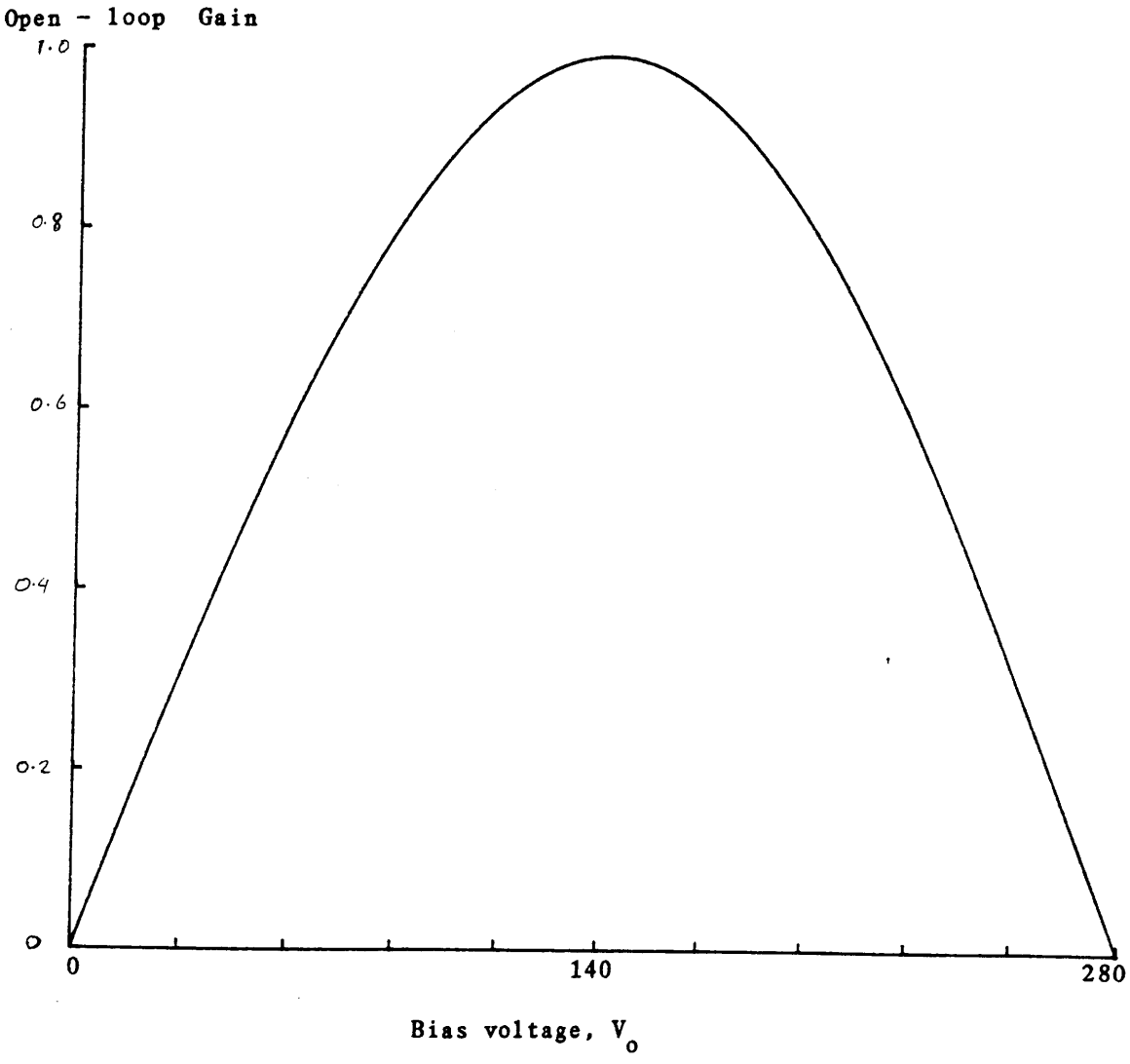

Figure 4.8 The variation of the open - loop gain of the intensity stabilisation system with the biassing voltage, V_o, over the range 0 - V_π. The maximum loop gain is achieved when $V_o = V_\pi$. However in this case 50% of the input laser light is rejected. This is undesirable when high laser powers are required. The practical operation of the servosystem involves a compromise between the desire for high gain and low losses of light.

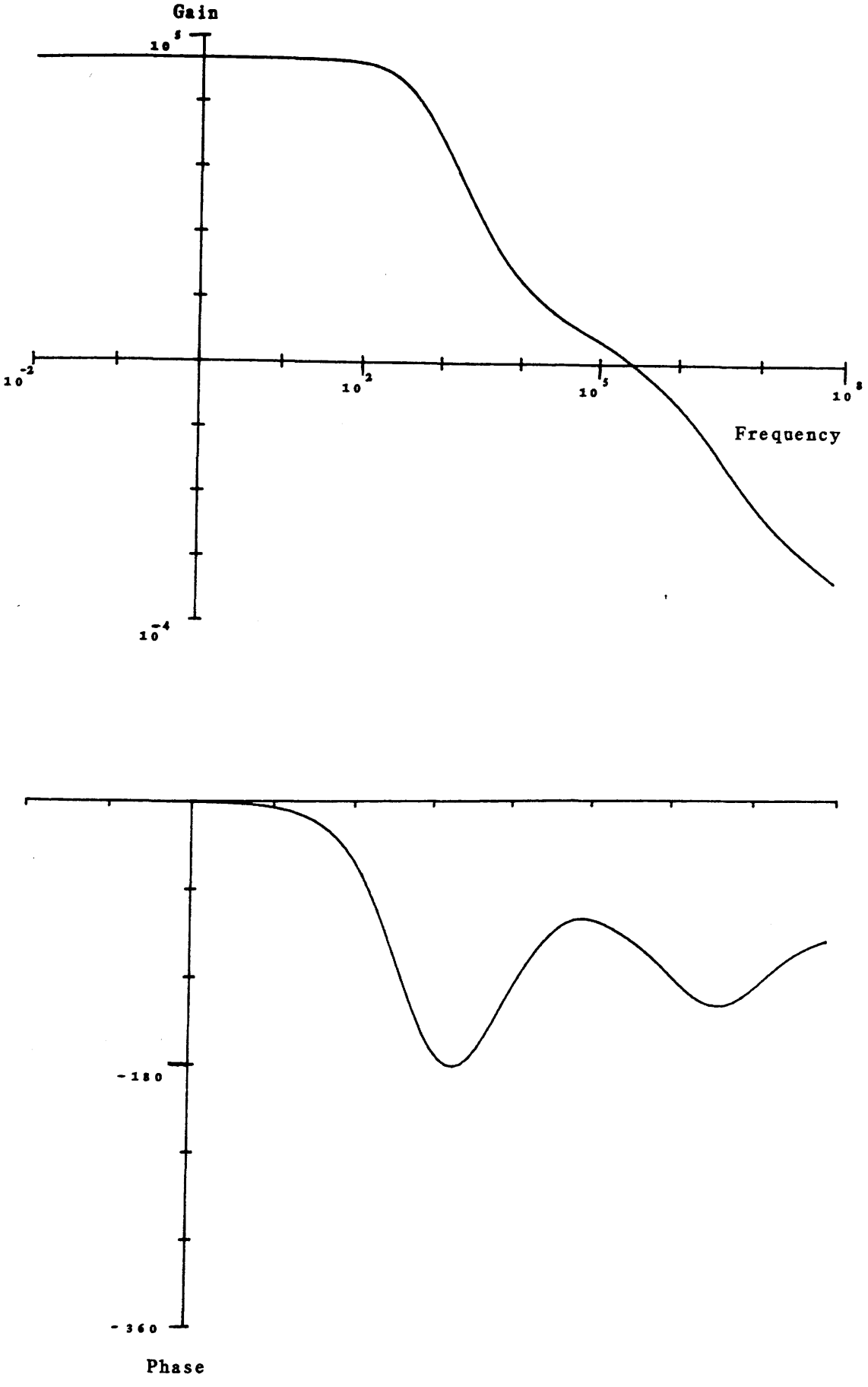

Figure 4.9 Bode plots of the transfer function of the intensity stabilisation system when $V_o = 0.7 * V_{\pi}$.

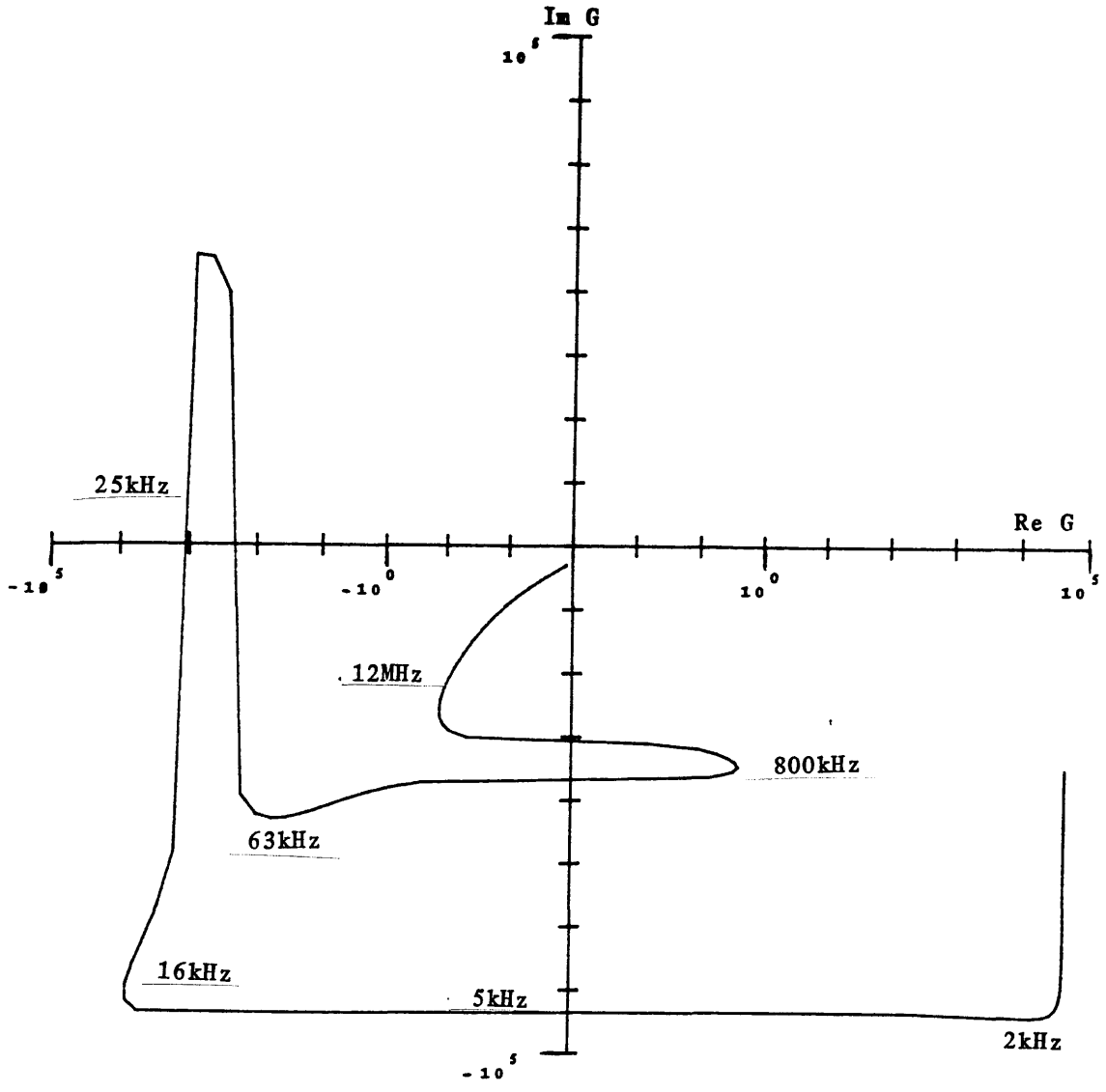

Figure 4.10 A Nyquist plot of the transfer function of the intensity stabilisation system when $V_o = 0.7 * V_\pi$.

(-1,0) point. However in practice the system is capable of attaining lock with the gain set higher than this and so it will not be a problem.

The observed open loop gain corresponded well to the calculated values. However as reported in the previous chapter the level of intensity stabilisation observed did not correspond to the gain available. The observed performance of the servosystem was limited by non-intensity noise sources which were detected as intensity noise. The use of a length of mono-mode stepped index fibre as a beam cleaner allowed the servosystem to approach its design performance over a wider range of frequencies.

CHAPTER 5

THE STABILISATION OF LASER BEAM GEOMETRY WITH OPTICAL FIBRES

5:1 AN INTRODUCTION TO OPTICAL FIBRES

The previous two chapters have been concerned with the reduction of intensity and frequency fluctuations in the light illuminating the cavities of an interferometric gravitational radiation detector. However, due to vibrations in the mirror mounts of the laser cavity and inhomogeneities of the laser medium the output light is also subject to geometrical fluctuations eg. position, angle, etc. Now, if the output beams of the interferometer are interfered at some angle, α, and the laser beam shows transverse fluctations, $\delta x(t)$, then there will be a spurious phase signal which will be observed as a fluctuation in the length of the cavities. This spurious signal is given by:

$$\delta l = k\, \alpha\, \delta x(t) \qquad (5.1)$$

Where k is a constant of proportionality. It has been shown that the geometrical fluctuations of a free-running argon ion laser can limit the displacement sensitivity of an interferometric gravitational radiation detector at a level as high as 10^{-15} m/Hz$^{1/2}$[67].

The reduction of otherwise seriously limiting fluctuations in the input laser beam has been achieved by the use of active systems in the foregoing chapters. A related development at Glasgow has been a beam position stabilisation system[78]. However, in some instances there are passive devices available which may provide ample

improvement in some aspect of beam quality and possibly a saving in lossy optical components. The waveguide properties of optical fibres may be useful in this context.

The geometrical fluctuations of a laser beam can be understood as variations in the mode structure of the propagating beam. Clearly if the optical fibre attenuates the higher order modes the emergent beam will have greater geometrical stability, provided that the end of the fibre is not free to vibrate. If the initial fluctuations are large enough to affect significantly the coupling of the beam into the fibre then the output will be intensity modulated. A combination of an intensity stabiliser and a fibre, with the fibre located after the transducer and prior to the sampling photo-diode, has the potential for providing a quiet, stable and clean beam (cf. Chapter 3). A possible limitation to the attractiveness of such a scheme is the maximum power which may be transmitted through a fibre and this will be discussed later.

An optical fibre typically consists of a glass (SiO_2) fibre with a GeO_2 doped core of small radius, typically a few microns, which is of slightly higher refractive index than the surrounding cladding. This type of fibre is known as stepped-index. Graded-index fibres have been constructed so that the refractive index falls off continuously from the fibre centre and so the core and cladding are essentially indistinguishable. The fibre is usually covered by a plastic sheath which provides protection and reduces the level of 'crosstalk' in fibre bunches. So, if n_{co} = refractive index of core and n_{cl} = refractive index of cladding then:

$$n_{co} - n_{cl} \ll 1 \qquad (5.2)$$

Now, applying Snell's law to a ray within the core striking the core/cladding interface it is clear that the critical angle will

be very large. For this reason optical fibres are known as weakly guiding. An appropriate choice of dimensions and refractive indices can reduce the number of waveguide modes a fibre can support. A mono-mode fibre is designed to support only the fundamental waveguide mode and it is this property which is useful for guiding the light into an interferometric gravitational wave detector.

The small size of the fibre core means that great care must be taken to introduce a laser beam into a fibre to achieve efficient coupling. A mode-matching lens is required to couple the input beam into the fibre and another to control the divergence of the output beam. The efficiency of the coupling will be treated in more detail later.

The glass core, which carries almost all of the power of the propagating beam, is slightly birefringent. The birefringence of the core changes with temperature, pressure and bending of the fibre. The effect of this is broadly the same as for the Pockels cell discussed in Chapter 3.

The fundamental mode in a fibre is not in fact one mode but consists of two orthogonal polarisation states. In a simple low birefringence fibre energy can be transferred easily from one polarisation state to another. However it is possible to construct a fibre which has a high value of birefringence which effectively reduces this coupling of the two states[83].

5:2 SUPPRESSION OF LASER BEAM POSITIONAL FLUCTUATIONS

To investigate in a simple way how optical fibres could be used to suppress beam position fluctuations several different lengths of a sample fibre were prepared and tested for suppression. To ensure that the light will couple into the fibre a flat, smooth surface must

be prepared. First the protective, plastic sheath was cut or burnt off. A light, scoring movement with a glass cutter was used to weaken the exposed fibre sufficiently so that bending caused a clean break. The new end was examined using a binocular microscope for any chips or 'spurs' which would reduce the coupling efficiency. With practice very good cleaves were possible with few attempts. For ease of handling, and to protect the fibre, each end was mounted in a piece of capillary tube as shown in Figure 5.1. A clear adhesive was used to bond the fibre into the tube and to affix a thin microscope cover slip over the end of the tube. Once the cover slip was in place the fibre was eased in until its end was in close contact with the cover. This meant that the fibre was well protected though without necessarily reducing the coupling efficiency.

A small fraction of the output of a Spectra Physics 165 Argon Ion laser running at 514.5nm was used to provide illumination. The test bed was a thick aluminium plate supported on rubber pads to minimise flexing and reduce vibrations coupling into the components. The input end of the mounted fibre was fixed to a precision mount which provided x, y and z movement and tilt and rotation.

To achieve efficient coupling of the input laser beam into the fibre it was necessary to use a mode-matching lens. Similarly, the divergence of the beam leaving the fibre was controlled with a second lens. The transmission was maximised by making repeated adjustments to each degree of freedom of the fibre mount until no further improvement was possible. In some instances very high transmissions were achieved due to the excitation of cladding modes. The light power is guided by the fibre but within the cladding which leads to a much more complex mode structure in the output beam. By curving the fibre slightly these modes can be suppressed and a true transmission level can be read. The longest length of fibre tested was arranged in

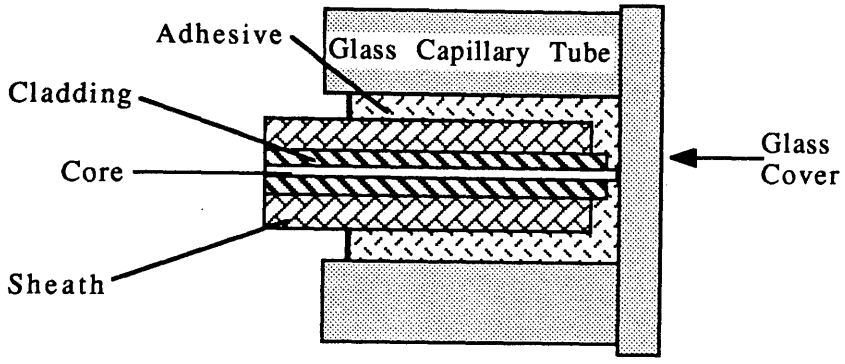

Figure 5.1 The handling and use of glass fibres can be eased by mounting in a suitable manner. This is one scheme which was tried but which had some disadvantages for use in an interferometric gravitational wave detector.

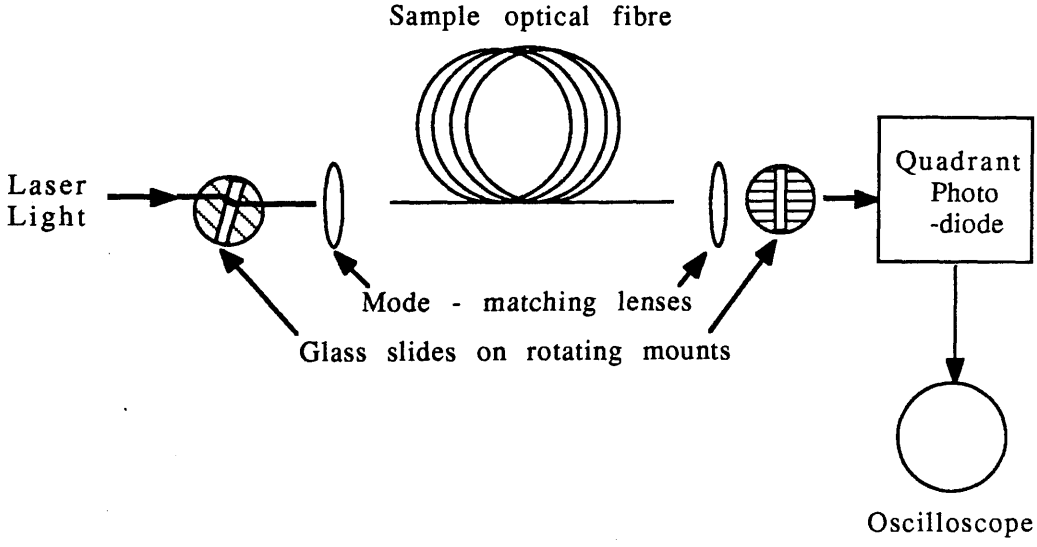

Figure 5.2 The mode - matching lenses and the sample of optical fibre are treated as a single unit. The degree of suppression of beam movement provided by the fibre can be found by comparing the signal from the quadrant photo - diode when a rotation is applied to the input and output beams. The bias current of the photo - diode is also recorded to ensure that the deviation does not affect the coupling of the light into the fibre.

coils of 30cm diameter.

To observe the effects of the fibre on the transmitted light a quadrant photo-diode was used with the signals from opposite quadrants subtracted to give signals for two orthogonal beam movements. The biasing current was also measured to ensure that intensity fluctuations could be detected.

To investigate the suppression of beam position motions two glass plates affixed to rotating mounts were placed before the input mode-matching lens and after the output lens. The arrangement is shown in Figure 5.2. A known rotation may be applied to a glass plate to introduce a detectable beam movement. Comparing the measured beam movement for the same rotation of the input and output plates gives a measure of the degree of suppression achieved by using the fibre. The advantage of this method is that readings can be taken quickly and easily repeated. The actual value of beam movement imposed is not required since the displacement can be calibrated in terms of the magnitude of rotation of the glass plates and the signal from the photo-diode. As mentioned above the photo-diode bias current was monitored to ensure that the input motion did not affect the coupling and that the laser output did not fluctuate while readings were taken.

Four different lengths of fibre were tested to see how the beam movement suppression varied. The birefringence of the fibre core meant that the output polarisation and intensity was susceptible to fluctuations due to flexing and small thermal changes. The longer the fibre being tested the more pronounced the effect became. This susceptibility of the longest fibre in particular made measurements quite difficult hence the large error bars on the graph shown in Figure 5.3. The suppression of beam position movements is plotted against fibre length. The slope of the graph gives a

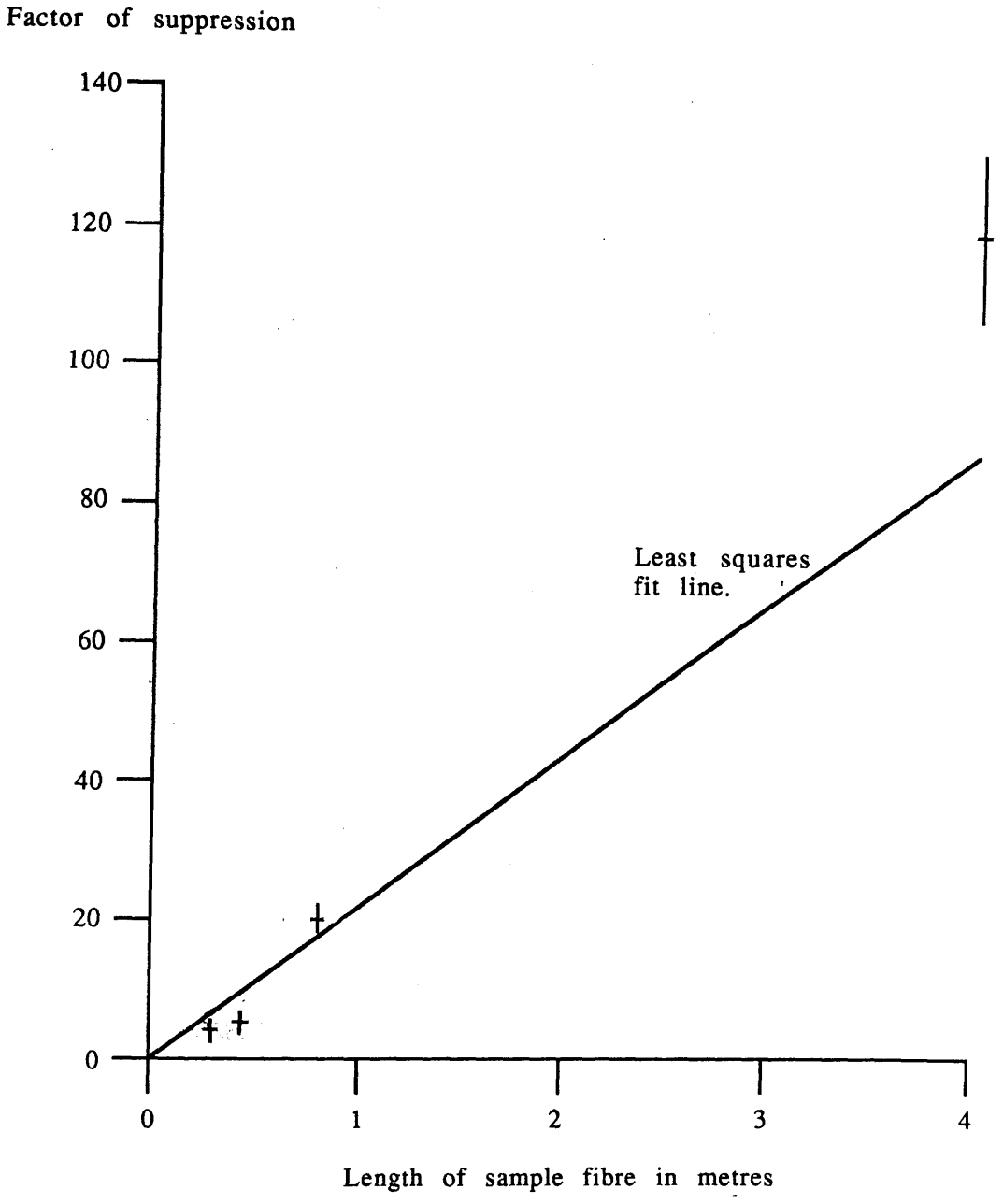

Figure 5.3 The degree of suppression of laser beam movement is plotted against the length of the sample fibre. The longer pieces of fibre show a great susceptibility to perturbations, eg. from temperature variations, and this makes it hard to reduce the size of the error bars for these measurements.

suppression factor of ~ 22/metre for this fibre. It is possible that the suppresion does not rise linearly but as some power of the fibre length; however the large errors in the reading do not allow this to be seen. In practice only a short length of fibre (~1 metre) would be used in the prototype detector and so the above result will be valid for this case.

The variation in the transmission achieved with each length of fibre suggests that the quality of the fibre mounting varied despite the care taken. The best transmission achieved was 80%, with the largest length of fibre, but this lasted only a few minutes and was very hard to recover. Usually around 50% was achieved and maintained for many minutes.

This experience led to the use of unmounted fibre for comparison of transmission levels and the finding that a clean, unprotected fibre end will survive well. This experiment also demonstrated that for work with the prototype gravitational radiation detector a more suitable choice of fibre would be a mono-mode, high birefringence type, ie. to preserve polarisation and to remove higher order modes. It is this type of fibre (obtained from York V.S.O.P. Ltd.) which was used to improve the observed performance of the intensity stabilisation system and which is currently installed in the prototype detector and routinely transmitting ~ 50%.

5:3 THEORETICAL TRANSMISSION OF A FUNDAMENTAL MODE

With this experience of using fibres and of some of the limitations it will be useful to calculate the maximum transmission that could be expected for a single-mode fibre optimised for green light. The fibre considered will be a simple stepped-index type as discussed above. The relevant parameters for the 'York' fibre will be

used so that a comparison of the expected transmission can be made with the achieved transmission.

A waveguide mode is a coherent distribution of light which propagates with phase velocity, $v = \omega/\beta$, where ω is the angular frequency of the light and β is the propagation constant of the fibre which will be determined from the boundary conditions. Using a cylindrical co-ordinate system $(r,\emptyset,z)$ with z along the axis of the fibre gives the z and time dependence of the wave function as $e^{i(\beta z - \omega t)}$.

5:3.1 THE FIELDS WITHIN THE FIBRE

In a non-magnetic, non-conducting fibre Maxwell's equations can be written:

$$V.E = 0 \tag{5.3a}$$

$$V.H = 0 \tag{5.3b}$$

$$VxE = -\mu_o \frac{\partial H}{\partial t} \tag{5.3c}$$

$$VxH = \varepsilon \frac{\partial E}{\partial t} \tag{5.3d}$$

Where $\varepsilon = \varepsilon_r \varepsilon_o$. Now taking the curl of equation 5.3c and using the identity:

$$Vx(VxE) = V.(V.E) - V^2E \tag{5.4}$$

Gives:

$$V^2E = \mu_o \varepsilon \frac{\partial^2 E}{\partial t^2} \tag{5.5}$$

Which becomes:

$$\nabla^2 E = -k^2 E \tag{5.6a}$$

This is the wave equation for E where $k = \omega n/c$, the plane wave propagation constant, and $n = \varepsilon_r^{1/2}$ the refractive index of the fibre. And similarly for H:

$$\nabla^2 H = -k^2 H \tag{5.6b}$$

In a cylindrical co-ordinate system the Laplacian of a vector is given by:

$$\nabla^2 V = \underset{\sim}{r} \left[\nabla^2 V_r - \frac{1}{r^2} V_r - \frac{2}{r^2} \frac{\partial V_\phi}{\partial \phi} \right]$$

$$+ \underset{\sim}{\phi} \left[\nabla^2 V_\phi - \frac{1}{r^2} V_\phi - \frac{2}{r^2} \frac{\partial V_r}{\partial r} \right]$$

$$+ \underset{\sim}{z} \nabla^2 V_z \tag{5.7}$$

Clearly the z-components of E and H can be solved as scalar wave equations. The solution for E will be of the form $E_z(r,\phi,z,t) = R(r).\underline{\Phi}(\phi)\ e^{i(\beta z - \omega t)}$ and H will be similar. So putting this solution in equation 5.6a and then separating variables gives:

$$r^2 \frac{\ddot{R}}{R} + r \frac{\dot{R}}{R} + r^2 (k^2 - \beta^2) = \frac{\ddot{\underline{\Phi}}}{\underline{\Phi}} \tag{5.8}$$

Where $\dot{R} = dR/dr$, etc. Now, since the two sides are independent they must equal a constant, n^2, say. Therefore:

$$\ddot{\underline{\Phi}} = - n^2 \underline{\Phi} \tag{5.9}$$

The solution is:

$$\underline{\Phi} = \cos (n\phi + \theta) \tag{5.10}$$

Similarly for the L.H.S. of equation 5.8, substituting $g^2 = r^2 (k^2 - \beta^2)$:

$$g^2 \frac{\partial^2 R}{\partial g^2} + g \frac{\partial R}{\partial g} + (g^2 - n^2) R = 0 \qquad (5.11)$$

Providing g is real the solution of this equation is given by Bessel's functions of the first and second type, where $k^2 - \beta^2$ is a scaling factor, i.e.:

$$R = A_1 J_n(g) + B_1 Y_n(g) \qquad (5.12)$$

However, the function $Y_n(g)$ goes to infinity at the axis and so the coefficient B_1 must equal zero. So, the field within the fibre is:

$$E_z = A_1 J_n(g) \cos(n\emptyset + \theta) \; e^{i(\beta z - \omega t)} \qquad (5.13)$$

This solution extends out to infinity without regard to the core/cladding interface, i.e. there is no attenuation. To confine the wave to the core it is surrounded by a medium of lower refractive index, n_2. From here the subscripts 1 and 2 will refer to the parameters of the core and cladding respectively. Hence in the core $g^2 = r^2 (k_1^2 - \beta^2)$ and in the cladding, defining $h^2 = r^2 (\beta^2 - k_2^2)$, where $r \geq a$ and a is the core radius, and substituting into the L.H.S. of equation 5.8 gives:

$$h^2 \frac{\partial^2 R}{\partial h^2} + h \frac{\partial R}{\partial h} - (h^2 - n_2^2) R = 0 \qquad (5.14)$$

The solution to this equation is given by Bessel's modified functions if h is real. So the propagation constant is defined $k_2 < \beta < k_1$. The solution is:

$$R = C_1 I_n(h) + D_1 K_n(h) \qquad (5.15)$$

However, Bessel's modified function of the first kind, I_n, tends to infinity at infinity and so the coefficient, C_1, must be zero. So, the field in the cladding can now be written as:

$$E_{2z} = D_1 K_n(h)\cos(n\phi + \theta)\ e^{i(\beta z - \omega t)} \tag{5.16}$$

The H_z fields produce similar results. In the core the coefficient, A_1, is the maximum amplitude, E_o say, of E_z and D_1 is the maximum amplitude, H_o say, of H_z.

Let the maximum values of the E_z and H_z fields in the cladding be represented by C and D. These values will be calculated from the boundary conditions. Now by taking the curl of the E_z and H_z fields in equations 5.3c and 5.3d and cross-substituting it is possible to compute the radial and angular fields for the core (substituting $\alpha_1^2 = k_1^2 - \beta^2$ and $\alpha_2^2 = \beta^2 - k_2^2$).

$$E_{1r} = \frac{i}{\alpha_1^2}\left[\beta\frac{\partial E_{1z}}{\partial r} + \frac{\mu_o\omega}{r}\frac{\partial H_{1z}}{\partial \phi}\right] \tag{5.17a}$$

$$E_{1\phi} = \frac{i}{\alpha_1^2}\left[\frac{\beta}{r}\frac{\partial E_{1z}}{\partial \phi} - \mu_o\omega\frac{\partial H_{1z}}{\partial r}\right] \tag{5.17b}$$

$$E_{1z} = E_o J_n\cos(n\phi + \theta)\ e^{i(\beta z - \omega t)} \tag{5.17c}$$

$$H_{1r} = \frac{-i}{\alpha_1^2}\left[\frac{k_1^2}{\mu_o\omega}\frac{1}{r}\frac{\partial E_{1z}}{\partial \phi} - \beta\frac{\partial H_{1z}}{\partial r}\right] \tag{5.17d}$$

$$H_{1\phi} = \frac{i}{\alpha_1^2}\left[\frac{k_1^2}{\mu_o\omega}\frac{\partial E_{1z}}{\partial r} + \frac{\beta}{r}\frac{\partial H_{1z}}{\partial \phi}\right] \tag{5.17e}$$

$$H_{1z} = H_o J_n\cos(n\phi + \gamma)\ e^{i(\beta z - \omega t)} \tag{5.17f}$$

And in the cladding:

$$E_{2r} = \frac{-i}{\alpha_2^2}\left[\beta\frac{\partial E_{2z}}{\partial r} + \frac{\mu_o\omega}{r}\frac{\partial H_{2z}}{\partial \phi}\right] \quad (5.18a)$$

$$E_{2\phi} = \frac{-i}{\alpha_2^2}\left[\frac{\beta}{r}\frac{\partial E_{2z}}{\partial \phi} - \mu_o\omega\frac{\partial H_{2z}}{\partial r}\right] \quad (5.18b)$$

$$E_{2z} = CK_n\cos(n\phi + \theta)\, e^{i(\beta z - \omega t)} \quad (5.18c)$$

$$H_{2r} = \frac{i}{\alpha_2^2}\left[\frac{k_2^2}{\mu_o\omega}\frac{1}{r}\frac{\partial E_{2z}}{\partial \phi} - \beta\frac{\partial H_{2z}}{\partial r}\right] \quad (5.18d)$$

$$H_{2\phi} = \frac{-i}{\alpha_2^2}\left[\frac{k_2^2}{\mu_o\omega}\frac{\partial E_{2z}}{\partial r} + \frac{\beta}{r}\frac{\partial H_{2z}}{\partial \phi}\right] \quad (5.18e)$$

$$H_{1z} = DK_n\cos(n\phi + \gamma)\, e^{i(\beta z - \omega t)} \quad (5.18f)$$

5:3.2 THE BOUNDARY CONDITIONS

The equations above have five unknowns: C, D, γ, Θ and β. From Maxwell's equations there is continuity of the tangential components of the E and H fields at the core/cladding interface. Let $p = \alpha_1 a$ and $q = \alpha_2 a$ and the boundary conditions are:

$$E_o J_n(p) = CK_n(q) \quad (5.19a)$$

$$E_o\frac{n\beta}{p^2}J_n(p)\sin(n\phi+\theta) + H_o\frac{\mu_o\omega}{p}J_n'(p)\cos(n\phi+\gamma)$$

$$= -C\frac{n\beta}{q^2}K_n(q)\sin(n\phi+\theta) - D\frac{\mu_o\omega}{q}K_n'(q)\cos(n\phi+\gamma) \quad (5.19b)$$

$$H_o J_n(p) = DK_n(q) \quad (5.19c)$$

$$E_o\frac{k_1^2}{\mu_o\omega p}J_n'(p)\cos(n\phi+\theta) - H_o\frac{n\beta}{p^2}J_n(p)\sin(n\phi+\gamma)$$

$$= -C\frac{k_2^2}{\mu_o \omega q} K_n'(q)\cos(n\phi+\theta) + D\frac{n\beta}{q^2} K_n(q)\sin(n\phi+\gamma) \quad (5.19d)$$

From here on the arguments of the J-Bessel functions will be taken to be g and that of the K-Bessel functions will be h unless explicitly shown. Now substituting from these boundary conditions into equations 17b, 17e, 18b and 18e and simplifying with the substitutions:

$$F_j = \frac{1}{p}\frac{J_n'(p)}{J_n(p)} \quad (5.20a)$$

$$F_k = \frac{1}{q}\frac{K_n'(q)}{K_n(q)} \quad (5.20b)$$

Gives:

$$\frac{(F_j + F_k)(k_1^2 F_j + k_2^2 F_k)}{n^2\beta^2(1/g^2 + 1/h^2)^2}$$

$$= -\frac{\sin(n\phi + \theta)\sin(n\phi + \gamma)}{\cos(n\phi + \theta)\cos(n\phi + \gamma)} \quad (5.21)$$

Now since the two sides of 5.21 are independent they must equal a constant. The R.H.S is constant and equal to one when $\theta - \gamma = +/- \pi/2$. Then from 5.21:

$$(F_j + F_k)(k_1^2 F_j + k_2^2 F_k) = n^2\beta^2(1/g^2 + 1/h^2)^2 \quad (5.22)$$

Now defining a ratio, P, which is the proportion of H_z and E_z fields in a mode as:

$$P = -\frac{\mu_o \omega}{\beta}\frac{H_o}{E_o} \quad (5.23)$$

And from the boundary conditions:

$$P = \frac{n(1/g^2 + 1/h^2)}{F_j + F_k} \tag{5.24}$$

Now by substituting for P and simplifying with the relations, $F_c = E_o \cos(n\phi)\, e^{i(\beta z - \omega t)}$ and $F_s = E_o \sin(n\phi)\, e^{i(\beta z - \omega t)}$ the components of the fields in the core are rearranged to give:

$$E_{1r} = \frac{i\beta F_c}{2a_1}\left[J_{n-1}(1-P) - J_{n+1}(1+P) \right] \tag{5.25a}$$

$$E_{1\phi} = \frac{-i\beta F_s}{2a_1}\left[J_{n-1}(1-P) + J_{n+1}(1+P) \right] \tag{5.25b}$$

$$E_{1z} = J_n F_c \tag{5.25c}$$

$$H_{1r} = \frac{ik_1^2 F_s}{2a_1\mu_o\omega}\left[J_{n-1}\left[1-\frac{\beta^2}{k_1^2}P\right] + J_{n+1}\left[1+\frac{\beta^2}{k_1^2}P\right]\right] \tag{5.25d}$$

$$H_{1\phi} = \frac{ik_1^2 F_c}{2a_1\mu_o\omega}\left[J_{n-1}\left[1-\frac{\beta^2}{k_1^2}P\right] - J_{n+1}\left[1+\frac{\beta^2}{k_1^2}P\right]\right] \tag{5.25e}$$

$$H_{1z} = \frac{-\beta}{\mu_o\omega} J_n P F_s \tag{5.25f}$$

And in the cladding:

$$E_{2r} = \frac{-\beta J_n(p) F_c}{2a_2 K_n(q)}\left[K_{n-1}(1+P) + K_{n+1}(1-P) \right] \tag{5.26a}$$

$$E_{2\phi} = \frac{i\beta J_n(p) F_s}{2a_2 K_n(q)}\left[K_{n-1}(1+P) - K_{n+1}(1-P) \right] \tag{5.26b}$$

$$E_{2z} = \frac{J_n(p)}{K_n(q)} F_c K_n \tag{5.26c}$$

$$H_{2r} = \frac{ik_2^2 J_n(p) F_s}{2\mu_o\omega a_2 K_n(q)}\left(K_{n-1}\left[1+\frac{\beta^2}{k_2^2}P\right] - K_{n+1}\left[1-\frac{\beta^2}{k_2^2}P\right]\right) \tag{5.26d}$$

$$H_{2\phi} = \frac{ik_2^2 J_n(p) F_c}{2\mu_o\omega a_2 K_n(q)}\left(K_{n-1}\left[1+\frac{\beta^2}{k_2^2}P\right] + K_{n+1}\left[1-\frac{\beta^2}{k_2^2}P\right]\right) \tag{5.26e}$$

$$H_{2z} = \frac{-\beta J_n(p)}{\mu_o \omega K_n(q)} F_s K_n P \qquad (5.26f)$$

5:3.3 THE FUNDAMENTAL FIBRE MODE

To identify the mode in the fibre it is necessary to know the energy distribution. This is given by the real part of the average Poynting vector:

$$\underset{\sim}{S} = \frac{1}{2} (E \times H^*) \qquad (5.27)$$

Where the asterisk indicates the complex conjugate. So $\underset{\sim}{S}$ is given by:

$$\underset{\sim}{S} = \frac{1}{2} [\underset{\sim}{r} (E_\phi H_z^* - E_z H_\phi^*) + \underset{\sim}{\phi} (E_r H_z^* - E_z H_r^*)$$

$$+ \underset{\sim}{z} (E_r H_p^* - E_p H_r^*)] \qquad (5.28)$$

By inspection of equations 5.25 and 5.26 it is clear that the only real part of the the Poynting vector is the z-component. The initial requirement that the energy is guided along the fibre axis is satisfied. The z-component is given by:

$$\underset{\sim}{S}_z = \frac{\beta k_1^2 E_o^2}{8\alpha_1^2 \mu_o \omega} \left[J_{n+1}^2 (1+P) \left[1 + \frac{\beta^2}{k_1^2} P \right] + J_{n-1}^2 (1-P) \left[1 - \frac{\beta^2}{k_1^2} P \right] \right.$$

$$\left. - J_{n+1} J_{n-1} \cos(2n\phi) \left[2 - 2\frac{\beta^2}{k_1^2} P^2 \right] \right] \qquad (5.29)$$

The fundamental mode has an energy distribution which is a maximum at r = 0, the centre of the core, and which decreases radially. There should be no angular dependence. To remove the angular dependence from equation 5.29 there are two possibilities:

1) $n = 0$,

or 2) $1 - \beta^2 P^2 / k_1^2 = 0$.

Now if $n = 0$ then from equation 5.24, $P = 0$ and substituting this into equation 5.29 and using the recurrence relation, $J_{-n} = (-1)^n J_n$ gives an energy distribution in the fibre:

$$\underset{\sim}{S}_{1z} = \frac{\beta k_1^2 E_o 2 J_1^2}{2\alpha_1^2 \mu_o \omega} \tag{5.30}$$

However, the Bessel function, J_1, goes to zero at $r = 0$, the energy of the propagating wave is distributed in a ring within the core, this is sometimes called a doughnut mode. Referring to equation 5.25f and substituting $P = 0$ produces a null H_z field. This is a transverse magnetic (TM) mode. There is also a solution $P = \infty$ when $n = 0$ which corresponds to the transverse electric (TE) solution.

The second condition yields the relation, $P = +/-(k_1/\beta)$. For most optical fibres the difference in refractive index between the core and the cladding is ~ 1%. Since β lies between k_1 and k_2 then $P \sim 1$ to the same accuracy. Referring back to equation 5.23, if $P \sim 1$ then the E_z and H_z fields are present in equal proportions. This is a hybrid mode which is designated HE. Substituting this value of P into equation 5.29 gives:

$$\underset{\sim}{S}_{1z} = \frac{E_o^2 \beta k_1^2}{2\alpha_1^2 \mu_o \omega} J_{n+/-1}^2 \tag{5.31}$$

For $P = +/-1$ respectively. Now the only Bessel J-function which rises to a maximum at $r = 0$ is J_o. Therefore for the fundamental mode $n = 1$ and $P = -1$. This fundamental mode is known as HE_{11}. The $P = +1$ solutions are known as the EH modes. Now by operating on equations 26a to 26f in the same way the energy distribution in the cladding for the fundamental mode is found to be:

$$\underset{\sim}{S}_{2z} = \frac{E_0^2 \beta k_2^2 J_1^2(p)}{2\mu_0 \omega a_1^2 K_1^2(q)} K_0^2 \qquad (5.32)$$

The foregoing description of the modes of a dielectric stepped index optical fibre is well documented[84,85] but to proceed further it will be necessary to see how this description fits the sample fibre under discussion.

5:3.4 CALCULATION OF BETA

The fibre supplied by York V.S.O.P. has a refractive index in the core, $n_1 = 1.463 \pm 0.001$, and in the cladding, $n_2 = 1.457 \pm 0.001$. The value of the propagation constant depends on these two values, the radius of the fibre core and the mode. As n_1 approaches n_2 or as r decreases the fibre will support fewer modes. As the cutoff of a mode approaches the scaling factor α_1 increases until the limit $\beta = k_2$. Substituting this value for β into g gives a cut-off parameter, u_{nm}, for each mode[84]:

$$u_{nm} = \frac{2\pi r}{\lambda}(n_1^2 - n_2^2)^{1/2} \qquad (5.33)$$

Where n is the mode number and m is the number of radial antinodes in the mode. If the value u_{nm} of a mode is less than the R.H.S. of equation 5.33 then the fibre will support the mode.

Now, by returning to the boundary conditions and using the Bessel function recurrence relations,

$$\frac{J_{n'}}{gJ_n} = \frac{J_{n-1}}{gJ_n} - \frac{n}{g^2} \qquad (5.34a)$$

$$-\frac{K_{n'}}{hK_n} = \frac{K_{n-1}}{hK_n} + \frac{n}{h^2} \qquad (5.34b)$$

it is possible to show that u_{nm} for the HE_1 and EH_1 modes is

given by the successive roots of:

$$J_1(u) = 0 \tag{5.35}$$

The first root of $J_1(u)$ is $u = 0$. The fundamental HE_{11} mode has no cut-off. Similarly the values of u_{nm} for the TM and TE modes ($P = 0$, $P = \infty$ respectively) and the HE_2 modes are given by the roots of equations 5.36a and 5.36b respectively:

$$J_o = 0 \tag{5.36a}$$

$$\frac{uJ_o}{J_1} = - \frac{n_1^2 - n_2^2}{n_2^2} \tag{5.36b}$$

But from equation 5.2 the R.H.S. of equation 5.36b ~ 0 and so the roots of equations 5.36a and 5.36b are similar. The cut-off values for the EH_2 modes are given by the roots of:

$$J_2 = 0 \tag{5.37}$$

Hence, the cut-off parameters for the first mode of each series is given by:

MODE	u_{nm}
HE_{11}	0
HE_{12}	3.832
TM_{01}, TE_{01}	2.405
HE_{21}	2.408
EH_{21}	5.136

Now the first modes to be guided after the fundamental are TE_{01} and TM_{01}. Hence, inserting the appropriate value of u_{nm} into equation 5.33 gives an upper limit to the core radius for single-mode operation, in the green, for the given values of refractive index. This upper limit is 1.48 microns. The manufacturers estimated the core radius to be 1.0 - 1.5 microns. For the purposes of this

calculation the radius will be taken to be, a = 1.45 microns. The cladding extends out 45 microns from the centre.

Now using the substitutions of equations 5.34a and 5.34b in equation 5.24 with:

$k_1 = (1.787 +/- 0.001) * 10^7\ m^{-1}$

$k_2 = (1.779 +/- 0.001) * 10^7\ m^{-1}$

$P = -k_1/\beta$ and n = 1. The root of the function was found using a NAG fortran library routine to yield the value for the propagation constant, $\beta = (1.783 +/- 0.001) * 10^7\ m^{-1}$.

This value of β may now be used in equations 5.31 and 5.32 to discover how well the mode is confined to the core of the fibre. A FORTRAN routine was written using Simpson's rule to integrate over the core and cladding to discover the proportion of power transmitted in the core. The result is:

$$\frac{{}_0\int^{2\pi}\ {}_0\int^{r}\ \underset{\sim}{S}_{1z}\ r\,dr\,d\phi}{{}_0\int^{2\pi}\ {}_0\int^{r}\ \underset{\sim}{S}_{1z}\ r\,dr\,d\phi + {}_0\int^{2\pi}\ {}_r\int^{\infty}\ \underset{\sim}{S}_{2z}\ r\,dr\,d\phi} = 82.0\% \quad (5.38)$$

And so in calculating the optimum waist size of the beam to be matched into the fibre the cladding may be neglected without significantly affecting the result.

5:3.5 THE WAIST OF THE INPUT BEAM

The beam which is to be coupled into the fibre is assumed to be the fundamental mode of a laser resonator, ie. a Gaussian beam. The diameter of this input beam will be larger than the fibre core and so a mode-matching lens will be required to effect efficient coupling of the beam into the fibre. Clearly the more tightly the input beam is focussed onto the fibre core the more light will be injected into the fibre. However, the beam will diverge

within the fibre and if the angle of divergence exceeds the critical angle then light will leak out through the fibre cladding.

When a Gaussian beam is focussed the wavefront is concave approaching the waist, planar at the waist and convex as the beam diverges. Choosing the beam waist as the point at which the beam enters the fibre offers the most efficient coupling. The plane wavefront meeting the plane face of the fibre will suffer least reflection losses. Another way of viewing this is that at the boundary the E_z and H_z fields are zero and there is continuity of the tangential components of the fields.

The optimum waist will admit the greatest fraction of the input beam with the least losses at the core/cladding boundary. To find the optimum waist requires the use of the orthogonality relation for Bessel functions of the first kind[86]:

$$\int_0^1 t\, J_\mu(\alpha_m t) J_\mu(\alpha_n t)\, dt = 0 \quad (m \neq n) \tag{5.39}$$

If it is assumed that the field distribution of the input Gaussian beam, of unity peak amplitude, is a superposition of Bessel functions of the first kind with parameters α_1, α_2, α_3..... then the amplitude of the fundamental mode of the fibre will be given by:

$$A_f = \frac{\int_0^1 t\, e^{-t(a^2/w^2)} J_o(\alpha_1 a.t)\, dt}{\int_0^1 t\, J_o^2(\alpha_1 a.t)\, dt} \tag{5.40}$$

Where a is the radius of the core, as before, and w is the waist of the input beam. However, the amplitude, A_f, will vary as w changes. The maximum amplitude, A_f, may be calculated by performing the above integral for a range of values of w to find the maximum. It should be noted that to ensure that the total amplitude of the input beam remains constant the integral must be multiplied by a factor

1/w. In this way the optimum input beam waist was calculated to be $1.52 * 10^{-6}$ metres and the optimised relative amplitude of the fundamental fibre mode was found to be 0.83.

5:3.6 COUPLING EFFICIENCY

To calculate the efficiency of the transmission, T, of the Gaussian beam into the fundamental fibre mode it is necessary to calculate the relative power in each over the area of the fibre core. This is achieved by the following integral:

$$T = \frac{\int_0^{2\pi} \int_0^{r} J_0^2(r\alpha_1)\, r\, dr\, d\phi}{\int_0^{2\pi} \int_0^{r} e^{-2r^2/w^2}\, r\, dr\, d\phi} \qquad (5.41)$$

$$= 75.7\%$$

It is reasonable to assume that a similar fraction of the light incident on the cladding will be transmitted as the fundamental fibre mode and so the total power transmitted will be approximately seventy-six per cent of that in the input beam.

Typical propagation losses for an optical fibre of this type is ~ 20dB/km. In the prototype detector at Glasgow only ~ 1m of fibre will be used and so the fibre propagation losses may be neglected. However, there will be Fresnel reflection losses at the input and output. The fraction of power transmitted at each interface assuming a plane wave is given by:

$$F = \frac{4}{n_1(1 + 1/n_1)^2} = 0.965 \qquad (5.42)$$

The wavefront may not be flat at the output end of the fibre but the radius of curvature of the wavefront within the fibre is constrained not to be so small that the angle of incidence of the

wavefront at the core/cladding boundary does not exceed the critical angle (~ 85^{o}) and so the assumption is valid. Therefore the actual power transmitted will be:

$$\text{Efficiency} \sim T * F^{2}$$

$$\sim 71\% \qquad (5.43)$$

Strictly speaking there will also be reflection losses associated with the mode-matching lenses, approximately 4% each, which will reduce the transmission to ~ 65%.

This figure is higher than that given initially for the fraction of power (~ 50%) actually transmitted through the fibre in use at Glasgow. The practical situation is probably limited by the effect on the coupling of laser beam geometry fluctuations, ie. the input beam is not a pure, fundamental Gaussian. The use of a rebuilt, quieter laser[77] or a fibre alignment system[86] may improve the transmission achieved. Another source of loss may be the contamination of the fibre input and output planes. Finally, this calculation has not taken account of the lossy effects of the 'bow-tie' stressing components in the real fibre. It seems likely however that 50 - 60% is a realistic transmission figure for a mono-mode fibre in this situation. The suppression of beam position fluctuations of ~ 2 metres of this fibre was measured to be at least 60dB[86].

However, as the power transmitted through a fibre is raised certain non-linear effects become significant. For instance, stimulated Raman scattering and stimulated Brillouin scattering have been observed in optical fibres. Experiments on the type of fibre under consideration have also shown a saturation effect which occurs with power densities of ~ 10^{11} Wm^{-2}[87], which limits the power

transmission of this type of fibre to a few hundred milli-Watts. This latter effect may be due to intensity dependent refractive index fluctuations leading to loss of transmitted power to the cladding or due to an intensity dependent absorption within the core. If fibres are to be used in laser interferometric gravitational radiation detectors then these limits must be raised to allow several Watts to be transmitted mono-mode. This could be achieved by using different materials or by increasing the fibre radius to lower the power density. In the latter case the difference in refractive index would have to be made even smaller than at present which would make the fibre very weakly guiding and possibly cause problems in construction.

CHAPTER 6

A SIMPLE DATA-COLLECTION SCHEME

6:1 INTRODUCTION

In the continued effort for better sensitivities it is important to remember that data analysis techniques must also be developed which will make full use of the information contained in the output of gravitational wave detectors. Because of the wider bandwidth of interferometric detectors compared to Weber bars data rates up to three orders of magnitude greater than those associated with bars will be common-place. The sheer physical volume in storage media that this represents is a problem in itself. Even new technology such as optical Write-Once-Read-Many (WORM) discs will produce storage problems. For instance one disc with a storage capacity of 100Mbytes will store only 20 minutes of data at the rates envisaged.

The analysis of such large volumes of data will clearly also be a source of problems. To achieve maximum benefit from the interferometric detectors it is desirable that as much analysis as possible should be conducted on-line.

However, even though the solution to such problems will require sophisticated equipment and techniques they do not preclude the construction of data collecting systems which employ fairly simple selection criteria to reduce the volume of data stored. This chapter will describe the design, construction and programming of such a system which might be used for storing certain events satisfying pre-set criteria.

6:2 THE DATA COLLECTION SYSTEM

The proposed system was required to select specific events from a continuous data stream. The incoming data would be provided by looking at the output from the servosystem maintaining the secondary cavity on resonance (signal proportional to the relative change in length of the two cavities). A specific sample of data would be selected when it contained an event which was larger than a preset value. This sample of data was then to be stored, with a record of the time at which it was captured, for future analysis. This pulse capture system would then provide a record of likely events which could also be investigated in the continuous data record at a later date. For timing purposes an accuracy of one tenth of a second was required.

The data selection scheme outlined above would be quite sufficient for simplifying searches for pulses in the signal from the detector except that many spurious events would also be stored. There are several effects, apart from a gravitational wave event, which might cause the level of the secondary feedback signal to rise above a given threshold value. For instance, despite the good isolation of the test masses from seismic noise a large disturbance might appear as a pulse on the output of the secondary feedback system. If the laser jumps from one mode to another, or the intensity stabilisation system is agitated then again a false event will be stored. The problem of reducing the number of spurious events may be resolved by monitoring all of the above sources of disturbance and generating a veto signal when a pulse is most likely not to be due to a gravitational wave event. By logically combining this veto signal with the event detection signal most spurious events will be

disregarded by the system.

The first requirement of the data collecting system was some device which could check the incoming data for an event and allow storage of the appropriate section of the signal. A discriminator and digital delay line* were used for this purpose. The discriminator could be preset to produce a TTL trigger pulse whenever the input signal rose above a certain voltage. The delay line allowed time for the system to respond to save the data.

The next requirement was a data sampling system which could be triggered as required to save the data temporarily and then output it for storage. The device chosen was a Tektronix 468 digital storage oscilloscope which was fitted with an IEEE 488 standard interface.

The details of the IEEE 488 standard are outside the scope of this text but in essence it provides a system for interconnecting up to fifteen devices under the control of one master device.

A BBC 8-bit microcomputer was chosen as the central controller of the proposed system because of its versatile interfacing capabilities and the excellent interface between ASSEMBLY language and BASIC which turned out to be very important and considerably simplified the programming. In addition the floppy diskettes used by the BBC microcomputer were well suited to save specific events in a manner available for random access.

The primary Input/Output facilities provided on the BBC microcomputer are the 1MHz bus which gives direct access to the data and address lines of the CPU and other special lines[88]. This scheme allows memory mapping of new peripherals. The second option is provided by one half of a 6522 Versatile Interface Adapter (VIA), the User Port, which is less flexible and somewhat restrictive for this task. It was therefore decided that for speed and

flexibility all of the I/O would proceed through the 1MHz bus. The IEEE 488 interface used was commercially available and plugged directly into the 1MHz bus.

The BBC was also investigated as a possible timing element for the system but it was found that the accuracy of its internal clock varied markedly depending on what other computing loads were placed on it. However an accurate time signal was available from the MSF 60kHz time and frequency service broadcast by the National Physical Laboratory. The MSF decoder used included a clock display but provided no direct means of interfacing to any other device. However it not only displayed the time accurately but also emitted a single TTL pulse on the minute.

A commercially available timer chip was selected as the time-keeping element using a good quality crystal. The timer chip registers were to be loaded from the BBC and then started by the MSF pulse.

Therefore the basic components of the system were a digital storage oscilloscope, a BBC microcomputer, a digital clock and the MSF standard. The next problem was linking these components in an efficient manner. A block diagram of the desired system configuration, Figure 6.1, will help to show how these problems were overcome.

To cope with the requirements of reading from, and writing to, the clock chip and also with the various other I/O requirements of the system an interface was constructed which incorporated three VIA's memory-mapped via the 1MHz bus. Although this is slower than using the 1MHz bus directly it combined the advantages of the 1MHz bus with those of the User Port. The three VIA's actually provided

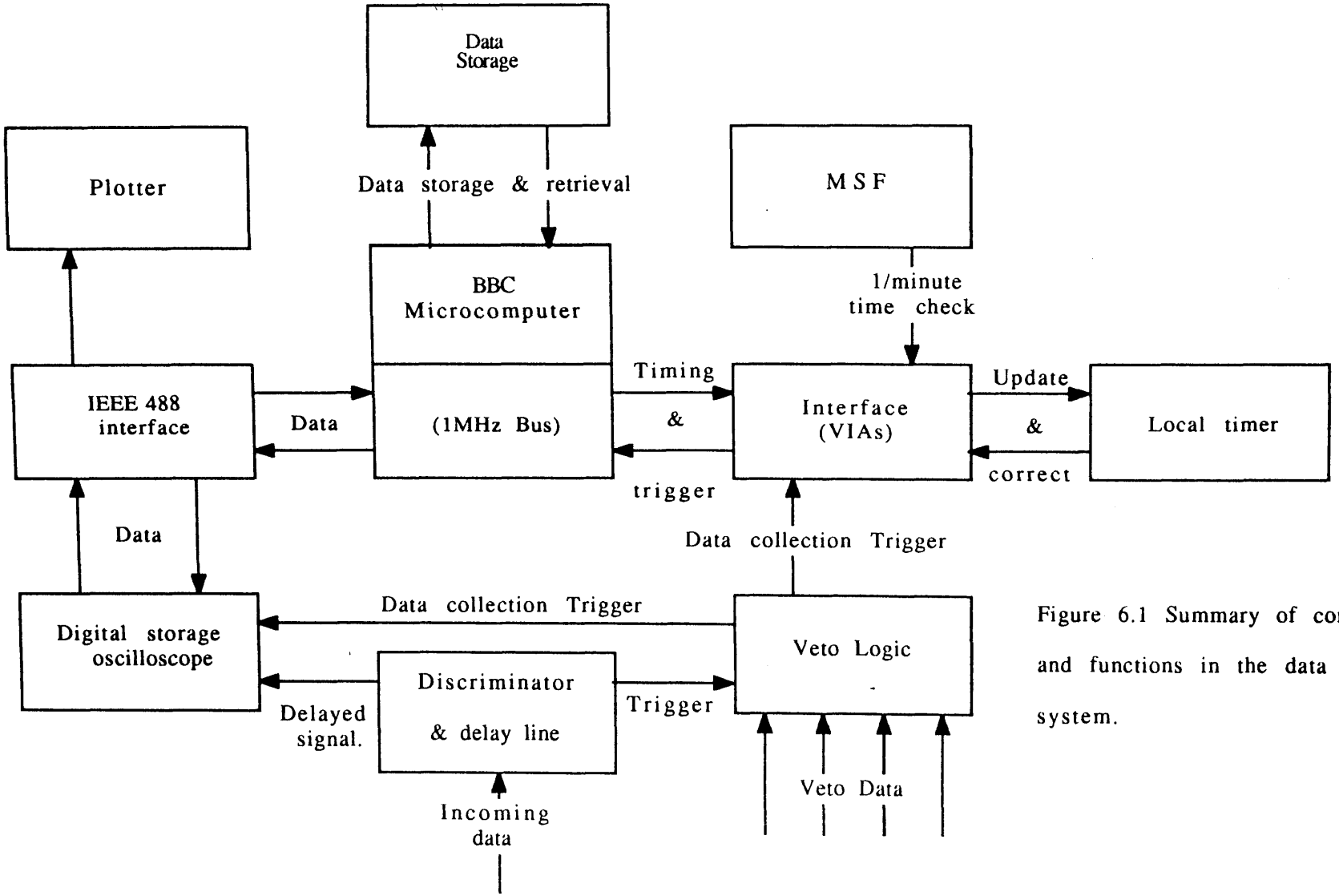

Figure 6.1 Summary of control lines and functions in the data collection system.

more scope than was strictly necessary for the application. In practice several pins were used where one might have sufficed to reduce the possibility of conflict and ease the programming.

In operation to ensure accurate timing it was necessary for the BBC to maintain updated copies of the timer chip registers. This continual updating represented the majority of the BBC's activity with the system in operation. The initial code for updating the registers was written in BASIC but proved prohibitively slow and so a routine was written in ASSEMBLER which even in the worst possible case would complete the updating of the registers within ~ 1mS.

As noted above a good quality crystal was used which in principle was accurate to 0.1 seconds in ~ 28hrs. In practice, however, temperature variations could prove important. To overcome the possibility of drift in the timer the MSF 1/minute pulse is used. Once every hour an interrupt is enabled which means that when any pulse arrives from the MSF a routine is run immediately (~ few μS) which compares the value in the tenths of second register in the timer chip to the expected value (0 if the timer is correct). Any difference is stored until one minute later when the clock is stopped and restarted or updated as required on the next MSF pulse. The effectiveness of the system was tested by slowing down the timer crystal to produce a net drift of ~ 0.3 seconds per hour. After more than 24 hours there was no perceptible difference in the displayed BBC and MSF times.

It was important that the storage of data did not occur while the registers in the BBC were being updated since this could result in incorrect timing information being stored with the sample. An interrupt would have been unsuitable in this situation for this reason. The simplest solution to this problem involved the use of a feature unique to the BBC, namely EVENTS. An EVENT is similar to an

interrupt except that the BBC will only respond to it when a BASIC statement is being executed. Therefore, although a signal pulse might arrive during the register updating (carried out in machine code) no action will be taken until this routine is finished and program control returns to BASIC.

Subsidiary programming tasks included routines to recognise a full disk, change drives and warn the operator of such an eventuality with a loud beep, and routines to recall the data from disc and to produce graphical output on a Hewlett-Packard 7221S plotter again employing the IEEE 488 interface. A copy of the program is included in Appendix B.

As yet it has not been practical to conduct a search for pulses. However the system has proved useful in other ways as discussed below.

6:3 ANALYSIS OF THE NOISE CHARACTERISTICS OF THE PROTOTYPE DETECTOR

On 24th February 1987 a supernova (SN1987A) was observed in the Large Magellanic Cloud which caused great interest in the astronomical community in general. Unfortunately there were no detectors operating at the time of the event apart from J. Weber's room temperature bar at the University of Maryland and a room temperature bar run by the University of Rome at Frascati. There have been reports from both groups of pulses in the data from the bars around the time of a neutrino burst detected at Mont Blanc. However there is still controversy over the significance of these events.

By putting some values into equation 1.16 it is possible to place a rough limit on the amplitude of gravitational radiation which would have reached the Earth from the burst. The supernova is approximately 160,000 light years away and if it had converted $0.2M_{\odot}$

into gravitational radiation then with this optimistic value we would expect a gravitational wave amplitude at the Earth of $h \sim 2 * 10^{-18}$ for the first burst.

Although all of the interferometer groups were in various stages of development work it was decided to attempt a coincident run of the interferometric detectors at the earliest possible opportunity. Due to the advanced state of rebuilding work on the German detector the Max Planck group were unable to join in this effort. Although there was a likelihood of a compact rapidly rotating remnant at the centre of the supernova it seemed unlikely that it would be emitting radiation at such a level as to be detectable on Earth by the present generation of interferometers. The purpose of the exercise was to achieve the first coincident run of interferometers, to collect coincident data and to determine any difficulties that might arise. Due to the haste in preparing for the run, conditions were far from ideal, none of the machines were optimised for detection and the M.I.T. and Californian groups did not have continuous data collection capability.

The group at Glasgow decided to use this as an opportunity to produce a sample of data which could be used to test various signal processing techniques which might be useful when gravitational wave observatories are a reality. To this end several waveforms similar to those expected from the coalescence of a compact-object binary system were super-imposed on the data with varying S/N ratios. Work on the analysis of these data is currently proceeding both at Glasgow and at University College Cardiff.

Because of the current sensitivity of the Glasgow prototype detector compared to likely sources (see Chapters 1 and 2) it was not really worthwhile to run the data collection system in a search for gravitational wave pulses. However data was also stored on magnetic

tape for later analysis of the noise statistics of the detector during the run.

If pulses of gravitational radiation are to be detected by statistical means it is vital that the noise statistics of the detector are well understood. If the noise is a truly random process then the pulse-height distribution should be Gaussian. Whether or not this is true may be tested by sampling the data (away from any superimposed signals) and plotting pulse-height against number of occurrences. This is a slightly different task than that for which the data collection system discussed above was originally designed. However this requires only a small modification in the way in which the system is triggered to collect data and so this has been done to test the system in operation.

The signal was stored on a Phillips Ana-log 7 tape drive after being passed through a high-pass filter at 2.5kHz. The response of the magnetic tape falls off at ~ 5kHz. The stored signal is not suitable for direct analysis because of a 'bump' in the frequency profile which is caused by the servosystem which maintains the cavity on resonance (see Figure 6.2a). This feature does not affect the sensitivity of the detector but in a pulse height analysis the data would be dominated by signals in a narrow band at ~ 1100Hz. The detector response also rises sharply below ~ 500Hz because of resonances in the wires supporting the test masses. To reduce the effect of these features the recorded signal was passed through a KEMO high-pass filter and a twin-T filter. The latter was an approximate match to the shape of the servosystem bump. The combination of this filtering gave a reasonably flat frequency profile in the range 1200-2500Hz (see Figure 6.2b). It may be possible to produce a more accurate match to the servosystem bump by using digital techniques and work on this is also in progress at

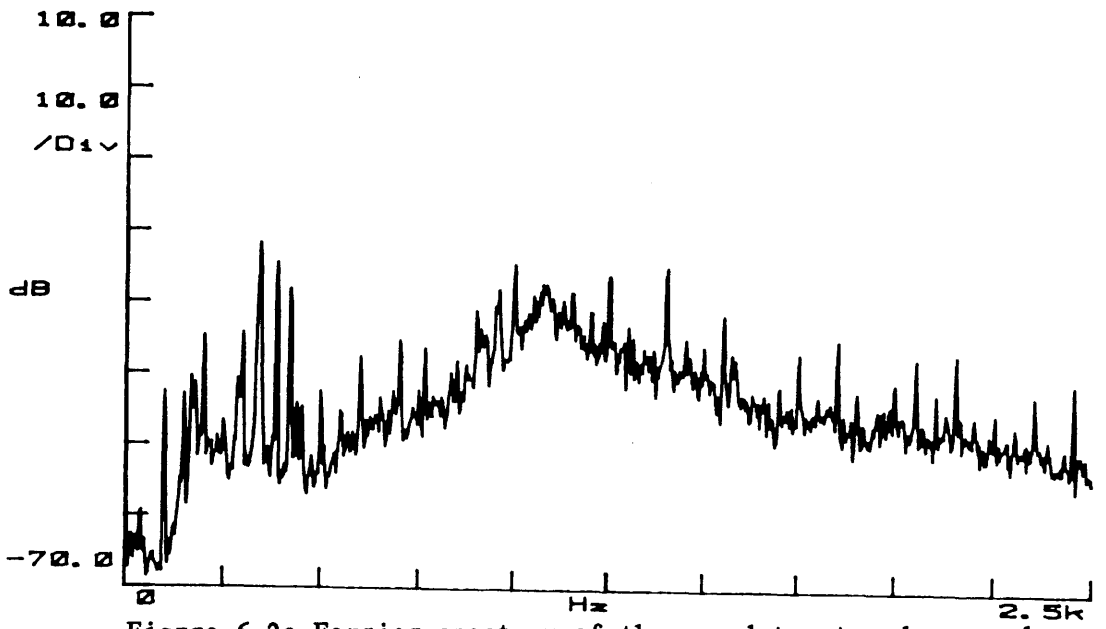

Figure 6.2a Fourier spectrum of the raw data stored on analogue tape during the coincident run of the interferometric detectors. Note the peaks due to wire resonances, below 500Hz, and the servo 'bump', which peaks around 1100Hz.

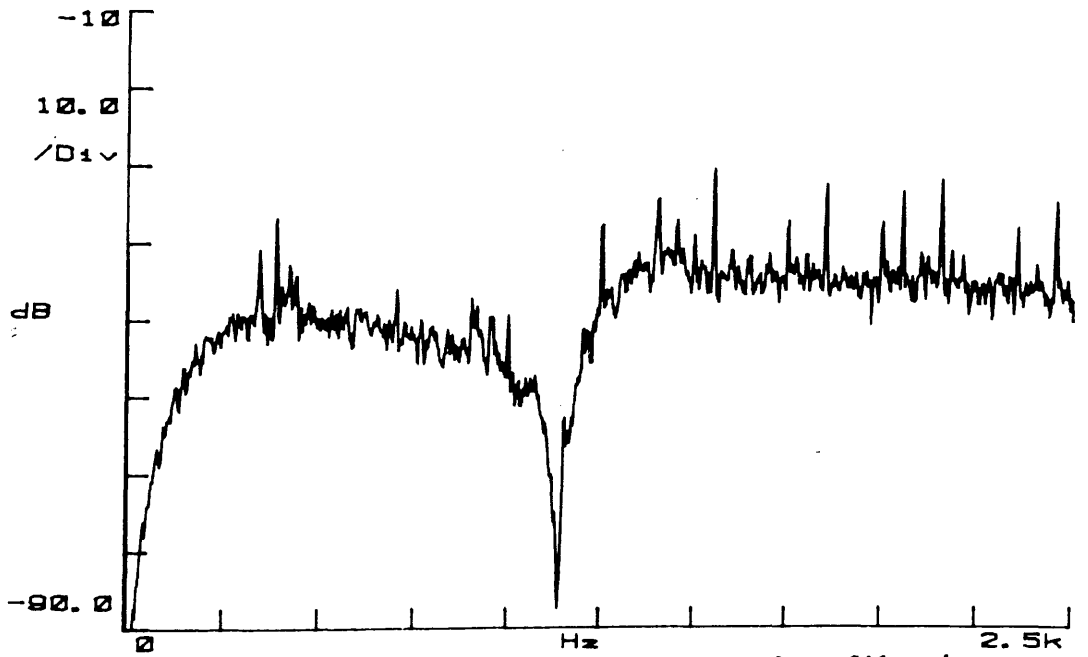

Figure 6.2b Fourier spectrum of the data after filtering, as described in the text. Note that the spectrum is now nearly flat between ~ 1200Hz and 2500Hz.

Glasgow.

The filtered signal was then fed to the data-collection system and data was collected by providing a pulse to the trigger input. The oscilloscope used stores 512 points in each sample and the window chosen was 20msec. Forty-three samples were collected giving a total of 22016 points.

Initially the standard deviation, σ, of each sample was obtained from:

$$\sigma^2 = \frac{\sum_i (x_i - \bar{x})^2}{N - 1} \qquad (6.1)$$

Where $\bar{x}$ is the sample mean and N is the number of points in the sample. There was a spread of values of the standard deviation from 10.2 to 28.2. It seemed unlikely that the statistics of the signal had changed very much from one sample to another and so the most likely explanation was that the scale of the output signal was varying in some manner. This would be caused, for example, by variations in the gain of the servosystem maintaining the secondary cavity on resonance. This could be caused by manual adjustments by an operator or such events as fluctuations in the input light level.

The assumption was made that this variation in the values of the deviation for each sample was the result of such a scaling factor and so the samples were rescaled to give a standard deviation of ~ 20. At this point the samples, individually, were too small to draw any conclusions about the statistics of the signal and so the points were sorted into 'bins' representing different values of voltage and then the values of each bin were summed. The final total produced the histogram shown in Figure 6.3. The shape appears to be Gaussian and this can be tested in various ways. The shape of the ideal Gaussian distribution is given by:

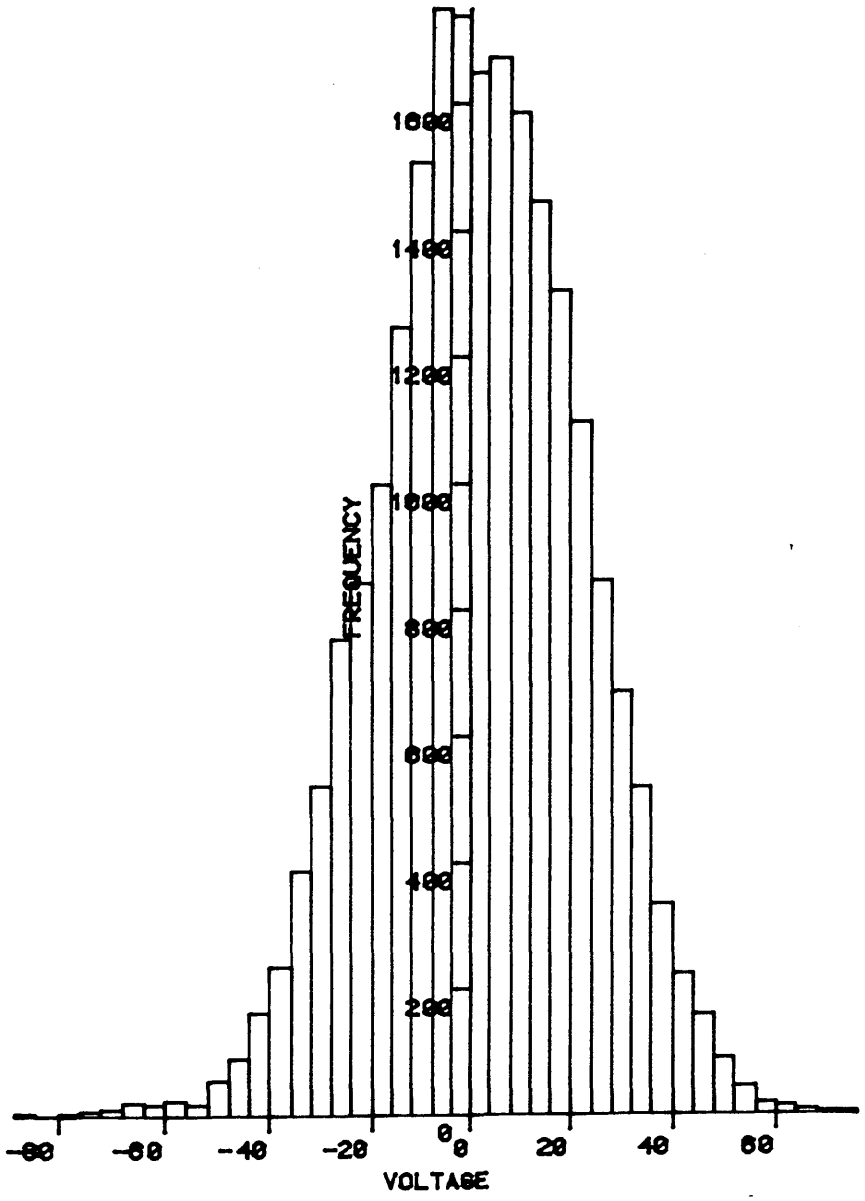

Figure 6.3 A plot of No. of counts against voltage (in arbitrary units).

$$y = A_o \, e^{-x^2/\sigma^2} \tag{6.2}$$

Where A_o is the peak of the distribution and σ is the standard deviation. This can be rewritten as:

$$\ln(y) = \ln(A_o) - x^2/\sigma^2 \tag{6.3}$$

Now the data in Figure 6.3 on a plot of ln(y) against x^2 should produce a straight line, see Figure 6.4. The large errors associated with a small number of events make it difficult to draw any conclusions about the detector statistics beyond the 2σ level. Two further tests may be made of the 'goodness' of the Gaussian[89]. The first is known as the ratio of skewness and indicates whether there is any excess in the density of distribution on the left (negative value) or the right (positive value) of the mean. This ratio lies between the values -1 and +1.

The ratio of skewness is given by:

$$S = \frac{\sum_i (x_i - \bar{x})^3}{N * \sigma^3} \tag{6.4}$$

The sample of 22016 points in Figure 6.3 has a ratio of skewness, S = -0.08, and so there is no significant bias to right or left.

The second test is of the kurtosis or excess of the distribution. This gives an indication of whether there is an excess in the density of the distribution about the mean, ie. whether the distribution is too sharply, or not sufficiently peaked. The ratio of kurtosis is given by:

$$K = \frac{\sum_i (x_i - \bar{x})^4}{N * \sigma^4} - 3 \tag{6.5}$$

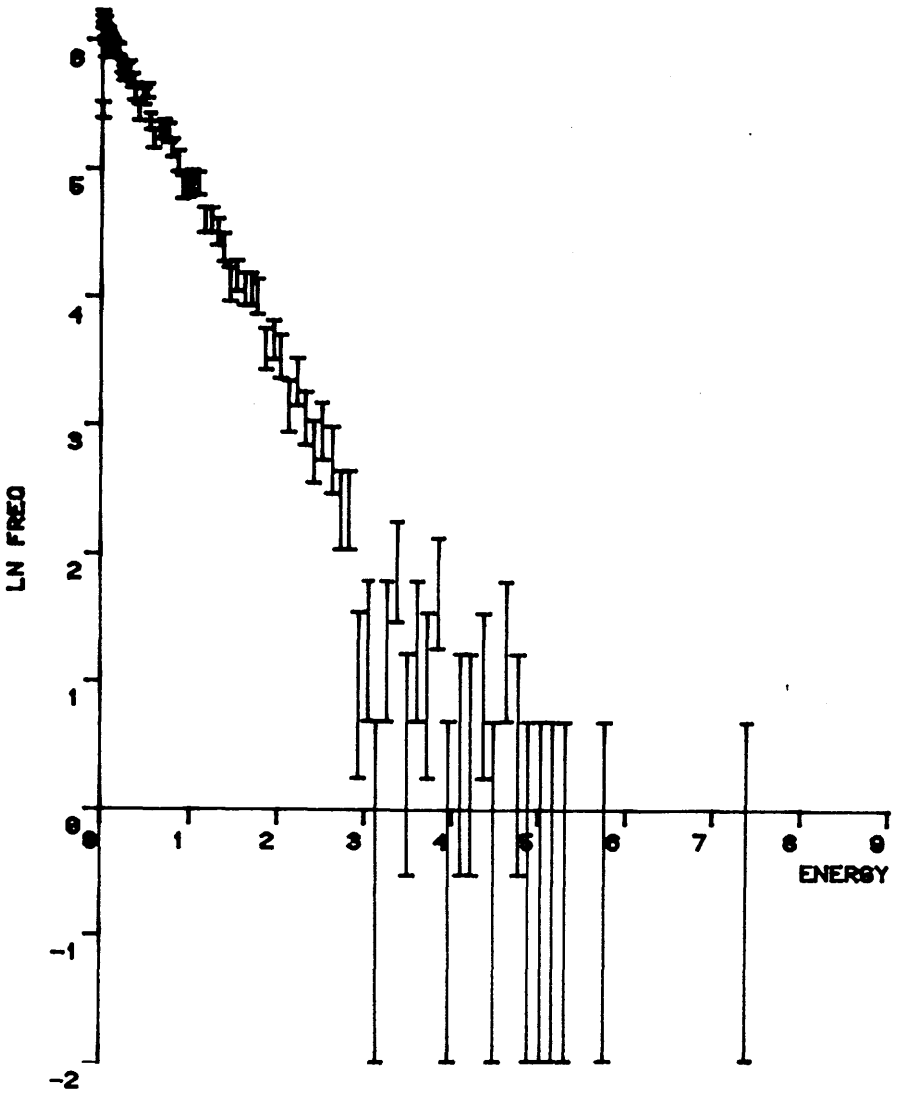

Figure 6.4 A plot of ln(no. of counts) against energy (in arbitrary units). The two sigma level is just above +2 on the y-axis. The error bars extending to -2 represent ln(0).

The sample here has a kurtosis, K = -0.0015.

These last two tests are not sufficient in themselves to show that the distribution is Gaussian in nature but when combined with the graphs of Figures 6.3 and 6.4 they show that the noise characteristics of the prototype detector are well-behaved and may be treated as Gaussian to 2σ. At the present time work is proceeding on the analysis of a much larger section of data using digital filtering techniques to investigate the statistics in the tails of the distribution.

In conclusion the data collection system has proved to be capable of collecting selected samples of data from the continuous stream from the detector. Although there has not as yet been any opportunity for the collection of pulses which might be due to gravitational wave events the system has been shown to be flexible and reliable.

The data collection system could have been used to collect more samples from the stored tape but not enough to alter the statistics significantly. For future data analysis the gain of the secondary cavity servosystem must be held constant to allow this type of analysis. This could be achieved, for example, by comparing the value of a calibration peak in the data stream to some voltage reference and using this signal to adjust the gain on-line.

CHAPTER 7

PROSPECTS FOR THE FUTURE

In the two decades since Weber announced his results a great deal of progress has been made. Much has been learnt by theorists about how to calculate the levels of gravitational radiation to be expected from a source. This has led to more realistic beliefs about the levels of radiation to be expected at Earth than was the case in the late 1960's.

However, detector development has also come a long way. The current generation of detectors have sensitivities close to $h \sim 10^{-18}$ and several systems now show the potential to operate at the levels required to detect events in the Virgo cluster of galaxies. This is necessary for the detection of several events per year. In particular laser interferometers have been shown to have potentially better sensitivities over wider bandwidths than the Weber bars. In fact now, as never before, workers in the field are poised on the brink of making gravitational wave astronomy a reality in the next decade.

Bar groups working at Perth in W. Australia, University of Rome (CERN), Louisiana State and Stanford Universities in America have recently collaborated to form GRAVNET, an organisation which attempts to co-ordinate detector running times and embodies provisional protocols for the exchange of data and publishing of results.

The detectors all have their resonant frequency near 900Hz and a bandwidth of ~ 1Hz and in April to July of 1986 an attempt was made to run all four bars in coincidence. Unfortunately the Niobium bar in

W. Australia developed problems with the superconducting parametric amplifier used to sense motion in the bar. During the run the Stanford-Rome and Louisiana-Rome combinations achieved a sensitivity to pulses of $h > 2.5 * 10^{-18}$. The Stanford and Louisiana instruments achieved a combined sensitivity to pulses of $h > 5 * 10^{-18}$.

Since this run the Louisiana group have been involved in rebuilding their detector to reduce mechanical noise and adding a larger cryostat to allow longer detection runs.

Stanford are presently constructing a new bar which has a design sensitivity to strain of $h \leq 3 * 10^{-20}$ and Rome also have plans for a new cooled detector. However it should be noted that it will be very difficult for Weber-type bars to to achieve sensitivities of $h \sim 10^{-21}$. To detect several gravitational wave events per year a sensitivity of $h \sim 10^{-22}$ over a bandwidth of a few hundred Hertz would be much better and interferometers hold more promise of ultimately achieving this goal.

In fact interferometers have been improving in sensitivity to such an extent that several groups now feel that the time is right to construct longer baseline detectors with sensitivities which should allow the detection of several events per year.

The Glasgow ten metre prototype currently has the best displacement sensitivity of any interferometer at $1.2 * 10^{-18}$ m/Hz$^{1/2}$ over a 1kHz bandwidth centred on 2kHz. At present effort is being concentrated on improving the frequency stability of the light illuminating the interferometer and on the coherent addition of high power Argon Ion lasers.

The British proposal is for the construction of one interferometer with an initial arm length of 1km, though sites have been selected to allow a possible later extension to ~ 3km.

A strain sensitivity for 1msec pulses of $h \sim 3 * 10^{-18}$ has been achieved on the interferometric detectors at Glasgow and at the Max Planck Institute in Germany, the latter having an arm length of 30 metres. At present the German group is involved in investigating the implementation of the recycling and squeezing techniques which will be required to achieve maximum sensitivity in a long baseline detector.

The group in Germany has suggested an ambitious scheme for a large detector involving the construction of three interferometers with arm lengths of three kilometres. However in their proposal the arms are not orthogonal but are arranged at 60^{o} to each other and so the whole apparatus forms an equilateral triangle of 3km on each side. Although the sensitivity of each interferometer will be slightly lower than if the arms were orthogonal this system has the advantage of providing full coverage of all polarisations of gravitational radiation of suitable orientation. The delay line technique developed by the German group requires larger mirrors than the Fabry-Perot and so experiments are under way to use multiple mirror systems which may present fewer difficulties than the development of very high quality large mirrors.

In America progress has also been made in reducing the effect of noise sources in the newest and largest protoype in California and current emphasis is on active systems to reduce the effects of seismic noise. Work is also proceeding on the shorter baseline detector at the Massachusetts Institute of Technology, the construction of a new detector with an arm length of 5 metres is under way and the use of high power YAG lasers to increase the light power available is being investigated.

The groups at Caltech and M.I.T. have collaborated to produce a proposal for two detectors with arm lengths of 4km. The proposal

calls for the two detectors to be the same type, ie. either Fabry-Perot or delay line, although a decision on the final design has not yet been made. However the prospects seem good that funding will be made available for the construction of two interferometers in the near future.

An exciting development in recent months has been a new proposal for a long baseline interferometer submitted by groups from Orsay, France, where work is proceeding on recycling and high power YAG lasers, and Pisa, Italy where the group is experienced in low frequency seismic isolation.

There is a good spirit of international cooperation between the groups in the field and it can be seen from the above that the work at these laboratories is complementary.

Clearly the provision of three detectors in Europe and two in America should provide the necessary redundancy to extract much useful information from a gravitational wave event. Also the more detectors that are available the better the sky coverage, and it is useful for detectors to be widely separated to prevent local disturbances producing coincident events. Further if the detectors are widely separated then the arrival times of gravitational waves at different detectors will allow the determinaton of the position of the source.

In conclusion, with the organised coincident running of several bar detectors of ever improving sensitivity and the very real prospects that several long baseline interferometer detectors will be built in the near future it is more likely than at any previous time that gravitational radiation will soon be seen by several independent detectors. The potential rewards of such observations can only be guessed at but it would be surprising if it was any less remarkable than the opening of other new areas in Astronomy.

APPENDIX A

It can be seen from Figures 3.4 and 4.3 that the feedback circuits for the intensity and frequency servosystems are complicated by several paths from the input to the output. Fortunately the overall transfer function may be determined by calculating the transfer function for each possible path individually. The two programs listed below were used for this task. The first program is concerned with calculating the values of a transfer function over a range of frequencies and storing these values on tape. The second program allows the recall of all or part of this stored data to calculate nyquist and bode plots.

Because of the complex nature of the response function it is necessary to calculate two values for the transfer function at each frequency, f. In the following program, arranged to calculate the transfer function of the intensity stabilisation system, the response functions of amplifier are stored in the G arrays, filters in F arrays and these are summed in A arrays. In all these cases a suffix one in the array name represents the real part of the function and a suffix two represents the imaginary values. The arrays storing the values of resistors and capacitors are set up at the end of the program.

```
10 ! ***** OPEN-LOOP RESPONSE FUNCTION OF THE LASER INTENSITY
STABILISATION CIRCUIT *****
20 ! ***** THE SYSTEM GAIN *****
30 RAD @ V5=280 @ V0=.9*V5 @ K=PI*V0/(V5*2)
40 G=.025*PI*SIN(K)*COS(K)/V5
50 OPTION BASE 1
60 P=100 @ GOSUB 980
```

```
70 DIM R1(3),R2(2),R3(3),R4(2),R(2),C1(1),C2(1),C3(1),C(2)
80 DIM A1(2),A2(2),D(4),R9(3),G1(4),G2(3)
90 DIM A$[6],B$[1]
100 GOSUB 560
110 END
```

Initially the transfer function of each amplifier is calculated in terms of a real denominator and real and imaginary numerators.

```
120 !
130 ! RATIONALISED DENOMINATOR EQUATIONS
140 !
150 D(1)=R1(1)*(1+W^2*C1(1)^2*R9(1)^2)
160 D(2)=R2(1)*(1+W^2*C2(1)^2*R9(2)^2)
170 D(3)=R3(1)*(1+W^2*C3(1)^2*R9(3)^2)
180 D(4)=R4(1)
190 !
200 ! NUMERATOR-REAL PART
210 !
220 G1(1)=-R1(2)*(1+W^2*C1(1)^2*R1(3)*R9(1))/D(1)
230 G1(2)=-R2(2)/D(2)
240 G1(3)=-R3(2)*(1+W^2*C3(1)^2*R3(3)*R9(3))/D(3)
250 G1(4)=-R4(2)/D(4)
260 !
270 ! NUMERATOR-IMAGINARY PART
280 !
290 G2(1)=W*C1(1)*R1(2)^2/D(1)
300 G2(2)=W*C2(1)*R2(2)^2/D(2)
310 G2(3)=W*C3(1)*R3(2)^2/D(3)
320 !
```

```
330 ! FILTERS - REAL PARTS
340 !
350 F1(1)=1/(1+(W*C(1)*R(1))^2)
360 F1(2)=1/(1+(W*C(2)*R(2))^2)
370 !
380 ! FILTERS - IMAGINARY PARTS
390 !
400 F2(1)=(-W*C(1)*R(1))/(1+(W*C(1)*R(1))^2)
410 F2(2)=(-W*C(2)*R(2))/(1+(W*C(2)*R(2))^2)
420 !
430 ! COMPONENTS-REAL PARTS
440 !
450 A1(1)=A*(G1(1)*(G1(2)*F1(1)-G2(2)*F2(1))-G2(1)*(G1(2)*F2(1)
+G2(2)*F1(1)))
460 A1(2)=B*G1(4)*C*(F1(2)*(G1(1)*G1(3)-G2(1)*G2(3))-F2(2)*(G1(1)
    *G2(3)+G2(1)*G1(3)))
470 !
480 ! COMPONENTS-IMAGINARY PARTS
490 !
500 A2(1)=A*(G1(1)*(G1(2)*F2(1)+G2(2)*F1(1))+G2(1)*(G1(2)*F1(1)
    -G2(2)*F2(1)))
510 A2(2)=B*G1(4)*C*(F2(2)*(G1(1)*G1(3)-G2(1)*G2(3))+F1(2)*(G1(1)
    *G2(3)+G2(1)*G1(3)))
520 T1=G*(A1(1)+A1(2))
530 T2=G*(A2(1)+A2(2))
540 RETURN
550 !
560 ! ***** SELECT OPTION *****
570 !
580 CLEAR @ DISP @ DISP "DO YOU WANT TO CALCULATE"
```

```
    @ DISP "    1) RESPONSE AT ONE FREQUENCY"
590 DISP "    2) RESPONSE OVER A RANGE";@ INPUT A1
600 ON A1 GOTO 620,760
610 !
620 ! ***** SINGLE RESPONSE *****
630 !
640 CLEAR @ DISP @ DISP "WHAT FREQUENCY ";@ INPUT A1@ IF A1<.001
    THEN GOTO 640
650 W=2*PI*A1 @ GOSUB 130
660 T3=SQR(T1^2+T2^2) @ P0=T2/T1 @ T0=ATN(P0)
670 IF P0>0 AND T1<0 THEN T0=T0-180
680 IF P0<0 AND T1<0 THEN T0=T0-180
690 IF P0>0 AND T1>0 THEN T0=T0-360
700 DISP @ DISP "    GAIN=";T3 @ DISP "    Re G=";T1
    @ DISP "    Im G=";T2 @ DISP "    PHASE=";T0
710 DISP @ DISP "ARE YOU FINISHED";@ INPUT B$
720 IF B$="N" THEN GOTO 620
730 IF B$<>"Y" THEN GOTO 710
740 RETURN
750 !
760 ! ***** STORE DATA ARRAY *****
770 !
780 CLEAR @ DISP @ DISP "NAME THE DESTINATION FILE ";@ INPUT A$
790 CREATE A$,P*2+11,8
800 ASSIGN# 1 TO A$
810 H1=-INF @ H2=-INF @ H3=-INF @ M1=INF @ M2=INF @ M3=INF @ F1=.01
820 S1=2*PI*F1 @ DISP "ENTER THE UPPER FREQUENCY LIMIT ";
    @ INPUT F2@ IF F2<F1 THEN GOTO 820
830 L2=10^INT(LGT(F2)) @ L2=LGT(INT(F2/L2+.5)*L2)
840 DISP @ DISP "COMPUTING ...."
```

```
850 M=(L2+2)/P @ FOR I=0 TO P-1
860 W=S1*10^(I*M)
870 GOSUB 130 @ PRINT# 1,2*I+12 ; T1 @ PRINT# 1,2*I+13 ; T2
880 IF T1<>0 THEN H1=MAX(H1,T1) @ M1=MIN(M1,T1)
890 IF T2<>0 THEN H2=MAX(H2,T2) @ M2=MIN(M2,T2)
900 T3=SQR(T1^2+T2^2) @ IF T3<>0 THEN H3=MAX(H3,T3) @ M3=MIN(M3,T3)
910 NEXT I
920 PRINT# 1,2 ; H1 @ PRINT# 1,3 ; H2 @ PRINT# 1,4 ; H3
    @ PRINT# 1,5 ; M1 @ PRINT# 1,6 ; M2 @ PRINT# 1,7 ; M3
930 PRINT# 1,8 ; F1 @ PRINT# 1,9 ; F2 @ PRINT# 1,10 ; M
    @ PRINT# 1,11 ; P940 BEEP @ DISP "CALCULATION COMPLETE."
950 ASSIGN# 1 TO *
960 RETURN
970 !
980 ! ENTER CAPACITOR VALUES
990 !
1000 C1(1)=.000000000172
1010 C2(1)=.00000000001 @ C3(1)=.0000000022
1020 C(1)=.0000000001 @ C(2)=.0000000011
1030 !
1040 ! ENTER RESISTOR  VALUES
1050 !
1060 R1(1)=100 @ R1(2)=1000000 @ R1(3)=20200 @ R2(1)=100 @ R2(2)=12000
1070 R3(1)=1000 @ R3(2)=270000 @ R3(3)=27000
1080 R4(1)=2000 @ R4(2)=2700
1090 R(1)=18000 @ R(2)=390000
1100 !
1110 ! ENTER ANY OTHER CONSTANTS
1120 !
1130 A=1 @ B=1 @ C=-110 @ ! 0=<A,B=<1:A#B
```

```
1140 !
1150 ! ENTER COMMON RELATIONSHIPS IN EQUATIONS
1160 !
1170 R9(1)=R1(2)+R1(3)
1180 R9(2)=R2(2)
1190 R9(3)=R3(2)+R3(3)
1200 RETURN
```

The following program was written to retrieve the data stored by the previous program. It will plot graphs using all of the stored points or a selected range and incorporates some simple checks to ensure that sufficient data points fall within the range to draw a graph.

```
10 ! *** A PROGRAM TO RETRIEVE CIRCUIT ANALYSIS DATA FROM TAPE AND TO
   PLOT GRAPHS ***
20 DIM A$[6],Q$[7],R$[11],S$[5],T$[5]
30 DEG
40 T=3 @ ! SMALLEST VALUE ON PLUS TO MINUS LOG SCALE=LGT(10^-T)
50 GOSUB 140
60 GOSUB 830
70 GOSUB 270
80 IF B$="Y" THEN GOSUB 490 ELSE GOSUB 620
90 GOSUB 1060
100 GOSUB 1280
110 IF R=1 THEN GOTO 50
120 END
130 !
140 ! ***** SET UP FOR RETRIEVE *****
150 !
```

```
160 CLEAR @ DISP @ DISP "NAME THE SOURCE FILE";@ INPUT A$
170 ASSIGN# 1 TO A$
180 READ# 1,2 ; H1@ READ# 1,3 ;  H2@ READ# 1,4 ; H3@ READ# 1,5 ; M1 @
    READ# 1,6 ; M2@ READ# 1,7 ; M3
190 READ# 1,8 ; F1@ READ# 1,9 ; F2@ READ# 1,10 ; M@ READ# 1,11 ; P
200 !
210 !  READ HIGHEST/LOWEST REAL/IMAG. H1,M1,H2,M2:HIGHEST/LOWEST  G.
    H3,M3:
220 ! READ LOWEST, HIGHEST FREQUENCY  F1,F2:
230 ! READ NO. OF POINTS P, POINT SPACING IN OMEGA M:
240 !
250 RETURN
260 !
270 ! ***** SELECT FREQUENCY SPAN *****
280 !
290 CLEAR @  DISP  @  DISP  "THE FREQUENCY RANGE IS ";F1;" TO ";F2; "
    HERTZ."
300 DISP @ DISP "DO YOU WANT TO  LIMIT  THE FREQUENCY RANGE"; @ INPUT
    B$
310 IF B$="N" THEN F3=F1 @ F4=F2 @ I1=0 @ I2=P-1 @ RETURN
320 IF B$<>"Y" THEN GOTO 300
330 DISP @ DISP "ENTER FREQUENCY RANGE    (lowest,highest)"; @ INPUT
    F3,F4
340 IF F3<F1 OR F3>F2 THEN GOTO 330
350 IF F4<F1 OR F4>F2 OR F4<F3 THEN GOTO 330
360 IF  X<>1  THEN  GOTO  440
370 IF X1=2 THEN GOTO 400
380 F3=INT(F3/10)*10
390 F4=INT(F4/10+.5)*10 @ GOTO 440
400 F5=10^INT(LGT(F3)-1)
```

```
410 F3=INT(F3/F5)*F5
420 F6=10^INT(LGT(F4))
430 F4=INT(F4/F6+.5)*F6
440 I1=INT(LGT(2*PI*(F3-F1))/M)
450 I2=INT(LGT(2*PI*(F4-F1))/M+1)
460 IF I2-I1<10 THEN DISP "NOT ENOUGH POINTS TO PLOT" @ GOTO 330
470 RETURN
480 !
490 ! ***** SET LIMITS OF AXES *****
500 !
510 H1=-INF @ H2=-INF @ H3=-INF @ M1=INF @ M2=INF @ M3=INF
520 FOR I=I1  TO I2
530 READ# 1,2*I+12 ; T1
540 READ# 1,2*I+13 ; T2
550 T3=SQR(T1^2+T2^2) @  IF T3=0 THEN GOTO 570
560 H3=MAX(H3,T3) @ M3=MIN(M3,T3)
570 IF T1=0 THEN  GOTO  590
580 H1=MAX(H1,T1) @ M1=MIN(M1,T1)
590 IF  T2=0   THEN  GOTO  610
600 H2=MAX(H2,T2) @ M2=MIN(M2,T2)
610 NEXT I
620 ON X GOTO 630,660
630 ON X1 GOTO 640,650
640 X2=F3 @ X3=F4  @  GOTO 700
650 X2=LGT(F3) @ X3=LGT(F4) @ GOTO 700
660 ON X1 GOTO 670,680
670 X2=INT(M1/10)*10 @ X3=INT(H1/10)*10 @ GOTO 700
680 X2=INT(LGT(ABS(M1))+1)*SGN(M1)
690 X3=INT(LGT(ABS(H1))+1)*SGN(H1)
700 ON Y GOTO 710,730,770
```

```
710 Y2=-360 @ Y3=0 @ Y4=0 @ Y5=60
720 GOTO  810
730 ON Y1 GOTO 740,750
740 Y2=INT(M2/10)*10 @ Y3=CEIL(H2/10)*10 @ GOTO 810
750 Y2=INT(LGT(ABS(M2))+1)*SGN(M2)
760 Y3=INT(LGT(ABS(H2))+1)*SGN(H2) @ GOTO 810
770 ON Y1 GOTO 780,790
780 Y2=INT(M3/10)*10 @ Y3=CEIL(H3/10)*10 @ GOTO 810
790 Y2=INT(LGT(M3))
800 Y3=INT(LGT(H3)+1)
810 RETURN
820 !
830 ! ***** SELECT QUANTITIES TO BE PLOTTED *****
840
850 ! ***** Y=QUANTITY  TO  BE  PLOTTED,  Y1=LOG/LIN, Y2=MIN, Y3=MAX,
Y4=INTERCEPT
860 ! Y5=MARK SPACING, Y6=DATA POINT.
870 !
880 ! X VARIABLES DITTO
890 !
900 CLEAR @  DISP @ DISP "SELECT THE VERTICAL AXIS "  @ DISP "     1)
    PHASE"
910 DISP "     2)   Im G" @ DISP "     3)   G";@ INPUT Y
    @ IF Y<1 OR Y>3 THEN GOTO 900
920 IF Y=1 THEN Q$=" PHASE " ELSE Q$=" Im G "
930 IF Y=3 THEN Q$=" GAIN "
940 IF Y=1 THEN Y1=1 @ GOTO 970
950 DISP @ DISP "SELECT SCALING:" @ DISP "     1)   LINEAR"
    @ DISP "     2)   LOG";@ INPUT Y1
960 IF Y1<1 OR Y1>2 THEN GOTO 950
```

```
970 IF Y1=1 THEN S$=" LIN." ELSE S$=" LOG."
980 CLEAR @ DISP @ DISP "SELECT THE HORIZONTAL AXIS:"
    @ DISP "     1)   FREQUENCY"
990 DISP "     2)   Re G";@ INPUT X@ IF X<1 OR X>2 THEN GOTO 980
1000 IF X=1 THEN R$=" FREQUENCY " ELSE R$=" Re G "
1010 DISP @ DISP "SELECT SCALING:" @ DISP "     1)   LINEAR"
     @ DISP "     2)   LOG";@ INPUT X1
1020 IF X1<1 OR X1>2 THEN GOTO 1010
1030 IF X1=1 THEN T$=" LIN." ELSE T$=" LOG."
1040 RETURN
1050 !
1060 ! ***** SET UP SCALES OF AXES *****
1070 !
1080 ! ***** Y SCALES *****
1090 !
1100 IF Y=1 THEN GOTO 1180
1110 IF Y=3 OR Y1=1 THEN GOTO 1140
1120 IF Y3<>Y2 THEN V=MAX(ABS(Y2),ABS(Y3)) @ Y2=-V @ Y3=V1130 Y4=0
     @ Y5=(Y3-Y2)/(Y3-Y2+2*T) @ GOTO 1180
1140 Y5=(Y3-Y2)/10 @ IF Y1=2 THEN Y5=1
1150 Y4=0 @ IF Y2>0 THEN Y4=Y2
1160 IF Y3<0 THEN Y4=Y3
1170 !
1180 ! ***** X SCALES *****
1190 !
1200 IF X=1 OR X1=1 THEN GOTO 1230
1210 IF X2<>X3 THEN V=MAX(ABS(X2),ABS(X3)) @ X2=-V @ X3=V
1220 X4=0 @ X5=(X3-X2)/(X3-X2+2*T) @ GOTO 1260
1230 X5=(X3-X2)/10 @ IF X1=2 THEN X5=1
1240 X4=0 @ IF X2>0 THEN X4=X2
```

```
1250 IF X3<0 THEN X4=X3
1260 RETURN
1270 !
1280 ! ***** READ AND PLOT *****
1290 !
1300 GCLEAR
1310 SCALE X2,X3,Y2,Y3
1320 PRINT @ PRINT "           ";A$ @ PRINT
1330 XAXIS Y4,X5
1340 YAXIS X4,Y5
1350 L=1
1360 FOR I=I1 TO I2
1370 READ# 1,2*I+12 ; T1
1380 READ# 1,2*I+13 ; T2
1390 GOSUB 1540
1400 IF L=0 THEN L=1 @ GOTO 1420
1410 PLOT X6,Y6
1420 NEXT I
1430 BEEP @ BEEP
1440 COPY @ PRINT @ PRINT
1450 PRINT "VERTICAL AXIS:" @ PRINT S$;Q$;"SCALE:";Y2;" - ";Y3;"."
1460 PRINT @ PRINT "HORIZONTAL AXIS:" @ PRINT T$;R$;"SCALE:";X2;
     " - ";X3;"."
1470 PRINT @ PRINT I2-I1+1;" POINTS PLOTTED."
1480 PRINT @ PRINT @ PRINT @ PRINT
1490 DISP @ DISP "DO YOU WANT ANOTHER GRAPH";@ INPUT A$
1500 IF A$[1,1]<>"Y" AND A$[1,1]<>"N" THEN GOTO 1490
1510 IF A$[1,1]="Y" THEN R=1 ELSE R=0
1520 RETURN
1530 !
```

```
1540 ! ***** ASSIGN PLOT VALUES *****
1550 !
1560 ON X GOTO 1570,1590
1570 X6=F1*10^(I*M) @ ON X1 GOTO 1640,1580
1580 X6=LGT(X6) @ GOTO 1640
1590 X6=T1 @ ON X1 GOTO 1640,1600
1600 IF 10^(-T)>ABS(X6) THEN L=0 @ GOTO 1790
1610 IF X6<0 THEN GOTO 1630
1620 X6=T*X5+LGT(X6)*X5 @ GOTO 1640
1630 X6=-T*X5-LGT(ABS(X6))*X5
1640 ON Y GOTO 1650,1710,1760
1650 T0=T2/T1
1660 Y6=ATN(T0)
1670 IF T0>0 AND T1<0 THEN Y6=Y6-180
1680 IF T0<0 AND T1<0 THEN Y6=Y6-180
1690 IF T0>0 AND T1>0 THEN Y6=Y6-360
1700 GOTO 1790
1710 Y6=T2 @ ON Y1 GOTO 1790,1720
1720 IF 10^(-T)>ABS(Y6) THEN L=0 @ GOTO 1790
1730 IF Y6<0 THEN GOTO 1750
1740 Y6=T*Y5+LGT(Y6)*Y5 @ GOTO 1790
1750 Y6=-T*Y5-LGT(ABS(Y6))*Y5 @ GOTO 1790
1760 Y6=SQR(T1^2+T2^2) @ ON Y1 GOTO 1790,1770
1770 IF Y6=0 THEN L=0 @ GOTO 1790
1780 Y6=LGT(Y6)
1790 RETURN
```

APPENDIX B

This appendix contains a listing of the program which was written for the BBC microcomputer to run the data collection system described in Chapter 6. Because the program is quite large it was split up into three sections which were loaded in and assembled individually. Each section contains many comments to explain the operation of the system.

```
 10 REM ---*** DATA1 ***---
 20 REM This section contains the clock R/W routines.
 30 MODE3:Z%=&0900:SETTIME=5:PASS=2
 40 REM Define VIA registers.
 50 DRB=&FCC0:DRA=&FCC1:DDRB=&FCC2:DDRA=&FCC3
 60 ACR=&FCCB:PCR=&FCCC:FLAG=&FCCD:IER=&FCCE
 70 PCR2=&FCDC:FLAG2=&FCDD:IER2=&FCDE
 80 REM Define clock registers for assembler.
 90 CLOCK=&70:FSEC=&71:SEC=&72:DSEC=&73:MINUTE=&74:DMINUTE=&75
100 HOUR=&76:DHOUR=&77:DATE=&78:DDATE=&79:WDAY=&7A:MONTH=&7B
110 DMONTH=&7C:YEAR=&7D:RESULT=&7E:REGISTER=&7F:TEMP=&80
120 S=HIMEM-&100:M=HIMEM-&100+&02:H=HIMEM-&100+&04
130 RUPTOFF=HIMEM-&100+&2B:RUPTON=HIMEM-&100+&36
140 REM Assemble the routines in page &0900.
150 FOR opt = 0 TO PASS STEP PASS
160 P%=Z%
170
180 [ OPT opt
190
200.VIA1
210    LDA #&7F    \Disable VIA
```

```
220     STA IER     \interrupts.
230     LDA #&00    \Write ACR with CB1
240     STA ACR     \latching disabled.
250     LDA #&FF    \Make port A
260     STA DDRA    \all outputs.
270.PULSE
280     LDA #&FF    \Make port B
290     STA DDRB    \all outputs.
300     LDA #&AE    \Set CA2 on manual high
310     STA PCR     \and CB2 for pulse output.
320     RTS
330
340.INIT            \Initialise clock for start.
350     LDA #&00    \Write 0 to DB3 of clock
360     STA DRB     \to initialise system.
370     LDA #&F0    \Write to address 15
380     STA DRB     \to disable interrupts.
390.HALT
400     LDA #&E0    \Write 0 to address 14 to
410     STA DRB     \stop clock and reset seconds.
420     RTS
430
440.GO
450     LDA #&FF    \Clear all
460     STA FLAG    \interrupt flags.
470.BEGIN
480     LDA FLAG    \Check flags.
490     CMP #&02    \Has MSF pulse arrived?
500     BNE BEGIN
510
```

```
520    LDA #&FF
530    STA FLAG    \Clear IFR flags.
540    LDA #&E1    \Write to address 14
550    STA DRB     \to start the clock.
560    RTS
570
580.OLDVECTOR
590
600 ]
610
620 P%=P%+2
630
640 [ OPT opt
650
660.VECTOR
670    SEI         \Prevent interrupt while vector is replaced.
680    LDA &0205
690    CMP #ROUTINE DIV 256
700    BNE DO      \Is vector already replaced?
710
720    LDA &0204
730    CMP #ROUTINE MOD 256
740    BEQ DONE    \If vector already replaced exit.
750
760.DO
770    LDA &0204   \Store old vector.
780    STA OLDVECTOR
790    LDA &0205
800    STA OLDVECTOR+1
810    LDA #ROUTINE DIV 256
```

```
 820    STA &0205  \Load new vector.
 830    LDA #ROUTINE MOD 256
 840    STA &0204
 850.DONE
 860    CLI
 870    RTS
 880
 890.ROUTINE       \Interrupt routine.
 900    LDA FLAG2  \Read IFR2.
 910    AND #&01   \Is interrupt set?
 920    BEQ ROUTINE2
 930
 940    LDA IER2   \Is interrupt enabled?
 950    CMP #&81
 960    BNE ROUTINE2
 970
 980    JSR RUPTOFF\Yes!
 990
1000    LDA &FF    \Emulate ESCAPE key press.
1010    ORA #&80
1020    STA &FF
1030    LDA &FC    \Restore accumulator.
1040    CLI
1050    RTI
1060
1070.ROUTINE2      \Check for MSF interrupt.
1080    LDA &041C  \Fetch G%.
1090    BNE CHECK  \If G%<>1 exit.
1100
1110    JMP (OLDVECTOR)
```

```
1120
1130.CHECK
1140    LDA FLAG
1150    AND #&02    \Check source of interrupt.
1160    BNE SERVICE\If not VIA exit.
1170
1180    LDA IER     \And is the interrupt set?
1190    CMP #&82
1200    BNE SERVICE\If not then exit.
1210
1220    JMP (OLDVECTOR)
1230
1240.SERVICE        \It is an MSF interrupt.
1250    LDA #&10    \Find value of FSEC.
1260    STA REGISTER
1270    JSR OUT
1280
1290    LDA RESULT \Retrieve FSEC.
1300    STA &044C  \Set S%.
1310    BNE FSET
1320
1330    LDA #&01    \The clock is on
1340    STA &0418  \time; set F%=1
1350    LDA #&05    \and S%=5.
1360    STA &044C
1370    JMP SET
1380
1390.FSET           \THE CLOCK IS OUT OF SYNCH.
1400    LDA #&00
1410    STA &0418  \Set F%=0.
```

```
1420.SET            \Disable the interrupt.
1430    LDA #&00    \Set G%=0 to
1440    STA &041C   \disable interrupt.
1450    LDA #&7F    \Disable VIA
1460    STA IER     \interrupts.
1470    LDA #&FF    \Clear VIA
1480    STA FLAG    \interrupts.
1490    LDA &FC     \Restore accumulator.
1500    CLI
1510    RTI
1520
1530.ENABLE
1540    LDA #&FF    \Clear VIA
1550    STA FLAG    \interrupt flags.
1560    LDA #&82    \Enable CA1
1570    STA IER     \interrupt.
1580    LDA #&01    \Set G%=1.
1590    STA &041C
1600    RTS
1610
1620.VIA2
1630    LDA PCR     \Read the PCR.
1640    ORA #&E0    \Disable CB2 pulse mode.
1650    STA PCR     \Write modified PCR.
1660    LDA #&F0    \Configure half of
1670    STA DDRB    \port B for input.
1680    RTS
1690
1700.OUT
1710    LDA REGISTER
```

```
1720    STA DRB     \Select clock register.
1730.REDO
1740    LDA #&EC
1750    STA PCR     \Write low CA2.
1760    LDA DRB     \Read data from B port.
1770    STA TEMP
1780    LDA #&EE    \Write high CA2.
1790    STA PCR
1800    LDA TEMP
1810    AND #&0F    \Mask most significant nibble.
1820    CMP #&0F    \Check for clock register update.
1830    BEQ REDO    \If found repeat read.
1840
1850    STA RESULT \Store the result for BASIC.
1860    RTS
1870
1880.SYNCH
1890    LDA &0418  \Is synchronisation selected?
1900    CMP #&02   \If F%=2 it isn't.
1910    BEQ EXIT
1920               \IF MINUTE<>SETTIME-F%-(S%<5) THEN EXIT.
1930    LDA #SETTIME
1940    SEC
1950    SBC &0418  \SETTIME-F%.
1960    LDY &044C  \Fetch S%.
1970    CPY #&05
1980    BCS GE
1990
2000    CLC        \S%<5.
2010    ADC #&01
```

```
2020.GE             \S%>=5.
2030    SEC
2040    SBC MINUTE \Does MINUTE equal the expression?
2050    BNE EXIT   \If not then exit.
2060
2070               \IF SEC<>-59*(S%>4) THEN EXIT.
2080    LDA &044C  \Fetch S%.
2090    CMP #&05
2100    BCS GE2
2110
2120    LDA #&00   \S%<5.
2130    CMP SEC    \Does SEC=0?
2140    BNE EXIT   \If not exit.
2150
2160    JMP TESTTWO
2170
2180.EXIT
2190    LDA IER2   \Is data collection
2200    CMP #&81   \interrupt set?
2210    BEQ EXIT5
2220
2230    JSR RUPTON \If not - enable.
2240
2250.EXIT5
2260    RTS
2270
2280.GE2            \S%>4.
2290    LDA #59
2300    CMP SEC    \Does SEC=59?
2310    BNE EXIT   \If not exit.
```

```
2320
2330.TESTTWO        \IF FSEC<>(1-S%)*(F%=0) THEN EXIT.
2340    LDY #&00    \Y=0.
2350    LDA &0418   \Fetch F%.
2360    BNE JUMP
2370
2380    LDA &044C   \F%=0 so fetch S%.
2390    SEC
2400    SBC #&01    \S%-1.
2410    TAY         \Y=S%-1.
2420.JUMP
2430    CPY FSEC    \Does FSEC=expression?
2440    BNE EXIT
2450
2460    LDA &0418   \Yes. Fetch F%.
2470    BEQ TEST1
2480
2490    JMP ENABLE \If F%=1 then enable the interrupt.
2500
2510.TEST1          \Correct the clock.
2520    LDA &044C
2530    CMP #&05    \If S%<5 then the clock is fast.
2540    BCS TEST2
2550
2560    JSR PULSE   \Enable VIA for output.
2570
2580    JSR HALT    \Stop the clock.
2590
2600    JMP EXIT4
2610
```

```
2620.TEST2          \The clock is slow.
2630    LDA #&40    \Examine minute register.
2640    STA REGISTER
2650    JSR OUT
2660
2670    JSR PULSE   \Enable VIA for output.
2680
2690    JSR HALT    \Stop the clock.
2700
2710    LDA RESULT
2720    ADC #&41    \Add 1 and include register address.
2730    STA DRB
2740    AND #&0F
2750    STA MINUTE \Set new minute.
2760    LDA #&30    \Set seconds display.
2770    STA S
2780.EXIT4
2790    JSR GO      \Wait for MSF pulse.
2800
2810    JSR VIA2    \Reset VIA.
2820
2830    LDA #&00    \Set
2840    STA SEC     \shadow
2850    STA FSEC    \counters.
2860    LDA #&01
2870    STA &0418   \Set F%=1.
2880    LDA #&05
2890    STA &044C   \Set S%=5.
2900    JMP EXIT
2910
```

```
2920.FRACS          \Read tenths of seconds register.
2930    LDA #&10    \Tenths of seconds address.
2940    STA REGISTER
2950    JSR OUT     \Read register.
2960
2970    LDA RESULT
2980    STA FSEC    \Store result.
2990    RTS
3000
3010.BOTH           \Find value of double registers.
3020    LDA CLOCK   \Select most significant register.
3030    STA REGISTER
3040    JSR OUT     \Read register.
3050
3060    LDA CLOCK
3070    SEC
3080    SBC #&10    \Select lower register.
3090    STA REGISTER
3100    LDA RESULT
3110    ASLA        \Multiply higher
3120    ASLA        \register by 10.
3130    CLC
3140    ADC RESULT
3150    ASLA
3160    STA CLOCK   \Temporary store.
3170    JSR OUT
3180
3190    LDA CLOCK   \Retrieve lower register.
3200    CLC
3210    ADC RESULT \Add higher result.
```

```
3220    STA CLOCK  \Store answer.
3230    LDA REGISTER
3240    CLC        \Reduce
3250    RORA       \lower
3260    RORA       \register
3270    RORA       \to lower
3280    RORA       \nybble.
3290    TAX
3300    LDA CLOCK  \Store answer in
3310    STA CLOCK,X\appropriate register.
3320    CPX #&07
3330    BCS EXIT2  \If this is not hours,minutes or seconds then
                    exit.
3340
3350    DEX
3360    DEX
3370    LDA #&0D   \Set display string null.
3380    STA S,X
3390    LDA CLOCK
3400    CMP #&0A   \Is result >=10?
3410    BCS EXIT2
3420
3430    LDA #&30   \Set display string = "0".
3440    STA S,X
3450.EXIT2
3460    RTS
3470
3480 ]
3490 NEXT opt
3500 CHAIN "DATA2"
```

```
 10 REM ---*** DATA2 ***---
 20 REM This section maintains the clock shadow registers, inserts
       the
 30 REM event handling routines and enables/disables the IEEE
       interrupt.
 40 HIMEM=HIMEM-&100
 50 REM Define parameters for assembly.
 60 PASS=2:FRACS=&0AAB:BOTH=&0AB7:CLOCK=&70:FSEC=&71:SEC=&72
    :MINUTE=&74
 70 PCR2=&FCDC:FLAG2=&FCDD:IER2=&FCDE:SCREENPLACE=&8E:?&8E=&88
    :?&8F=&72
 80 FOR opt=0 TO PASS STEP PASS
 90 P%=HIMEM
100 [ OPT opt
110
120.S EQUS "0"      \Set up strings
130   EQUB &0D      \for clock display.
140.M EQUS "0"
150   EQUB &0D
160.H EQUS "0"
170   EQUB &0D
180
190.UPDATE          \Keep display and clock shadow registers
updated.
200
210     JSR FRACS   \Update tenths of secs.
220
230     LDA FSEC    \Read tenths of secs.
```

```
240     BNE EXIT3
250
260     LDA #&30    \If zero then time to update seconds.
270     STA CLOCK
280     JSR BOTH
290
300     LDA SEC     \Read secs.
310     BNE EXIT3
320
330     LDA #&50    \If zero then time to update minutes.
340     STA CLOCK
350     JSR BOTH
360
370     LDA MINUTE \Read mins.
380     BNE EXIT3
390
400     LDA #&70    \If zero then time to update hours.
410     STA CLOCK
420     JSR BOTH
430
440.EXIT3
450     RTS
460
470.RUPTOFF         \Disable IEEE interrupt.
480     LDA #&7F    \Disable CA2
490     STA IER2    \interrupt.
500     LDA #&FF    \Clear all of the
510     STA FLAG2   \interrupt flags.
520     RTS
530
```

```
540.RUPTON          \Enable IEEE interrupt.
550     LDA #&02    \Set CA2 of VIA2 to
560     STA PCR2    \independent interrupt.
570     LDA #&FF    \Clear the interrupt
580     STA FLAG2   \flag register.
590     LDA #&81    \Enable the CA2
600     STA IER2    \interrupt bit.
610     RTS
620
630.OLDVECTOR
640
650 ]
660
670 P%=P%+2
680
690 [ OPT opt
700
710 .VECTOR2
720     LDA &0221   \Has vector already been replaced?
730     CMP ROUTINE DIV 256
740     BNE DO
750
760     LDA &0220
770     CMP ROUTINE MOD 256
780     BEQ DONE
790
800.DO
810     LDA &0220   \Store old vector.
820     STA OLDVECTOR
830     LDA &0221
```

```
 840       STA OLDVECTOR+1
 850       LDA #ROUTINE DIV 256
 860       STA &0221  \Load new vector.
 870       LDA #ROUTINE MOD 256
 880       STA &0220
 890.DONE
 900       RTS
 910
 920.ROUTINE          \Event handling routine.
 930       PHP
 940       CMP #&02   \Is this a keyboard press?
 950       BNE EXIT   \If not leave.
 960
 970       PHA
 980       TXA
 990       PHA
1000       TYA
1010       PHA
1020       CPY #&44   \Was the key pressed D?
1030       BNE EXIT1  \If not leave.
1040                  \Erase the disc change message.
1050       LDA #&00   \by poking value of blank space.
1060       LDY #&00   \There are 38 characters to be erased.
1070.CHAR             \i.e. that is 38*8 bytes.
1080       STA (SCREENPLACE),Y
1090       DEY
1100       BNE CHAR
1110                  \256 bytes done.
1120       CLC
1130       LDA SCREENPLACE+1
```

```
1140       ADC #&01    \Move 256 bytes.
1150       STA SCREENPLACE+1
1160       LDY #&00    \Do last 48 bytes.
1170       LDA #&00
1180.CHAR2
1190       STA (SCREENPLACE),Y
1200       DEY
1210       BNE CHAR2
1220
1230       SEC         \Reset screenplace for future use.
1240       LDA SCREENPLACE+1
1250       SBC #&01
1260       STA SCREENPLACE+1
1270       LDX #&02    \Use an OSBYTE call
1280       LDA #&0D    \to disable the event.
1290       JSR &FFF4
1300
1310.EXIT1
1320       PLA
1330       TAY
1340       PLA
1350       TAX
1360       PLA
1370.EXIT
1380       PLP
1390       JMP (OLDVECTOR)
1400
1410 ]
1420 NEXT opt
1430 CHAIN"DATA3"
```

```
10 REM ---*** DATA3 ***---
20 REM This section displays time and implements the IEEE data
       collection.
30 REM Define all the variables for the rest of the program.
40 REM Suppress cursor and define decimal for clock display.
50 VDU 23,240,0,0,0,0,24,24,0,0,0:VDU 23;8202;0;0;0;
60 REM Define the variables for the display.
70 DIM MONTH$(11),DAY$(11),THE$(2)
80 REM Variables for IEEE data collection.
90 DIM wave%1023,bc%(3),ID$(3)
100 FOR I%=1 TO 180:ID$(0)=ID$(0)+" ":NEXT:FOR I%=1 TO 3:
    ID$(I%)=ID$(0):NEXT
110 FOR I%=0 TO 3:bc%(I%)=0:NEXT I%
120 REM Define VIA registers.
130 DRB=&FCC0:DRA=&FCC1:DDRB=&FCC2:DDRA=&FCC3
140 ACR=&FCCB:PCR=&FCCC:FLAG=&FCCD:IER=&FCCE
150 PCR2=&FCDC:FLAG2=&FCDD:IER2=&FCDE
160 REM Define parameters: If F%=1 then once an hour enable
       MSF interrupt.
170 REM If F%=0 then there is a discrepancy in tenths of seconds
       in S%.
180 REM If S%=5 then the clock is synchronised. If G%=0 the MSF
190 REM interrupt is disabled. R% is the active disc drive.
200 F%=1:G%=0:R%=0:S%=5:trace1%=1
210 REM Disable escape key.
220 *FX 200,1,0
230 REM Define machine language calls.
240 VIA1=&0900:INIT=&091A:GO=&092A:VECTOR=&0943:VIA2=&09E1:
```

```
    OUT=&09EF
250 SYNCH=&0A0E:FRACS=&0AAB:BOTH=&0AB7:CLOCK=&70:FSEC=&71:
    SEC=&72
260 DSEC=&73:MINUTE=&74:DMINUTE=&75:HOUR=&76:DHOUR=&77:
    DATE=&78
270 DDATE=&79:WDAY=&7A:MONTH=&7B:DMONTH=&7C:YEAR=&7D:
    RESULT=&7E
280 REGISTER=&7F:TEMP=&80:S=HIMEM:M=HIMEM+&02:H=HIMEM+&04
290 UPDATE=HIMEM+&06:RUPTON=HIMEM+&36:RUPTOFF=HIMEM+&2B
300 VECTOR2=HIMEM+&48
310 PROCinit:ON ERROR GOTO 470
320 CALL VECTOR:CALL VECTOR2:REM Insert interrupt and event
    vectors.
330 CLS:PRINT TAB(22,5) "OPTIONS"
340 PRINT TAB(22,6) "-------"
350 PRINT TAB(10,8) "1)    Load and start clock."
360 PRINT TAB(10,10) "2)    Read out time from clock."
370 INPUT TAB(10,12) "Select 1 or 2 ";I%
380 IF I%<1 OR I%>2 PRINT TAB(24,12) "    ":GOTO 370
390 PRINT TAB(10,14) "Select MSF synchronisation: 1) ON."
400 INPUT TAB(38,16) "2) OFF.";F%:IF F%<1 OR F%>2 PRINT TAB(45
    ,16) "    ":GOTO 390
410 ON I% GOSUB 430,440
420 PROCdisplay:END
430 CALL VIA1:PROCload:RETURN
440 INPUT TAB(10,18) "Enter the year ";Y1%:Y1%=Y1%-INT(Y1%/100)
    *100+1900
450 CALL VIA1:CALL VIA2:CLS:PRINT TAB(22,2) "The clock is
    running.":RETURN
460 REM Error handling routines.
```

```
470 IF ERR=17 THEN PROCdata:PROCsave:PROCdisplay
480 IF ERR<>190 AND ERR<>198 THEN REPORT:PRINT" at line ";ERL
    :STOP
490 VDU 7:PRINT TAB(17,20) "CHANGE DISC IN DRIVE ";R%;" THEN
    PRESS ""D"".."
500 IF ERL=2030 THEN OSCLI("DELETE I"+event$)
510 R%=R% EOR 1:DAY$="DR. "+STR$(R%):OSCLI(DAY$):VDU 7:VDU 7:*FX
    14,2
520 trace1%=trace%:PROCsave:PROCdisplay
530
540 DEFPROCload
550 REM Load the clock registers.
560 CLS:PRINT:INPUT"Enter the year ";TAB(40);Y1%:PRINT
570 Y1%=Y1%-(INT(Y1%/100)*100)+1900:REM Y1%=19xx.
580 ?YEAR=Y1%-(INT(Y1%/4)*4):REM ?YEAR=LEAP YEAR PLUS 0,1,2,3
590 ON ?YEAR+1 GOTO 600,610,620,630
600 ?YEAR=8:GOTO 640
610 ?YEAR=4:GOTO 640
620 ?YEAR=2:GOTO 640
630 ?YEAR=1
640 ?YEAR=&D0+?YEAR:REM ADDRESS+DATA
650 INPUT"Enter the month (1-12) ";TAB(40);?MONTH:PRINT
660 IF ?MONTH<1 OR ?MONTH>12 GOTO 650
670 ?DMONTH=INT(?MONTH/10):?MONTH=?MONTH-?DMONTH*10
680 ?DMONTH=&C0+?DMONTH:?MONTH=&B0+?MONTH
690 INPUT "Enter the day (Monday - 1)";TAB(40);?WDAY:PRINT
700 IF ?WDAY<1 OR ?WDAY>7 GOTO 690
710 ?WDAY=&A0+?WDAY
720 INPUT "Enter the date ";TAB(40);?DATE:PRINT
730 IF ?DATE<1 OR ?DATE>31 GOTO 720
```

```
 740 ?DDATE=INT(?DATE/10):?DATE=?DATE-?DDATE*10
 750 ?DDATE=&90+?DDATE:?DATE=&80+?DATE
 760 INPUT "Enter the hour ";TAB(40);?HOUR:PRINT
 770 IF ?HOUR<0 OR ?HOUR>23 GOTO 760
 780 ?DHOUR=INT(?HOUR/10):?HOUR=?HOUR-?DHOUR*10
 790 ?DHOUR=&70+?DHOUR:?HOUR=&60+?HOUR
 800 INPUT "Enter the minutes ";TAB(40);?MINUTE:PRINT
 810 IF ?MINUTE<0 OR ?MINUTE>59 GOTO 800
 820 ?DMINUTE=INT(?MINUTE/10):?MINUTE=?MINUTE-?DMINUTE*10
 830 ?DMINUTE=&50+?DMINUTE:?MINUTE=&40+?MINUTE
 840 CALL INIT
 850 REM Load clock from shadow registers.
 860 FOR C%=4 TO 13:?DRB=?(CLOCK+C%):NEXT C%
 870 CLS:PRINT TAB(8,5) "The clock registers are loaded. Waiting
     for MSF signal...."
 880 CALL GO
 890 CALL VIA2:CLS
 900 ENDPROC
 910
 920 DEFPROCdisplay
 930 PRINT TAB(22,2) "The clock is running."
 940 PRINT TAB(17,6)"It is";:PRINT TAB(21,10)"The time is ";
 950 PROCmonth:?CLOCK=&70:CALL BOTH:IF ?HOUR>9 $H=""
 960 ?CLOCK=&50:CALL BOTH:IF ?MINUTE>9 $M=""
 970 ?CLOCK=&30:CALL BOTH:IF ?SEC>9 $S=""
 980 PROCweekday
 990 PROCdate:IF ?DATE<>1 GOTO 1010
1000 PROCmonth:IF ?MONTH=1 AND ?HOUR=0 AND ?MINUTE=0 AND ?SEC=0
     Y%=Y%+1
1010 PRINT TAB(22,6)DAY$;?DATE;THE$;MONTH$;Y1%;".        "
```

```
1020 CALL UPDATE:IF ?HOUR=0 GOTO 980
1030 PRINT TAB(33,10)$H;?HOUR;":";$M;?MINUTE;":";$S;?SEC;CHR$(240)
     ;?FSEC
1040 CALL SYNCH
1050 GOTO 1020
1060 ENDPROC
1070
1080 DEFPROCmonth
1090 REM Find out what month it is.
1100 ?CLOCK=&C0
1110 CALL BOTH
1120 ON ?MONTH GOSUB 1140,1150,1160,1170,1180,1190,1200,1210,1220,
     1230,1240,1250
1130 ENDPROC
1140 MONTH$=" January ":RETURN
1150 MONTH$=" February ":RETURN
1160 MONTH$=" March ":RETURN
1170 MONTH$=" April ":RETURN
1180 MONTH$=" May ":RETURN
1190 MONTH$=" June ":RETURN
1200 MONTH$=" July ":RETURN
1210 MONTH$=" August ":RETURN
1220 MONTH$=" September ":RETURN
1230 MONTH$=" October ":RETURN
1240 MONTH$=" November ":RETURN
1250 MONTH$=" December ":RETURN
1260
1270 DEFPROCdate
1280 ?REGISTER=&80:CALL OUT
1290 ?DATE=?RESULT
```

```
1300 THE$="th"
1310 IF ?DATE=1 THE$="st"
1320 IF ?DATE=2 THE$="nd"
1330 IF ?DATE=3 THE$="rd"
1340 ?REGISTER=&90:CALL OUT
1350 IF ?RESULT=1 THE$="th"
1360 ?DATE=?DATE+?RESULT*10
1370 ENDPROC
1380
1390 DEFPROCweekday
1400 ?REGISTER=&A0:CALL OUT
1410 ON ?RESULT GOSUB 1430,1440,1450,1460,1470,1480,1490
1420 ENDPROC
1430 DAY$=" Monday ":RETURN
1440 DAY$=" Tuesday ":RETURN
1450 DAY$=" Wednesday ":RETURN
1460 DAY$=" Thursday ":RETURN
1470 DAY$=" Friday ":RETURN
1480 DAY$=" Saturday ":RETURN
1490 DAY$=" Sunday ":RETURN
1500
1510 DEFPROCinit
1520 *IEEE
1530 CLOSE#0
1540 cmd%=OPENIN("COMMAND")
1550 data%=OPENIN("DATA")
1560 scope%=OPENIN("12")
1570 PRINT#cmd%,"BBC DEVICE NO",6
1580 PRINT#cmd%,"CLEAR"
1590 PRINT#cmd%,"REMOTE ENABLE"
```

```
1600 *DISC
1610 ENDPROC
1620
1630 DEFPROCdata
1640 REM Disable the clock interrupt.
1650 F%=1:G%=0:S%=5
1660 *IEEE
1670  FOR I%=0 TO 3:ID$(I%)="":NEXT
1680 trace%=1
1690 PRINT#cmd%,"TALK",scope%
1700 PRINT#cmd%,"READ BINARY",0
1710 REPEAT
1720 REPEAT
1730 result%=BGET#data%
1740 IF result%=10 trace%=6:PRINT#cmd%,"CLEAR":GOTO 1760
1750 ID$(trace%-1)=ID$(trace%-1)+CHR$(result%)
1760 UNTIL result%=37 OR result%=10
1770 IF result%=10 GOTO 1840
1780 bc%(trace%-1)=256*BGET#data%+BGET#data%
1790 FOR J%=0 TO bc%(trace%-1)-2
1800 wave%?(J%-(bc%(0)-1)*(trace%>=2)-(bc%(1)-1)*(trace%>=3)
     -(bc%(2)-1)*(trace%=4))=BGET#data%
1810 NEXT
1820 CS%=BGET#data%
1830 trace%=trace%+1
1840 UNTIL trace%=6
1850 *DISC
1860 ENDPROC
1870
1880 DEFPROCsave
```

```
1890 FOR trace%=trace1% TO 4
1900 IF ID$(trace%-1)="" GOTO 2100
1910 REM Store second, minute,hour,day and month in 60-decimal
     ** 0-9,A-Z,a-x.
1920 E%=?SEC+48:E%=E%-7*(E%>57)-6*(E%>83)
1930 D%=?MINUTE+48:D%=D%-7*(D%>57)-6*(D%>83)
1940 C%=?HOUR+48:C%=C%-7*(C%>57)
1950 B%=?MONTH+48:B%=B%-7*(B%>57)
1960 A%=?DATE+48:A%=A%-7*(A%>57)
1970 event$=CHR$(A%)+CHR$(B%)+CHR$(C%)+CHR$(D%)+CHR$(E%)+
     STR$(trace%)
1980 REM Store waveform(W) and identifying information(I)
     followed by
1990 REM the trace number and coded second, minute, hour,
     day and month.
2000 ID=OPENOUT("I"+event$)
2010 PRINT#ID,ID$(trace%-1)+STR$(?FSEC)
2020 CLOSE#ID
2030 WF=OPENOUT("W"+event$)
2040 BPUT#WF,INT(bc%(trace%-1)/256)
2050 BPUT#WF,bc%(trace%-1)-INT(bc%(trace%-1)/256)*256
2060 FOR I%=0 TO bc%(trace%-1)-2
2070 BPUT#WF,wave%?(I%-(bc%(0)-1)*(trace%>=2)-(bc%(1)-1)
     *(trace%>=3)-(bc%(2)-1)*(trace%=4))
2080 NEXT
2090 CLOSE#WF
2100 NEXT
2110 trace1%=1
2120 ENDPROC
```

This fourth section was written for the retrieval and analysis of the data stored on the discs. The example shown here contains routines for plotting out the data although it is simple to replace these with, for example, routines for statistical analysis as was done in Chapter 6.

```
10 REM ---*** DATA4 ***---
20 MODE7:VDU 14:VDU23;8202;0;0;0;
30 REM Variables for IEEE data collection.
40 DIM ID$(3),WFID$(3),XUNITS$(3),YUNITS$(3),FILE$(1,14),bc%(3)
   ,xinc%(3)
50 DIM XSCALE(3),YSCALE(3),ymult%(3),yoff%(3),wave%1023
60 FOR I%=0 TO 3:bc%(I%)=0:FOR J%=0 TO 14:FILE$(I% DIV 2,J%)=""
   :NEXT,
70 PROCinit
```

PROCinit sets up the BBC as controller of the IEEE 488 interface bus and prepares any devices for operation.

```
80 PROCmenu1
```

PROCmenu1 loads the disc directory into memory.

```
90 PROCmenu2
```

PROCmenu2 decodes the filenames to present an intelligible menu to the operator showing the time that the data was stored and how many traces.

```
100 PROCload
```

This routine reads in the selected data from disc.

```
110 PROCsort
```

PROCsort decodes the waveform information transmitted by the scope along with the actual data.

```
120 PROCaxes
130 PROCplot
```

These routines operate the HP7221S Plotter to produce hard copy if required.

```
140 GOTO 90
150 END
160
170 DEFPROCinit
180 *IEEE
190 CLOSE#0
200 cmd%=OPENIN("COMMAND")
210 data%=OPENIN("DATA")
220 plotter%=OPENIN("1")
230 PRINT#cmd%,"BBC DEVICE NO",6
240 PRINT#cmd%,"CLEAR"
250 PRINT#cmd%,"REMOTE ENABLE"
260 *DISC
270 ENDPROC
280
290 DEFPROCsort
300 trace%=trace1%
310 REPEAT
320 pos%=14-(trace%=1)*23 :L$=""
330 REPEAT
```

```
340 WFID$(trace%-1)=WFID$(trace%-1)+L$
350 pos%=pos%+1
360 L$=MID$(ID$(trace%-1),pos%,1)
370 UNTIL ASC(L$)=34
380 pos%=pos%+8 :L$="" :PROCpick
390 V%=VAL(L$)
400 pos%=pos%+16 :L$="" :PROCpick
410 xinc%(trace%-1)=VAL(L$)
420 pos%=pos%+16 :L$="" :PROCpick
430 trig%=VAL(L$)
440 pos%=pos%+7 :L$="" :PROCpick
450 XUNITS$(trace%-1)=L$
460 pos%=pos%+7 :L$="" :PROCpick
470 ymult%(trace%-1)=VAL(L$)
480 pos%=pos%+14 :L$="" :PROCpick
490 yoff%(trace%-1)=VAL(L$)
500 pos%=pos%+7 :L$="" :PROCpick
510 YUNITS$(trace%-1)=L$
520 sec$=RIGHT$(ID$(trace%-1),1)
530 trace%=trace%+1
540 UNTIL trace%=trace2%+1
550 ENDPROC
560
570 DEFPROCpick
580 REPEAT
590 L$=L$+MID$(ID$(trace%-1),pos%,1)
600 pos%=pos%+1
610 UNTIL MID$(ID$(trace%-1),pos%,1)=","
620 ENDPROC
630
```

```
640 DEFPROCload
650 event$=FILE$(0,15-CHOICE%)
660 FOR trace%=trace1% TO 4
670 ID=OPENIN(LEFT$(event$,6)+STR$(trace%))
680 IF ID=0 trace2%=trace%-1:trace%=4:GOTO 780
690 INPUT#ID,ID$(trace%-1)
700 CLOSE#ID
710 WF=OPENIN("W"+MID$(event$,2,5)+STR$(trace%))
720 bc%(trace%-1)=BGET#WF*256+BGET#WF
730 FOR I%=0 TO bc%(trace%-1)-2
740 wave%?(I%-(bc%(0)-1)*(trace%>=2)-(bc%(1)-1)*(trace%>=3)-(bc%(2)
    -1)*(trace%=4))=BGET#WF
750 NEXT I%
760 CLOSE#WF
770 IF trace%=4 trace2%=4
780 NEXT trace%
790 ENDPROC
800
810 DEFPROCaxes
820 *IEEE
830 PRINT# cmd%,"LISTEN",plotter%,"EXECUTE"
840 PRINT# data%,"IN","IP3000,3000,10500,9000"
850 PRINT# data%,"SP2","PA 10500,3000","PD"
860 PRINT# data%,"PA3000,3000,3000,9000,10500,9000,10500,3000","PU"
870 PRINT# data%,"SC 0,511,0,255","SP4","PA 255,0","PD","PA 255,2"
    ,"YT"
880 FOR I%=2 TO 253 STEP 25 :PRINT# data%,"PA 255,"+STR$(I%),"YT"
    :NEXT I%
890 PRINT# data%,"PA 255,255","PU","PA 0,127"
900 PRINT# data%,"PD","PA 5,127","XT" :FOR I%=5 TO 506 STEP 50
```

```
910 PRINT# data%,"PA "+STR$(I%)+",127","XT":NEXT I%
920 PRINT# data%,"PA 511,127","PU","SP0"
930 ENDPROC
940
950 DEFPROCplot
960 *IEEE
970 FOR trace%=trace1% TO trace2%
980 PRINT#data%,"SP"+STR$(2-(trace% MOD 2))
990 IF trace%>2 PRINT#data%,"LT2" ELSEPRINT#data%,"LT"
1000 PRINT# data%,"PA 0,"+STR$(yoff%(trace%-1)),"PD","XT","YT","PU"
1010 J%=0:PRINT# data%,"PA0,"+STR$(wave%?0),"PD"
1020 FOR I%=0 TO 511 STEP (512/(bc%(trace%-1)-1))
1030 PRINT# data%,"PA"+STR$(I%)+","+STR$(wave%?(J%-(bc%(0)-1)*
     (trace%>=2)-(bc%(1)-1)*(trace%>=3)-(bc%(2)-1)*(trace%=4)))
1040 J%=J%+1:NEXT I%:PRINT# data%,"PU":NEXT trace%
1050 PRINT# data%,"LT","SP4","PA"+STR$(trig%*(512/(bc%(trace2%
     -1)-1)))+",0","PD","PR0,12,-3,-3,3,3,3,-3,-3,3","PU","SP0"
1060 PRINT#data%,"SC","IP;","PA4500,9500","SP1","LB"+LEFT$(FILE$
     (1,15-CHOICE%),26)+"."+sec$+CHR$(3)
1070 PRINT#data%,"SP4","PA11000,8500","LBKEY:"+CHR$(3),"SP0"
1080 PRINT#data%,"PU":Y%=8200:FOR trace%=trace1% TO trace2%
1090 PRINT#data%,"SP"+STR$(2-(trace% MOD 2))
1100 IF trace%>2 PRINT#data%,"LT2" ELSE PRINT#data%,"LT"
1110 PRINT#data%,"PA11300,"+STR$(Y%),"LB"+WFID$(trace%-1)+CHR$(3)
     ,"PR300,80","PD","PR800,0","PU"
1120 Y%=Y%-300
1130 NEXT trace%
1140 PRINT#data%,"LT","SP4","PA11300,"+STR$(Y%),"LBTrig. Point:-"
     +CHR$(3),"PR300,0","PD","PR0,240,-60,-60,60,60,60,-60,-60,60","PU"
1150 FOR trace%=trace1% TO trace2%
```

```
1160 XSCALE(trace%-1)=25*(512/(bc%(trace%-1)-1))*xinc%(trace%-1)
     *10^(3*(XUNITS(trace%-1)="MS")+6*(XUNITS(trace%-1)="US")+9*
     (XUNIT(trace%-1)="NS"))
1170 XUNITS(trace%-1)=STR(XSCALE(trace%-1))+" S/DIV"
1180 IF XSCALE(trace%-1)<10^-6 XUNIT(trace%-1)=STR(XSCALE
     (trace%-1)*10^9)+" NS/DIV"
1190 IF XSCALE(trace%-1)<10^-3 XUNIT(trace%-1)=STR(XSCALE
     (trace%-1)*10^6)+" US/DIV"
1200 IF XSCALE(trace%-1)<1 XUNITS(trace%-1)=STR(XSCALE
     (trace%-1)*10^3)+" MS/DIV"
1210 YSCALE(trace%-1)=25*ymult%(trace%-1)*10^(3*(YUNITS
     (trace%-1)="MV")+6*(YUNITS(trace%-1)="UV"))
1220 YUNITS(trace%-1)=STR(YSCALE(trace%-1))+" V/DIV"
1230 IF YSCALE(trace%-1)<10^-3 YUNITS(trace%-1)=STR(YSCALE
     (trace%-1)*10^6)+" UV/DIV"
1240 IF YSCALE(trace%-1)<1 YUNITS(trace%-1)=STR(YSCALE
     (trace%-1)*10^3)+" MV/DIV"
1250 NEXT trace%
1260 trace%=trace1%:PRINT#data%,"SP"+STR(2-(trace% MOD 2))
1270 Y%=6100:PRINT#data%,"PA11000,"+STR(Y%),"LB"+XUNITS
     (trace%-1)+CHR(3)
1280 IF trace1%>3 OR trace2%<3 GOTO 1310
1290 trace%=trace%+1:IF trace%>trace2% GOTO 1310
1300 Y%=Y%-300:IF XUNITS(trace1%-1)<>XUNITS(trace2%-1)
     PRINT#data%,"SP"+STR(2-(trace2% MOD 2)),"PA11000,"+STR(Y%),
     "LB"+XUNITS(trace2%-1)+CHR(3)
1310 trace%=trace1%:PRINT#data%,"SP"+STR(2-(trace% MOD 2))
1320 Y%=2600:PRINT#data%,"PA6000,"+STR(Y%),"LB"+YUNITS
     (trace%-1)+CHR(3)
1330 trace%=trace%+1:Y%=Y%-300:IF trace%>trace2% GOTO 1410
```

```
1340 PRINT#data%,"SP"+STR(2-(trace% MOD 2)):IF YUNITS(trace%-1)
     <>YUNITS(trace%-2)PRINT#data%,"PA6000,"+STR(Y%),"LB"+
     YUNITS(trace%-1)+CHR(3)
1350 IF trace1%>1 OR trace2%<3 GOTO 1390
1360 trace%=trace%+1:Y%=Y%-300:IF trace%>trace2% GOTO 1410
1370 PRINT#data%,"SP"+STR(2-(trace% MOD 2)):IF YUNITS(0)<>
     YUNITS(2) PRINT#data%,"PA6000,"+STR(Y%),"LB"+YUNITS(trace%
     -1)+CHR(3)
1380 trace%=trace%+1:Y%=Y%-300:IF trace%>trace2% GOTO 1410
1390 IF trace1%>2 OR trace2%<4 GOTO 1410
1400 PRINT#data%,"SP"+STR(2-(trace% MOD 2)):IF YUNITS(1)<>
     YUNITS(3) PRINT#data%,"PA6000,"+STR(Y%),"LB"+YUNITS(trace%
     -1)+CHR(3)
1410 PRINT#data%,"SP0","PA15760,11180"
1420 INPUT TAB(4,20)"DO YOU WANT THE PLOT ADVANCED";TEMP:IF
     LEFT(TEMP,1)="N" GOTO 1450
1430 IF LEFT(TEMP,1)<>"Y" THEN PRINT TAB(34,20)"       "
     :GOTO 1410
1440 PRINT# data%,"EC","AF","EC0"
1450 *DISC
1460 ENDPROC
1470
1480 DEFPROCmenu1
1490 FOR I%=0 TO 1:FOR J%=0 TO 14:FILE(I%,J%)="":NEXT,
1500 Y%=wave% DIV 256:X%=wave% MOD 256:A%=8
1510 !(wave%+1)=wave%+&0D:!(wave%+&05)=&1F:!(wave%+&09)=&00
     :CALL &0FFD1
1520 K%=0:F%=0
1530 REPEAT:J%=?(wave%+&0D+K%)
1540 IF ?(wave%+&0D+K%+1)<>73 THEN K%=K%+J%+1:GOTO 1580
```

```
1550 FOR K%=1+K% TO J%+K%-1
1560 FILE(0,F%)=FILE(0,F%)+CHR(?(wave%+&0D+K%))
1570 NEXT K%:F%=F%+1
1580 UNTIL J%=0 OR F%=15
1590 FOR I%=0 TO 14:FOR L%=2 TO 7
1600 TEMP=MID(FILE(0,I%),L%,1)
1610 CODE%=ASC(TEMP)-48+7*(ASC(TEMP)>57)+6*(ASC(TEMP)>91)
1620 ON L%-1 GOSUB  1980,1820,2080,2080,2080,2130
1630 IF L%>3 AND L%<6 THEN FILE(1,I%)=FILE(1,I%)+":"
1640 NEXT,
1650 ENDPROC
1660
1670 DEFPROCmenu2
1680 CLS:PRINT TAB(17,0);"MENU"
1690 FOR I%=15 TO 1 STEP -1
1700 PRINT TAB(1,16-I%+1);~(16-I%)": ";FILE(1,I%-1)
1710 NEXT
1720 LAST%=1
1730 REPEAT
1740 KEY=INKEY(0):IF KEY<>-1 THEN CHOICE%=KEY-48+7*(KEY>57)
     ELSE 1770
1750 IF CHOICE%>=1 AND CHOICE%<=15 THEN PRINT TAB(0,LAST%+1)
     ;CHR(135)
1760 PRINT TAB(0,CHOICE%+1);CHR(133):LAST%=CHOICE%
1770 UNTIL INKEY(-74)
1780 *FX15,0
1790 trace1%=VAL(RIGHT(FILE(1,15-CHOICE%),1))
1800 ENDPROC
1810
1820 REM Find out what month it is.
```

```
1830 ON CODE% GOSUB 1850,1860,1870,1880,1890,1900,1910,1920,
     1930,1940,1950,1960
1840 FILE(1,I%)=FILE(1,I%)+MONTH+" at ":RETURN
1850 MONTH=" January  ":RETURN
1860 MONTH=" February ":RETURN
1870 MONTH=" March    ":RETURN
1880 MONTH=" April    ":RETURN
1890 MONTH=" May      ":RETURN
1900 MONTH=" June     ":RETURN
1910 MONTH=" July     ":RETURN
1920 MONTH=" August   ":RETURN
1930 MONTH=" September":RETURN
1940 MONTH=" October  ":RETURN
1950 MONTH=" November ":RETURN
1960 MONTH=" December ":RETURN
1970
1980 REM Subroutine to print date.
1990 THE="th"
2000 IF CODE% MOD 10=1 THE="st"
2010 IF CODE% MOD 10=2 THE="nd"
2020 IF CODE% MOD 10=3 THE="rd"
2030 IF CODE% DIV 10=1 THE="th"
2040 IF CODE%<10 THEN TEMP=" " ELSE TEMP=""
2050 FILE(1,I%)=FILE(1,I%)+TEMP+STR(CODE%)+THE
2060 RETURN
2070
2080 REM Subroutine to print time.
2090 TEMP="":IF CODE%<10 THEN TEMP="0"
2100 FILE(1,I%)=FILE(1,I%)+TEMP+STR(CODE%)
2110 RETURN
```

```
2120

2130 REM Print out the trace number.

2140 FILE(1,I%)=FILE(1,I%)+" - tr:"+TEMP

2150 RETURN
```

REFERENCES

1) Einstein, A., Sitzber, Preuss. Akad. Wiss., Berlin, K1. Math. Physik. UTech., 688, (1916)

2) Einstein, A., Sitzber. Preuss. Akad. Wiss., Berlin, K1. Math. Physik. UTech., 154, (1916)

3) Press, W. H. and Thorne, K. S., Ann. Rev. Astron. and Astrophys., 10, 355 (1972)

4) Misner, C. W., Thorne, K. S., Wheeler, J. A., 'Gravitation', Freeman (1973)

5) Thorne, K. S., O. A. Series, Nuc., Atomic and Th. Astro., 575 (1979)

6) Davies, P. C. W., 'The Search for Gravity Waves', Cambridge University Press (1980)

7) Nagabirov, V. R., Kopvillem, U. Kh., JETP Lett., 5, 360 (1967)

8) Nagabirov, V. R., Kopvillem, U. Kh., Izv. VUZ Fiz., 9, 66 (1967)

9) Nagabirov, V. R., Kopvillem, U. Kh., Sov. Phys. - JETP, 29, 112 (1969)

10) Braginskii, V. B., Rudenko, V. N., Sov. Phys. - Usp., 13, 165 (1970)

11) Wood, L., Zimmerman, G., Nuckolls, J., Chapline, G., Bull. Am. Phys. Soc., 16, 609 (1971)

12) Iben, I., Tutukov, A. V., Astrophys. J. Supp., 54, 335 (1984)

13) Evans, C. R., Iben, I., Smarr, L., Astrophys. J. (1987)

14) Wheeler, J. C., 'Supernovae: A Survey of Current Research', Rees, M. J., Stoneham, R. J., (eds.), Reidel (1982)

15) Wilson, J. R., Phys. Rev. Lett., 32, 849 (1974)

16) Schram, D. N., Arnett, W. D., Astrophys. J., 198, 629 (1975)

17) Douglass, D. H., Braginskii, V. B., Chapter 3 in 'General Relativity: An Einstein Centenary Survey', Hawking, S. W., Israel, W. (eds.), Cambridge University Press (1979)

18) Endal, A. S., Sofia, S., Phys. Rev. Lett., 39, 1429 (1977)

19) Hough, J., Meers, B. J., Newton, G. P., Robertson, N. A., Ward, H., Schutz, B. F., Drever, R. W. P., Tolcher, R. and Corbett, I. F., 'A British Long Baseline Gravitational Wave Observatory', Design Study Report GWD/RAL/86-001

20) Schutz, B. F., Am. J. Phys., 52, 412 (1984)

21) Arnett, W. D., 'Supernovae and their remnants', Brancozio, P. J., Cameron, A. G. W. (eds.), New York: Gordon and Breach (1969)

22) Thorne, K. S., 'Gravitational Radiation' submitted to '300 Years of Gravitation', Hawking, S. W., Israel, W. (eds.), Cambridge University Press (1987)

23) Peters, P. C., Mathews, J., Phys. Rev., 131, 435 (1963)

24) Schutz, B. F., Nature, 323, 310 (1986)

25) Blinnikov, S. I., Novikov, I. D., Perevodchikova, T. V., Polnarev, A. G., Soviet Astron. - AJ, 10, 177 (1984)

26) Lyne, A., Private communication to B. F. Schutz (1986)

27) Shapiro, S. L., Teukolsky, S. A., Astrophys. J. (Lett.), 292, L41 (1985)

28) Quinlan, G., Shapiro, S. L., Paper in preparation (1987)

29) Rees, M. J., in 'Gravitational Radiation', Deruelle, N., Piran, T. (eds.), North-Holland (1982)

30) Haugan, M. P., Shapiro, S. L., Wasserman, I., Astrophys. J., 257, 283 (1982)

31) Detweiler, S. L., Szedenits, E., Astrophys. J., 231, 211 (1979)

32) Kojima, Y., Nakomura, T., Prog. of Theor. Phys., 71, 79

(1984)

33) Zimmerman, M., Phys. Rev. D, 21, 891 (1980)

34) Alpar, M. A., Pine , D., Nature, 314, 334 (1985)

35) Chandrasekhar, S., Phys. Rev. Lett., 24, 611 (1970)

36) Friedman, J. L., Schutz, B. F., Astrophys. J., 222, 281, (1978)

37) Wagoner, R. V., Astrophys. J., 278, 345 (1984)

38) Priedhorsky, W., Stella, L., White, N. E., IAU Circ. No. 4247 28th August (1984)

39) Bond, J. R., Carr, B. J., Mon. Not. Roy. Astr. Soc., 207, 585 (1984)

40) Matzner, R. A., ASTROPHYS J., 154, 1123 (1968)

41) Ruffini, R., Wheeler, J. A., 'Relativistic Cosmology and Space Platforms' in Proc. ESRO Colloq., European Space Research Organisation, Neuilly-sur-Seine, France, September 1969

42) Davies, M. M., Taylor, J. H., Weisberg, J. M. and Backer, D. C., Nature, 315, 547 (1985)

43) Hogan, C. J., Rees, M. J., Nature, 311, 109 (1984)

44) Carr, B., Nature, 315, 540 (1985)

45) Weber, J., Phys. Rev., 117, 306 (1960)

46) Weber, J., Phys. Rev. Lett., 22,1320 (1969)

47) Drever, R. W. P., Hough, J., Bland, R., Lessnoff, G.W., Nature, 246, 340 (1973)

48) Kerr, G. A., Ph.D. Thesis, Univ. of Glasgow (1986)

49) Unruh, W. G., Phys. Rev. D., 19, 2888 (1979)

50) Caves, C. M., Drever, R. W. P., Sandberg, V. D., Thorne, K. S., Zimmerman, M., Rev. Mod. Phys., 52, 341 (1980)

51) Moss, G. E., Miller, L. R., Forward, R. L., Appl. Opt., 10, 2495 (1971)

52) Forward, R. L., Phys. Rev. D., 17, 379 (1978)

53) Newton, G. P. et al, Proc. 4th Marcel Grossman Meeting on Recent Developments in Relativity and Gravitation, Rome 1985, Ed. R. Ruffini, Elsevier Science Publishers BV, 599 (1986)

54) Drever, R. W. P. et al, ibid.

55) Shoemaker, D. H. et al, ibid.

56) Livas, J. et al, ibid.

57) Drever, R. W. P., Hough, J., Munley, A. J., Lee, S. A-., Spero, R., Whitcomb, S. E., Ward, H., Ford, G. M., Hereld, H., Robertson, N. A., Kerr, I., Pugh, J. R., Newton, G. P., Meers, B., Brooks III, E. D., Gursel, Y., Proc. of the NATO Adv. Study Inst., Bad Windsheim, West Germany in 'Quantum Optics, Expt. Grav. and Meas. Theory', Meystre, P., Scully, M. O. (eds.), Plenum Press (1981)

58) Caves, C. M., Phys. Rev. D., 23, 1693 (1981)

59) Slusher, R. E., Hollberg, L. W., Yurke, B., Mertz, J. C., Valley, J. F., Phys. Rev. Lett., 55, 2409 (1985)

60) Edelstein, W. A., Hough, J., Pugh, J. R., Martin, W., J. Phys. E: Sci. Instrum., 11, 710 (1978)

61) Braginsky, V. B., Gertsenshtein, M. E., Sov. Phys.-JETP Lett., 5, 287 (1967)

62) Anderson, A. J., Nature, 229, 547 (1971)

63) Hellings, R. W., Callahan, P. S., Anderson, J. D., Moffat, A. T., Phys. Rev. D., 23, 844 (1981)

64) Smarr, L., Vessot, R. F. C., Lundquist, C. A., Decher, R., Gen. Rel. and Grav., 15, 129 (1983)

65) Faller, J. E., Bender, P. L., Hall, J. L., Hils, D., Vincent, M. A., in 'Proceedings of the Colloquium: Kilometric Optical Arrays in Space', ESA SP-226, Cargese, Corsica, Oct. 1984

66) Drever, R. W. P., Hall, J. L, Kowalski, F. V., Hough, J., Ford, G. M., Munley, A. J., Ward, H., Appl. Phys. B, 31, 97-105 (1983)

67) Meers, B. J., Ph.D. Thesis, Univ. of Glasgow (1983)

68) Robertson, N. A., Ph.D. Thesis, Univ. of Glasgow (1981)

69) Billing, H., Maischberger, K., Rudiger, A., Schilling, R., Schnupp, L. and Winkler, W., J. Phys. E: Sci. Instrum., 12, 1043 (1979)

70) Layer, H.P., Appl. Optics., 18, 2947-2949 (1979)

71) Hall, J.L. et al, IEEE/OSA Conf. on Laser Engineering and Applications. Digest of papers [IEEE Cat. No. 77 CH-1207.0] p.45 (1977)

72) Yariv, A.,'Quantum Electronics', 2nd Edition, Chap. 14

73) Goldstein, R., Pockels cell primer, Laser Focus Magazine (1968)

74) Ley, J.M., Electron. Lett., 2, 12-13 (1966)

75) Clayson, C.H., Electron. Lett., 2, 138 (1966)

76) Fang-Shang Chen, 'Modulators for Optical Communications', Proc. IEEE, 58, 1440-1457 (1970)

77) Kerr, G. A., Robertson, N. A., Hough, J., Man, C. N., Appl. Phys. B, 37, 11-16 (1985)

78) Meers, B.J., Optics Communications, 47, 237-242 (1983)

79) Rudiger et al, Optica Acta, 28, 641-658 (1981)

80) Distefano III, J. J., Stubberud, A. R., Williams, I. J., 'Feedback and Control Systems', Schaum (1976)

81) Hammond, P. H., 'Feedback Theory and its Applications', English Universities Press (1958)

82) Thaler, G. J., 'Design of Feedback Systems', Dowden, Hutchinson and Ross (1973)

83) Birch, R. D., Payne, D. N., Varnham, M. P., Electron. Lett., 18, 1036 (1982)

84) Snitzer, E., J. Opt. Soc. Am., 51, 491 (1961)

85) Gloge, D., Appl. Opt., 10, 2252 (1971)

86) Dholen, K., Final Year Project Report, Department of Physics and Astronomy, University of Glasgow (1986)

87) Brown, R. G. W., Jackson, D. A., Jones, J. D. C., Chan, R. K. Y., International Commision for Optics - 13, P. 322, Conference Digest of 'Optics in Modern Science and Technology', Sapporo, Japan, August (1984)

88) Bray, A. C., Dickens, A. C., Holmes, M. A., 'The Advanced User Guide for the BBC Microcomputer', Cambridge Microcomputer Centre (1983)

89) Mood, A. M., Graybill, F. A., Boes, D. C., 'Introduction to the Theory of Statistics' 3rd. Ed., McGraw-Hill (1985)

'All right,' said the (Cheshire) Cat; and this time it vanished quite slowly, beginning with the end of the tail, and ending with the grin, which remained some time after the rest of it had gone.

Lewis Carroll (Alice's Adventures in Wonderland, 1865)